2017

Hydrogen Peroxide and Pharmacological Agent Modulation of TRPV2 Channel Gating

Tuoxin Cao
Virginia Commonwealth University

Hydrogen peroxide and pharmacological agent modulation of TRPV2 channel gating

Dissertation Submitted to the Faculty of Graduate School of Virginia Commonwealth University

In partial fulfillment of the requirements for the degree of

Doctor of Philosophy in Neuroscience

at Virginia Commonwealth University.

By

Tuoxin Cao

BS. University of Kentucky 2011

Dissertation under the guidance of Ian Scott Ramsey Ph.D.,

Assistant Professor, Department of Physiology and Biophysics

Virginia Commonwealth University

Richmond, Virginia

May, 2017

Acknowledgements

First, I must express my sincere gratitude for Dr. Ian Scott Ramsey, who has supported my graduate research. When I started this project, I had very little knowledge about electrophysiology. I only knew the basic mechanism of the action potential; Dr. Ramsey taught me the much more than just the theories and techniques of electrophysiology, including: experimental design and analysis, whole cell voltage and excised inside-out voltage clamp, and writing and presenting research findings. Most importantly, Dr. Ramsey taught me how to construct a testable hypothesis and use logic arguments to determine whether the experimental data support or refute the hypothesis. Dr. Ramsey constantly challenged me to be more creative in science and to challenge my assumptions. His door is always open, and I appreciated the many opportunities I had to discuss concerns and questions. Dr. Ramsey is a patient teacher and always made sure I had a good grasp of the concepts behind my research. Instead of providing simple answers to my questions, he challenged me to deduce the meaning of data by myself first. Furthermore, Dr. Ramsey neither forced nor or assigned a research project; instead, he respected my interest in microglia and allowed me to pursue a new direction for the lab. As the result, I was able to pursue a thesis project that describes a novel mechanism of gating in TRPV2 channels that is also relevant to microglial biology. My thesis research provided me with opportunities to participate in a variety of research strategies, including structural analysis of proteins, redox signaling, stretch/mechanosensation, and microglial cell culture. I am proud of this study of ion channel biophysics in the primary innate immune cell of the central nervous system, and consider it to have been a singular experience. My thesis project certainly took longer turned out to be more convoluted than I had initially expected we explored many dead ends before successfully arriving at this terminus. Despite my initial difficulties, Dr. Ramsey supported me academically, financially and emotionally by

providing the encouragement I needed to complete my studies. For the aforementioned reasons I provide my thanks to Dr. Ramsey for helping me complete this thesis research project.

I also thank members of Ramsey lab: Victor De La Rosa Jimenez, Ph.D., a post-doctoral researcher; Ashely Bennett, my fellow Ph.D. student; and Aaron L. Randolph, a former Ph.D. student in Ramsey lab. Victor and Ashely have been great assets, both academically and emotionally. They helped me in with many elements of the research design and with analysis of experimental data. Ashely provided great insight into the structure of TRPV2 and helped me learn to use Visual Molecular Dynamics software for this purpose. Victor is a talented fellow electrophysiologist who provided important mentorship into the study of TRPV ion channels using biophysical techniques. He also provided constructive criticism of my oral presentations and provided sound career advice. Aaron was a great help when I first entered the lab and was instrumental in getting me started with electrophysiology and the patch clamp technique.

I would also like to express my present sincere thanks to all of the members of my Thesis Advisory Committee. First, I would like to thank Dr. Michelle Block for generously providing the BV-2 microglia-like cell line and for dissociated neonatal mouse microglia-enriched primary cell cultures. Furthermore, as a microglial expert, she provided valuable insight on how to study these cells. During Advisory Committee meetings, she never put untoward pressure on the student, but instead stimulated me to think ‘outside of the box’. She also provided personal advice on how to manage my responsibility as a researcher and provided much-needed encouragements for continuing my research career, and I would not have been able to complete this project without her help.

I am also indebted to Dr. Pamela Knapp and Sarah Kim, a student in the Knapp laboratory. They each provided valuable dissociated neonatal mouse microglia-enriched cultures for immunocytochemical and electrophysiological analysis. Dr. Knapp was also provided valuable critiques of my work, addressing changes that improved my research and scientific writing.

Dr. Clive Baumgarten and Dr. Sung Park, a former student in his laboratory generously provided DCPIB for my study on TRPV2. Most importantly, I appreciate Dr. Baumgarten's unique ability to provide constructive criticism of my electrophysiological studies. He also provided valuable suggestions about the design of studies to test the effects of LPS and H_2O_2 on TRPV2 channel activity.

Dr. Roland Pittman provided additional insights into the process of H_2O_2 production and helped me understand potential differences between the effects of the exogenous H_2O_2 used in my study and H_2O_2 that is physiologically produced in cells. His advice encouraged me to more carefully consider the biological relevance of my studies.

I also thank Dr. John Bigbee, Director of the Neuroscience Graduate Program, who offered support at committee meetings and provided valuable perspective on the relevance of ion channels and microglia to neurological function. Dr. Bigbee also provided encouragement during my studies and sound career advice. His effort to ensure the wellbeing of Neuroscience students meant that I never felt isolated from the Program.

Although the studies are not included here, I am thankful to Dr. Diomedes Logothetis, Ph.D. and Junghoon Ha, Ph.D. Drs. Logothetis and Ha provided valuable suggestions in the study of TRP channels by membrane lipids and kindly provided reagents.

Table of Content

List of Figures

List of Equations

List of Tables

List of Abbreviations

TRP: transient receptor potential channel

TRPC: TRP channel, canonical subfamily

TRPV: TRP vanilloid subfamily

TRPA: TRP ankyrin subfamily

TRPM: TRP melastatin subfamily

TRPP: TRP polycystin subfamily

TRPML: TRP mucolipin subfamily

TRPV1: TRP vanilloid subfamily, member 1 channel

TRPV2: TRP vanilloid subfamily, member 2 channel

TRPV3: TRP vanilloid subfamily, member 3 channel

TRPV4: TRP vanilloid subfamily, member 4 channel

TRPV5: TRP vanilloid subfamily, member 5 channel

TRPV6: TRP vanilloid subfamily, member 6 channel

TRPA1: TRP ankyrin subfamily, member 1 channel

TRPM1: TRP melastatin subfamily, member 1 channel

TRPM2: TRP melastatin subfamily, member 2 channel

TRPM8: TRP melastatin subfamily, member 8 channel

Ca^{2+}: calcium ion

Na^+: sodium ion

$[Ca^{2+}]_i$: intracellular free calcium concentration

2-APB: 2-aminophyenyl borinate, 2-Aminoethoxydiphenyl borate

CAP: capsaicin

$PI(4,5)P_2$: phosphatidylinositol(4,5)bisphosphate

Cryo-EM: electron cryomicroscopy

ARD: ankyrin repeat domain

TM: transmembrane

DkTx: *Chilobrachys guangxiensis* (spider) toxin

RTx: resiniferatoxin

HLH: helix-loop-helix

CTD: C-terminal domain

Kv: voltage-gated potassium channel

MNG: maltose neopentyl glycol

RuR: Ruthenium Red

mRNA: messenger RNA

THC: Δ^9-tetrahydrocannabinol

CBD: cannabidiol

PBC: probenecid

Tra: tranilast

Po: open probability

EC_{50}: half-maximal response concentration

RNAi: RNA interference

NF-κB: nuclear factor kappa-light-chain-enhancer of activated B cells

LPS: lipopolysaccharide

IL-6: interleukin 6

TNFα: tumor necrosis factor alpha

IL1β: interleukin 1 beta

fMLP: formyl-Met-Leu-Phe peptide

CNS: central nervous system

H_2O_2: hydrogen peroxide

$O_2^{-}\cdot$: superoxide anion

ROS: reactive oxygen species

HEK-293: Human embryonic kidney 293 cell

DMEM: Dulbecco's modified Eagle's medium

FBS: fetal bovine serum

P/S: penicillin and streptomycin

CO_2: carbon dioxide

EGFP: enhanced green fluorescent protein

DMSO: dimethyl sulfoxide

SOC: catabolite repression

LB: Luria broth

AITC: allyl isothiocyanate

CZP: capsazepine

DCPIB: 4-[(2-Butyl-6,7-dichloro-2-cyclopentyl-2,3-dihydro-1-oxo-1H-inden-5-yl)oxy]butanoic acid

$I_{Cl,swell}$: swell activated chloride channel

PBS: phosphate-buffered saline

BSA: bovine serum albumin

BMD: 2-Mercaptoethanol

I_{tail}: instantaneous tail current

I-V: current-voltage

$V_{0.5}$: half-maximal voltage

t: time

i: unitary current

V_M: membrane potential

E_{REV}: reversal potential

N: number of functional channels

SEM: standard error of the mean

I_{CRAC}/Orai: store-operated calcium release-activated calcium channel

Abstract

HYDROGEN PEROXIDE, LIPOPOLYSACCHARIDE AND PHARMACOLOGICAL AGENT MODULATION OF TRPV2 CHANNEL GATING

By Tuoxin Cao

BS. University of Kentucky 2011

A dissertation submitted in partial fulfillment of the requirements for the degree of Doctor of Philosophy at Virginia Commonwealth University. Virginia Commonwealth University, 2017.

Dissertation under guidance of Ian Scott Ramsey, Ph.D. Assistant Professor, Department of Physiology and Biophysics

Transient receptor potential vanilloid 2 channel (TRPV2) is a Ca^{2+}-permeable ion channel that is highly expressed in leukocytes but is also present in skeletal and cardiac muscle and endocrine cells. The TRPV2 function is implicated in a number of physiological processes, including bacterial phagocytosis, pro-inflammatory cytokine production, cardiac hypertrophy, and cancer development. TRPV2 knockout mice exhibit a high incidence of perinatal mortality, arguing that the channel plays essential roles in physiology. Despite the importance of TRPV2 for normal homeostasis, the mechanisms that control TRPV2 gating in response to pharmacological agonists, heating, membrane stretch, bioactive lipids and reactive oxygen species (ROS) remain poorly understood. Here we demonstrate that TRPV2 is functionally expressed in microglia (i.e., 'brain macrophages') and the microglia-like BV-2 cell line, and demonstrate that the gating of an endogenous TRPV2-like conductance is positively modulated by the bacterial toxin lipopolysaccharide (LPS), which is known to cause pro-inflammatory (M1) activation and increase ROS production by NADPH oxidase. To determine how TRPV2 gating is modulated by ROS, we recorded single channel activity in inside-out patches excised from HEK-293 cells expressing GFP-rTRPV2. Unitary currents elicited by the TRPV2 agonist 2-aminophenyl borinate (2-APB) or cannabidiol (CBD) are linear in monovalent recording solutions and give rise to an estimated unitary conductance of ~100pS, which is similar to TRPV1 but significantly smaller than TRPV3. Intriguingly, we find that although TRPV2 is insensitive to ROS (in the form of exogenously applied H_2O_2) alone, apparent open probability is synergistically enhanced when H_2O_2 is applied together with CBD. We identify two intracellular Cys residues that are necessary for TRPV2 responses to H_2O_2 sensitivity and find that these residues are located close to one another, albeit in different subunits, in the TRPV2 structure, suggesting that ROS promote the formation of an inter-subunit disulfide bond that alters sensitivity to pharmacological agonists. We hypothesize that ROS-dependent modulation of TRPV2 activity may be an important contributor to pro-

inflammatory activation of microglia underline central nervous system diseases and that TRPV2 antagonism could be a useful therapeutic strategy in the treatment of neuroinflammation.

Chapter I. Introduction

1. The TRP channel superfamily

The superfamily of transient receptor potential (TRP) channel genes contains six subfamilies that encode more than 20 different ion channel proteins in mammals[2]. TRP channels are grouped based on primary sequence similarity rather than biological function, and include canonical (TRPC), vanilloid (TRPV), ankyrin (TRPA), melastatin (TRPM), polycystin (TRPP) and mucolipin (TRPML) subfamilies[3]. Even within a subfamily, sequence identity can be as low as 20%[3]. The overall architecture of TRP channel proteins is similar to other voltage-gated cation channels: six transmembrane helices (S1 – S6) compose the transmembrane-spanning structure and formation of a tetrameric quaternary structure is necessary for function[3]. S5 - S6 and the intervening 'pore loop' from each of 4 subunits jointly form the pore domain that contains the ion 'selectivity filter'[1,4-6].

A common theme among TRP channels is their weak selectivity between monovalent and divalent cations[3], and most TRP channels are thus permeable to the pleiotropic second messenger calcium (Ca^{2+}). Ca^{2+} permeability endows TRP channels with the ability to function as cellular sensors and to directly participate in intracellular signaling cascades. When activated, TRP channels both depolarize the membrane (due to inward currents carried by Na^{+} and/or Ca^{2+}) and increase intracellular calcium concentration ($[Ca^{2+}]_i$) by allowing an influx of Ca^{2+} from the extracellular space[7]. Physiologically, free $[Ca^{2+}]_i$ is approximately 100 nM, which is significantly lower than the extracellular Ca^{2+} concentration (~2 mM); the Ca^{2+} concentration gradient thus strongly favors Ca^{2+} entry over efflux[2].

TRP channel gating mechanisms are crucial to understanding the biological functions of TRP channels. TRP channel activation mechanisms are complex and vary widely even between members of the same subfamily. A general feature of TRP channel gating is 'polymodal gating', in which multiple stimuli can activate the same channel[3,7]. Examples include activation by membrane depolarization (i.e., voltage), changes in temperature, mechanical force or membrane stretch, pharmacological ligands such as 2-aminophyenyl borinate (2-APB), capsaicin (CAP), menthol and cannabinoids, membrane lipids (i.e.,

phosphatidylinositol(4,5)bisphosphate or PI(4,5)P_2) and ions such as Ca^{2+} [3,7]. TRPV1, TRPV2, and TRPV3 are activated by heating[8-11], while TRPM8 and TRPA1 are known to be activated by cooling[12-14]. Gating in each of the aforementioned channels is also modulated by changes in voltage, PI(4,5)P_2 and chemical ligands[3,7,15-18]. Some thermosensitive TRP channels contribute to thermal nociception: knockout of TRPV1 from mice, for example, attenuates behavioral responses to noxious heat and pain transduction[19,20]. Ligand-dependent activation of TRP channels also elicits specific behavioral responses. TRPV1 is activated by the vanilloid compound capsaicin from hot chili peppers[21], while TRPM8 and TRPA1 are activated by menthol, a compound found in the mint plant; as a result, eating chili pepper causes the sensation of heat while mint elicits a cooling sensation[12,13].

The TRPV channel subfamily contains six members, (TRPV1 - TRPV6) that share 20% amino acid (aa) identity. The TRPV subfamily can be further subdivided into two groups: TRPV1-4 and TRPV5-6 based on the primary sequence: TRPV5 and TRPV6 share approximately 75% aa sequence identity, but are only ~20% identical to TRPV1-4[3,22]. TRPV5 and TRPV5 are constitutively active (i.e., they lack gating sensitivity to changes in temperature, voltage, and chemical ligands), and are thus distinct from TRPV1-4[3,7,22]. TRPV1-3 share pharmacological activation by 2-APB, psychoactive and non-psychoactive cannabinoids, sensitivity to heating, and are modulated by PI(4,5)P_2[15,17,18]. TRPV4 is distinct from TRPV1-3 in being mechanosensitive and activated by phorbol esters[23,24]. TRPV2 is most closely related to TRPV1, with which it shares approximately 50% aa sequence identity[7,8,22].

Despite recent advances enabling the cloning and functional expression of TRP channels in mammalian cells, gating mechanisms, and physiological functions remain elusive. For example, the pharmacology of activators and inhibitors at TRPV1 has been extensively characterized, biophysical properties have been carefully analyzed, and physiological functions have been examined in transgenic animals[4,7,22,25,26]. Recently, several TRPV1 structures in different conformations and in complex with different ligands were solved by cryo-electron microscopy (cryo-EM), and the structural basis for vanilloid and PI(4,5)P_2 sensitivity is known[26-28]. The recent availability of rat and rabbit TRPV2 cryo-EM structures have guided

mutagenesis strategies to successfully reconstitute vanilloid sensitivity in TRPV2, suggesting that differences in the molecular function of TRPV1 and TRPV2 are mainly attributable to specific amino acid side chain substitutions[1,29]. The emergence of cryo-EM structures now facilitates other rationally designed studies to investigate mechanistic similarities and differences between TRPV1 and TRPV2.

2. TRPV2 channel structure

The cytoplasmic N-terminus in TRPV2 contains a ~70 aa distal N-terminal region of the unknown structure followed by the ~250 aa ankyrin repeat domain (ARD), and a ~60 aa membrane-proximal linker region that connects the ARD to the S1 helix in the heptahelical transmembrane (TM) domain[30]. This distal N-terminal region is not resolved by the crystal structure, suggesting its structure is dynamic[31], and deletion of up to 65 N-terminal residues does not significantly alter channel function in rat TRPV2[32]. Although their length varies, ankyrin repeat domains are commonly found in TRP channels. In TRPV1 and TRPV2, the ARD contains 6 interconnected ankyrin repeats each of which contains a similar helix-β-hairpin-helix motif[1,29]. Ankyrin repeats stack to create the ARD, and the 5 consecutive β-hairpin structures (referred to as finger 1-5) compose a continuous external cytoplasmic surface[1,29]. ARDs are clearly resolved in cryo-EM structures of TRPV2, suggesting that ARDs form relatively rigid structures[31]. Molecular dynamics (MD) simulations of TRPV1 channels based on putative closed (apo)[26] and open (bound to an activating peptide toxin, DkTx, and the vanilloid compound resiniferatoxin)[4] TRPV1 structures predict that channel opening elicited by heat results from a sequence of conformational changes that begin in the intracellular ARDs; rotation of ARDs relative to one another is thus thought to be a crucial step in the gating process[33]. Reorganization of the ARDs subsequently causes changes in pore domain at both pore and cytoplasmic gates, resulting in channel opening[33]. Heating could result in similar conformational changes, but a definitive test of this hypothesis has not yet been reported.

The ARD (Fig 18A, purple) is connected to the TM domain (Fig 18A, cyan) by a highly conserved 60 amino acid helix-loop-helix (HLH) linker (Fig 18A, blue) that forms a V-shaped cradle at the membrane-

cytosol interface; the HLH linker is surrounded by the pre-S1 helix and TRP helix in both TRPV1 and TRPV2 cryo-EM structures[1,29] and the TRPV6 X-ray structure[5]. The pre-S1 helix directly connects S1 to the ARD and the TRP helix (Fig 18A, 18B dark purple), which projects horizontally (i.e., parallel to the membrane inner leaflet) from the cytoplasmic C-terminal domain (CTD; Fig 18A, green) of S6 underneath the S1-S4 bundle[1,29]. Thus the HLH motif may transduce the movement of ARD to the transmembrane domain and channel gate[1,29]. Consistent with this hypothesis, a chimeric TRPV1-TRPV2 channel protein study indicated this region is crucial for thermal sensation in TRPV2, as swapping TRPV1 and TRPV2 cytosolic N-terminus can shift the thermal sensitivity between the two channels[34].

The TM domain comprised of S1-S6 helical segments contains the vestigial S1-S4 voltage sensor domain and pore (S5-S6) domains that are structurally homologous to voltage-gated K^+ channels (Kv). The selectivity filter regions in TRPV1 and TRPV2 contain a highly conserved Gly-Met-Gly-Asp/Glu motif that is similar to the Gly-Tyr-Gly-Asp in K^+ channel selectivity filter structures[1,29]. Pore architectures in TRPV1 and TRPV2 differ slightly from one another, but the reasons remain unknown[1]. One possibility is that differences in the purification methods used for TRPV1 and TRPV2 account for structural differences. TRPV1 was purified in A8–35 amphipol while TRPV2 was purified using the maltose neopentyl glycol (MNG) class of detergents[1,4]. Furthermore, some TRPV1 channel structures are stabilized by an activating spider toxin (DkTx) or truncation of the extracellular S5 'turret' region[29,35]. A prediction, based on molecular dynamics simulation, is that the presence of the turret region would change the pore architecture in TRPV1[36]. The analogous turret region is present in TRPV2 cryo-EM expression constructs, but its structure is poorly resolved in the structures, suggesting that this region is highly dynamic[1].

The conserved TRP helix is connected to the C-terminal end of S6 and, as mentioned previously, extends perpendicular to the S1-S4 helices to interact with the HLH linker domain via the pre-S1 helix, potentially allowing allosteric communication between the transmembrane and the cytoplasmic regions of TRPV1 and TRPV2 channels[1,29]. Studies in TRPV1 show that the TRP helix is likely to directly participate in PI (4,5)P_2 binding site and to regulate desensitization of capsaicin- and heat-activated TRPV1 channel activity[28,37].

Interestingly, the C-terminal end of the TRP helix in TRPV2 forms a hook-like structure (Fig. 18A, green) that is absent from TRPV1 structures. The hook contains a series of ionizable amino acids and one Cys that may be exposed, but the functional significance of this hook structure is unknown. At the C-terminal end of the hook, the remaining CTD sequence forms an extended loop that forms part of the inter-subunit interface together with the ARD (see Fig. 21)[1,29]. The CTD forms a single β-strand that contains C704/C748 (TRPV2/TRPV1) and is located adjacent to the N-terminal 'finger' formed by the ARD (Fig. 21); this β-strand is also close to the N-terminal helix of the proximal membrane linker domain and pre-S1 helix[1,29].

Recent studies have shown that the CTD is crucial for inter-subunit interactions in TRPV channels. For example, Ogawa, et al. (2016) show that in rTRPV1, C258 (C219 in rTRPV2) and C742 (C704 in rTRPV2) form an intracellular disulfide bond under oxidizing conditions, and that C258S or C742S mutations prevent the formation of the covalently-linked tetramer[38]. However, the atomic distances between sulphur atoms in C258 and C742 (> 8 Å) appear to be too large to readily allow for inter-subunit disulfide bond formation far away from their putative partners in participating in a disulfide bond (Fig. 21). Relatively subtle changes in the local structures near C258 and C742 could enable inter-subunit interactions to influence channel gating[29,38], but the hypothesis that inter-subunit disulfide bonds influence TRPV1 gating has not been directly tested. Given the similarity between TRPV1 and TRPV2 ARD structures, we hypothesize that similar interactions could also occur in TRPV2. However, TRPV2 contains two Cys residues (C206 and C334) at the inter-subunit interface that are not present in TRPV1; C219 and C704 in TRPV2 are equivalent to C258 and C748 in TRPV1, respectively (Fig. 21). Thus the number of possible disulfide bonds that could be formed in this region is larger in TRPV2, and intra- as well as inter-subunit bonds are each possible. No studies have investigated the roles of Cys residues at the inter-subunit interface on TRPV2 channel function.

In summary, TRPV1 and TRPV2 cryo-EM structures are highly similar, suggesting that the structural basis of gating are also likely to be shared. Movement of ARD domains in adjacent subunits are thought to underlie temperature-dependent gating in TRPV1, and ARD interactions could also be important for transducing other types of gating stimuli. Both N- and C-terminal residues contribute to the proposed ARD

interaction motif, and the proximity of this structure to the TM domain and TRP helix is consistent with the hypothesis that ARD motions function to control pore opening at the cytoplasmic gate. Differences between TRPV1 and TRPV2 structures (i.e., hook structure at the C-terminal end of the TRP helix) could be responsible for subtle but important differences in TRPV1 vs. TRPV2 gating. Finally, although the structure of TRPV6 solved by X-ray crystallography[5,6] exhibits remarkable overall similarity to TRPV1 and TRPV2 cryo-EM structures, ambiguity about the organization of subunits in TRPV6 complicates a direct comparison of the ARD-TM interface. Future studies are needed to ascertain the relationship(s) between channel structure and function in constitutively active (TRPV5 and TRPV6) vs. polymodal stimulus-dependent (TRPV1-4) channels.

3. TRPV channel pharmacology

Synthetic and plant-derived small organic molecules are known to activate, block, or antagonize TRPV1-3 channels. In some cases, ligands (i.e., capsaicin) are selective for one channel isoform or species orthologue; other agents (i.e., 2-APB) act similarly to agonize TRPV1-3 but antagonize other TRP channels; and some ligands (i.e., ruthenium red; RuR) universally modulate most or all TRP channels [22,39,40]. Selective ligands have been useful for identifying TRP channels and dissecting their physiological roles. For example, TRPV1 is potently activated by the plant-derived vanilloid compound capsaicin, and this activity was instrumental in the initial identification and cloning of TRPV1 from mRNA in dorsal root ganglion neurons[11,22]. Capsaicin also functions as a neurotoxin that can be used to selectively ablate TRPV1-expressing cells during development[41]. In contrast, TRPV2 and TRPV3 are essentially capsaicin-insensitive[3,8,42]. However, limited mutagenesis was used to show that TRPV2 can become vanilloid-sensitive, suggesting that the binding pockets are conserved and functional differences are attributable to specific interactions between drug molecules and protein side chains[43].

Phytocannabinoids, including Δ^9-tetrahydrocannoiabinol (THC) and cannabidiol (CBD), which are psychoactive and non-psychoactive compounds, respectively, isolated from the marijuana plant, act as agonists of TRPV1 and TRPV2 with similar (micromolar) potency[44]. Although the cannabinoid binding site is not known, studies suggest that it may be least partly overlap with the vanilloid binding site. The putative $PI(4,5)P_2$ binding site also partially overlaps with the vanilloid binding site in TRPV1, suggesting a common mechanism of gating modulation by phosphoinositides[45]. Although $PI(4,5)P_2$ is reported to negatively affect channel open probability (P_O) in both TRPV1 and TRPV3[46-48], contrasting reports suggest that TRPV1 and TRPV2 may also be positively gated by $PI(4,5)P_2$ and other phosphoinositide [18,49,50], and the existence of additional interaction sites in TRP channel has not been ruled out.

TRPV1-3 are also commonly activated by 2-APB, which functions as an antagonist at other ion channel targets[27]. Membrane depolarization, 2-APB, heating, and $PI(4,5)P_2$ appear to cooperatively gate TRPV1 and TRPV3 channels, suggesting that these disparate stimuli impinge on a common downstream gate[3]. Voets, et al. and Brauchi, et al. proposed allosteric gating schemes to explain cooperative gating by diverse stimuli[51,52]. The reason(s) why TRPV2 appears to exhibit different sensitivities to voltage, heating, and $PI(4,5)P_2$ remain to be determined. Interestingly, 2-APB potency is ~10-fold lower in human vs rat TRPV2, and residues in the ARD appear to be responsible for this difference[32]. This suggests that 2-APB could directly interact with residues that are near the putative ARD interaction motif (i.e., close to C748 in TRPV1) described earlier[32]. However, the existence of additional 2-APB binding sites in TRPV1-3 has not been ruled out. Ruthenium red serves as a voltage-dependent pore blocker in a number of TRP channels and exerts its effect by binding voltage-dependently in the selectivity filter region of the TRPV4 pore domain[8]. Consistent with this hypothesis, extracellular RuR rapidly and potently blocks inward currents in many TRP channels, but outward currents block is less robust (see Figs. 4, 5).

Although TRPV2 pharmacology is less well characterized than TRPV1, two synthetic compounds are reported to selectively modulate TRPV2. Probenecid (PBC), a blocker of organic cation transport, selectively activates TRPV2 (EC_{50} = 32 μM), as measured by calcium imaging[47]. Neither the molecular

determinants of the putative PBC binding site nor the drug's mechanism of action at TRPV2 has been reported. TRPV2 is also reported to be selectively antagonized by anti-allergic medicine tranilast (Rizuben)[46,53-55]. Together with commonly used TRPV channel agonist 2-APB and CBD, synthetic compounds provide a limited but useful tool for identification of TRPV2 channel current.

4. The physiological role of TRPV2

The physiological roles of TRPV2 are not well established, but the severe phenotype (which includes a high incidence of perinatal lethality) in a constitutive, global TRPV2-null transgenic mouse line argues that TRPV2 channels are likely to be necessary for a broad variety of essential physiological processes[56]. In contrast, knockout of TRPV1, TRPV3 or TRPV4 in mice does not lead to overt morphological defects or loss of viability[19,20,57-59]. Similar to TRPV1-4, TRPV2 channel is activated by heating, but the apparent thermal activation threshold for expressed TRPV2 (>52° C) is supra-physiological[8]. In contrast to TRPV1 knockout mice[20], TRPV2-null mice do not manifest behavioral deficits to thermal stimuli[56], indicating that TRPV2 is not responsible for heat sensation.

In contrast to other TRPV channels, TRPV2 is abundantly expressed in the immune system. TRPV2 mRNA is expressed in high amount compared to other TRPV channels in human blood lymphocytes[60]. Ca^{2+}-permeable ion channels of the Transient Receptor Potential (TRP) family are also reported to be expressed in both macrophages and microglia, where they may mediate Ca^{2+} entry and thereby modulate inflammatory activation. Both TRPV1, TRPV4 protein have been reported to present in microglia[61-63]. TRPV2 is reported to be present in macrophage[64-66], and recently in BV-2BV-2 microglia like-cells[67]. RNA interference (RNAi)-mediated knockdown of the TRPV2 or pharmacological block by ruthenium red (RuR) dramatically attenuates lipopolysaccharides (LPS)-induced interleukin 6 (IL-6) production and nuclear factor kappa-light-chain-enhancer of activated B cells (NF-κB) nuclear translocation in the macrophage-like RAW264 cell line[66]. As expected from the inhibition of NF-κB nuclear translocation, LPS induced transcription of pro-inflammatory cytokine tumor necrosis factor alpha (TNFα) and interleukin 1 beta

(IL1β) are attenuated in TRPV2 knockdown macrophage[66]. Targeted deletion of TRPV2 in mice causes a defect in peritoneal macrophage phagocytosis[64]. However, one contradicting result shows that the targeted deletion of TRPV2 in mice did not alter IL6 production[64]. The reasons for contradictory results are unknown, but the difference may potentially be compensation mechanisms in cytokine production. Finally, TRPV2 is associated with podosome formation in the macrophage. The addition of the chemokine formyl-Met-Leu-Phe (fMLP) peptide has been shown to cause translocation of TRPV2 from cytosol to podosome[65,68]. The translocation of TRPV2 to podosome is coupled by elevated basal calcium level in the cell[68]. Removal of extracellular Ca^{2+} abolishes the elevation of basal calcium level in macrophage, indicating calcium influx is the cause of elevated basal $[Ca^{2+}]_i$ [65,68]. Furthermore, knockdown of TRPV2 as well as the application of TRPV channel blocker ruthenium red (RuR), prevents the elevated basal $[Ca^{2+}]_i$ following fMLP peptide stimulation[65,68], indicating TRPV2 channel translocation and activation in podosome is needed to mediate fMLP induced Ca^{2+} influx and macrophage motility.

TRPV2 is also suggested to be functionally expressed in other leukocyte cell lines, including RBL-2H3[69] and Jurkat[70] cells. Leukocytes also express a variety of other TRP channels that can be discriminated based on pharmacological criteria[39]. Endocannabinoids[44] and lysophosphatidylcholine (LPC)[71,72], which activate both TRPV1 and TRPV2 channels. Both TRPV1 and TRPV2 channels are reported to be expressed in BV-2BV-2 cells[67], which are widely used as a cell culture model for microglia[73]. However, it is not known whether TRPV2 is expressed in primary microglia cells. Whether TRPV3 is expressed in BV-2BV-2 microglia is not known. Although TRPV1 and TRPV2 are thermosensitive, the apparent threshold for temperature-dependent gating of expressed TRPV2 channels (~52˚ C) is well above the physiological range[8]. In contrast, studies indicate that TRPV2 is an important mediator of immune cell function. Despite knockdown and knockout studies indicate the importance of TRPV2 in macrophage phagocytosis[64], LPS induced NF-κB nuclear translocation[66], cytokine production[66], and chemotaxis[65,68]; the mechanism of TRPV2 activation in immune cells remains poorly understood.

5. TRPV channels in microglia

Microglia are innate immune cells of the central nervous system (CNS). Microglia are phagocytes derived from a common myeloid lineage as monocytes, neutrophils, and osteoclasts[74]. They comprise approximately 12% of cells in the mammalian brain[75]. Microglia in the brain is thought to exist in a 'resting' state under normal physiological conditions[76,77]. Resting microglia are characterized by a small cell body with highly ramified processes, dynamically extending and contracting for continuous surveillance of the surrounding environment[77]. Microglia is readily activated by traumatic injury or immunological stimuli[77,78]; once activated, microglia can mediate both beneficial and detrimental functions[75,79,80].

Microglia, by design, is capable of recognizing and responding to diverse stimuli. Factors known to activate microglia include molecules of infectious agents, damaged neuronal cells, environmental toxins, cytokines, chemokines, and heavy metals[76,78,81-84]. Despite the wide variety of the potential stimuli common factors can be found to modulate microglia activation. One common signaling molecule is hydrogen peroxide (H_2O_2)[75]. Microglia, macrophages and other phagocytic leukocytes produce reactive oxygen species (ROS) including superoxide ($O_2^{-}\cdot$) after exposure to pro-inflammatory stimuli, including bacterial peptides (i.e., fMLP) and the endotoxin lipopolysaccharide (LPS)[76]. $O_2^{-}\cdot$ is readily converted to membrane-permeable H_2O_2 [85], and H_2O_2 is suggested to alter the function of TRPV1, TRPV4[86], TRPM2[87,88] and TRPA1 [89-91]. Autocrine or paracrine signaling by H_2O_2 and other ROS positively modulates inflammatory activation of leukocytes. In the CNS, ROS-dependent reactive microgliosis appears to contribute to neurotoxicity associated with environmental toxicants, ischemic damage following stroke, neurodegenerative diseases, and age-related cognitive impairment[75,76]. Ca^{2+} influx through TRP channels has not been directly linked to leukocyte pathophysiology, but redox modulation of TRP channel gating nonetheless represents a compelling mechanistic hypothesis that has not previously been tested.

A rise in the concentration of $[Ca^{2+}]_i$ is required for inflammatory activation of phagocytic leukocytes such as macrophages and microglia[85,92,93]. For example, chelation of $[Ca^{2+}]_i$ by incubation of macrophages with BAPTA-AM reduces lipopolysaccharide (LPS)-dependent cytokine and nitric oxide production[85]. Other

markers of inflammatory activation in macrophages, including nuclear translocation of NF-κB, production of cytokines such as TNFα, and NLRP-3 inflammasome formation also require elevated $[Ca^{2+}]_i$ [92-95]. Since nuclear translocation of NF-κB is required for transcription of pro-inflammatory genes, and NLRP-3 inflammasome is required for the production of the mature form of IL-1β in macrophage and microglia, the ion channels regulating the basal $[Ca^{2+}]_i$ can play a significant role in regulating macrophage and microglia activation. As demonstrated by Nagasawa et al, TRPV2 channels may mediate the Ca^{2+} influx from the extracellular fluid into macrophages, and perhaps it is not surprising that knockdown of TRPV2 attenuates LPS induced nuclear translocation of NF-κB and cytokine production in macrophages[66].

Here we hypothesize that similar to the related TRPV1 and TRPV3, TRPV2 channels are also regulated by H_2O_2 and mediate calcium influx in microglia like cells. In this thesis, we examine both previously unknown TRPV2 channel gating characteristics and enhanced activation of TRPV2 by pro-inflammatory stimuli such as LPS and H_2O_2. Specifically, we demonstrate that 1. TRPV2 have similar single channel properties compared to TRPV1; 2. TRPV2 single channel properties can be modulated by pharmacological reagents; 3. TRPV2 are functionally expressed in both BV-2BV-2 and primary mouse brain microglia; 4. Application of exogenous H_2O_2 is sufficient to potentiate the agonist-dependent activity of expressed TRPV2 channels; 5. Acute treatment of microglia with LPS is sufficient to positively modulate the gating of endogenous TRPV2 currents. Our results suggest that endogenously produced ROS in macrophages and microglia is likely to augment Ca^{2+} influx through TRPV2 channels and thereby exacerbate pro-inflammatory leukocyte activation.

Chapter II. Method

1. Cell culture

Human embryonic kidney 293 (HEK-293) cells and murine BV-2 microglia-like cells (BV-2, a generous gift from Dr. Michelle Block; Stark Neurosciences Research Institute, Indiana University School of Medicine, Indianapolis, IN) are cultured in Dulbecco's modified eagle's medium (DMEM) media with 10% fetal bovine serum (FBS) and 1% penicillin and streptomycin (P/S) solution. Culture enriched in neonatal mouse microglia (a generous gift from Dr. Michelle Block; Stark Neurosciences Research Institute, Indiana University School of Medicine, IL and Dr. Pamela Knapp; Department of Anatomy and Neurobiology, Virginia Commonwealth University, VA) are cultured in DMEM media with 2% FBS and 1% P/S solution. The cells are maintained at 37°C under 5% carbon dioxide (CO_2) environment until the experiment.

Prior to the experiment, enhanced green fluorescent protein (EGFP)-tagged rat-TRPV1 (rTRPV1), rat-TRPV2 (rTRPV2) or human-TRPV3 (hTRPV3) channels cloned into the pEGFP-C1 vector (Clontech) are transfected into HEK-293 cells with Lipofectamine 2000 reagent (Invitrogen) following manufacture's protocol. Briefly, 0.5µg of plasmid DNA is mixed with Lipofectamine 2000 in Opti-MEM (Gibco) solution. Plasmid DNA is allowed to mix with Lipofectamine 2000 at room temperature for 30 minutes, and then DNA-Lipofectamine solution is applied to HEK-293 cells. HEK-293 cells are cultured at 37°C with 5% CO_2 for at least 8 hours to ensure successful transfection. Transfected HEK-293 cells are incubated at 37°C for at least 24 hours prior to the experiment.

BV-2 cells and neonatal murine primary microglia enriched cultures are incubated with either treatment media (DMED media with 2% FBS and 1% P/S) or treatment media containing 2µg/ml in at 37°C for 20-30 minutes prior to experiments.

2. TRPV channel mutagenesis

Site-directed point mutations are introduced into TRPV channels by polymerase chain reaction (PCR), and then cloned into HEK-293 cells. The mutagenesis primer is designed by either SeqBuilder software (DNASTAR Lasergene 8) or Serial cloner software (Serial Basics) and synthesized by Integrated DNA Technologies, Inc. PCR reactions are prepared by mixing 25μl of Phusion® High-Fidelity DNA Polymerase (New England Biolab, Inc.), with 100ng DNA, 300ng forward and reverse primers, 4μl Dimethyl sulfoxide (DMSO) and 17μl distilled water. The cyclic parameters of PCR are 98°C for 1 minute followed by 20 cycles of 98°C for 1 minute, 50°C for 1 minute, and 72°C for 5 minutes. Methylated DNA are removed from PCR products by DPN1 digestion, 37°C for 1 hour. PCR products are then transformed into XL10-Gold® Ultracompetent Cells (Stratagene) according to manufacturer's protocol. Briefly, XL-10 gold cells are defrosted on ice and mixed with 1μl Dimethyl sulfoxide (DMSO). PCR products are then added to XL10 gold cells and incubated on ice for 30 minutes. XL-10 gold cells are then subjected to 42°C heat shock of either 30 or 45 seconds and incubated in 200ml super optimal broth with catabolite repression (SOC) medium in 37°C for 1 hours. Transformed E.coli are then selected on Luria broth (LB) agar plate with 30μg/ml kanamycin incubated for at least 24 hours in 37°C. Surviving colonies are selected and cultured in LB broth with 30μg/ml kanamycin are incubated for at least 24 hours at 37°C. Finally, plasmid DNAs are isolated using QIAprep Spin Miniprep Kit (Qiagen).

3. Preparation of TRPV agonists and antagonists

Table 1 Agonist and antagonist of TRP channels.

Compound name	Abbreviation	Functions	Solvent
2-Aminoethoxydiphenyl borate	2-APB	TRPV1-3 agonist	DMSO
Allyl isothiocyanate	AITC	TRPA1 agonist	DMSO
Capsaicin	CAP	TRPV1 agonist	DMSO
Cannabidiol	CBD	TRPV1, V2 agonist	Methanol
Hydrogen peroxide	H2O2	ROS	H_2O
Probenecid	PBC	TRPV2 agonist	DMSO
Capsazepine	CZP	TRPV1 antagonist	DMSO
4-[(2-Butyl-6,7-dichloro-2-cyclopentyl-2,3-dihydro-1-oxo-1H-inden-5-yl)oxy]butanoic acid	DCPIB	Swell activated Cl channel antagonist	DMSO
Ruthenium Red	RuR	Ca channel blocker	H_2O
Tranilast	Tra	TRPV2 antagonist	DMSO

Compound name and their abbreviation are listed with their targeted TRP channel and solvent used to create stock solutions. All compounds are diluted by bath solution and applied by bath superfusion or pipetting.

The compounds used for electrophysiology are listed above. 2-APB (Cayman chemical) is prepared in dimethyl sulfoxide (DMSO; Fisher Scientific) as concentrated stock, and diluted and applied to cells by bath superfusion as non-selective TRPV channel agonist. AITC (Sigma), CAP and PBC (Cayman chemical) are prepared in DMSO as concentrated stock, and then diluted and applied to the cells by bath solution superfusion as a TRPA1, TRPV1, and TRPV2 selective agonist respectively. CBD (Cerillant) is prepared in methanol (EMD Millipore Biochemicals) as concentrated stock and diluted and applied to the cell by pipetting as a TRPV2 agonist. H_2O_2 (EMD Millipore Biochemicals) is prepared in HyClone HyPure Molecular Biology Grade Water (Thermo Scientific) and applied to the cell by pipetting to enhance TRPV2 current. CZP (Cayman chemical), DCPIB (generous gift from Dr. Clive Baumgarten, Department of Physiology and Biophysics, Virginia Commonwealth University, VA) and Tranilast (Toics Bioscience) are prepared in DMSO as concentrated stock, and then diluted and applied to cell by bath superfusion as TRPV1,

swell activated chloride channel ($I_{Cl,swell}$) and TRPV2 antagonist respectively. Finally, RuR (Cayman chemical) is prepared in HyClone HyPure Molecular Biology Grade Water as concentrated stock, and then diluted and applied to the cell by bath superfusion or pipetting to block TRP channels.

4. Immunocytochemistry

Non-treated HEK-293 cells, EGFP-tagged-rTRPV2-transfected HEK-293 cells, EGFP-tagged-hTRPV3-treansfected HEK-293 cells, BV-2 cells or dissociated neonatal mice primary microglia cells are plated onto glass coverslips. Cells on coverslips are then washed with ice-cold Phosphate-buffered saline (PBS), and then fixed by incubating in 4% paraformaldehyde containing PBS (American bioanalytical) solution for 30 minutes to 1 hour. Fixed cells are permeabilized by 0.1% Triton X-100 (Sigma) for 1hour, and blocked with 1% bovine serum albumin (BSA) containing PBS solution for 1 hour. Following permeabilization, serial exposure to rabbit anti-TRPV2 (1:1000 dilution, Oncogene), rabbit anti-TRPV3 antibody (1:1000 dilution, custom antiserum, the gift of Dr. David E. Clapham, HHMI, Children's Hospital Boston) or mouse anti-TRPA1 antibody (1:1000 dilution; Alomone Labs) at 4°C overnight. After overnight incubation cells are subjected to incubation with Alexa fluoro647 secondary antibody (1:1000 dilution, Cell Signaling Technology) for 1 hour at room temperature. Fluoregel with tris buffer (Electron Microscopy Science) is applied to preserve immunofluorescence. Images are captured by confocal laser scanning microscopy (Olympus LSM710, VCU Department of Anatomy and Neurobiology Microscopy Facility, supported in part by funding from NIH-NINDS Center core grant 5P30NSD47463). The images are captured and processed by ZEN software (Carl Zeiss). The fluorescence intensity was normalized to positive control (EGFP-tagged-rTRPV2 or EGFP-tagged-hTRPV3-transfected HEK-293 cells).

5. Western blotting

HEK-293 cells transfected with rTRPV2 or hTRPV3 and BV-2 microglia like-cells are grown in a 10cm petri-dish until reaching approximately 90% confluency. Cells are collected by scraping in cold PBS. BV-2 cells are lysed in 1% Triton X solution with complete mini protease inhibitor (Roche Diagnostics) in PBS, and protein is collected from the supernatant of whole cell lysate after spinning 15,000xg for 10 minutes. Protein concentration is measured by Pierce BCA protein standard assay (Thermo Scientific) according to the manufacturer's protocol. Then proteins are denatured by heat and 2-Mercaptoethanol (BME; MP Biomedicals). Proteins are separated by size by SDS-PAGE using Mini-PROTEAN Tetra System (Biorad) for 100 to 120 V for 1 to 2 hours. Separated proteins were transferred onto PVDF transfer membrane (Thermo Scientific) using Pierce fast semidry blotter (Thermo Scientific) for 15V for 1 hours. PVDF transfer membrane is exposed to rabbit anti-TRPV2 (1:1000 dilution Oncogene), rabbit anti-TRPV3 (1:1000; dilution custom antiserum, gift of Dr. David E. Clapham, HHMI, Children's Hospital Boston), mouse anti-TRPA1 (1:1000 dilution; Alomone Labs) or mouse anti-βactin (1:1000 dilution, Chemicon) described above in 4°C overnight. HRP-conjugated goat anti-mouse or HRP conjugated goat-anti-rabbit antibody (1: 1000; Pirce) is applied for 1 hour at room temperature on the following day. Finally, PVDF transfer membrane is developed by Supersignal West Pico reagent (Thermo Scientific) and developed on Blue Ultra Autorad Film (GeneMate).

6. Electrophysiological recording

HEK-293 cells expressing EGFP-tagged rTRPV1, EGFP-tagged rTRPV2, EGFP-tagged hTRPV3, BV-2 cells, or dissociated neonatal mouse primary microglia are plated onto glass coverslips and maintained at 37°C with 5% CO_2. Whole cell voltage clamp electrophysiology is performed in a bath solution containing approximately (in mM) 150 NaCl and 2 $MgCl_2$ 1 EGTA, 10 HEPES, pH 7.4. The pipette solution contains (in mM): 150 $CsMeSO_3$, 2 $MgCl_2$, 10 NaCl, 2 $CaCl_2$, 1 EGTA, 10 HEPES pH 7.4. Final [free $Ca^{2+}]_i$ is ~100 nM (estimated using Maxchelator, C. Patton, Stanford University). The osmolality of the bath and pipette

solutions is adjusted to 290-310 mmol/kg. Currents were elicited by repeated application of 1 s voltage ramps (-80 to +80 mV with 10 kHz sampling rate, repeated every 4 seconds) or voltage step (-80 to 120mV voltage step followed by -80mV voltage step, 10 kHz sampling rate). Currents are low-pass filtered at 5 kHz and digitized at 20 kHz. Single channel currents are measured by the excised inside-out patch clamp technique. Excised inside-out patches are pulled from cells into symmetrical bath and pipette solutions containing (in mM): 150 NaCl, 1 EGTA, 10 HEPES, pH 7.4. Osmolality is adjusted to 290-310mmlo/kg. Single-channel currents are measured during repeated voltage steps (1 or 2s duration at 15 kHz sampling rate, repeated every 5 seconds). Membrane voltage is stepped to +80mV and -80mV unless otherwise indicated. Currents were low-pass filtered at 2 kHz and digitized at 15 kHz. Data are captured by JustAcequire program and analyzed by Clampfit 10 software (Molecular devices).

7. Analysis of electrophysiological recordings

a. Whole cell recording analysis

The whole cell voltage clamp recording is processed and analyzed by Clampfit 10 software (Molecular devices) and Origin 6.0 (Origin Lab). In the voltage ramp and voltage step protocol, membrane currents are recorded in the form of current change over time (I-t plot). Raw data are presented as I-t curves where time (ms) is presented in the x-axis and current is presented in the y-axis (nA; see F4B, result). The ramp protocol consist of 50 or 300ms -80mV step to measure steady state -80mV step current, followed by voltage ramp consistently increase membrane potential from -80mV to +80mV in 1s to construct an current-voltage (I-V) curve, followed by a 100ms +80mV membrane step to measure steady state step +80mV current, and finally a 500ms -80mV membrane step to measure -80mV instantaneous tail current (I_{tail}; see F4A, result). The voltage ramp is repeated every 4 seconds. In the voltage step protocol, membrane potential is stepped to -60mV for 200ms, and then stepped to various membrane voltage for 500ms. Finally, membrane voltage is stepped to -80mV for 300ms to measure I_{tail} (see F36A, result section).

b. Construction of Current-Voltage relation curve (IV curve)

The -80 to 80mV ramp protocol is used to construct IV curve of TRPV channel. In the voltage ramp protocol, membrane potential is raised from -80mV to +80mV in 1 second. Hence the voltage (V) at any given time is time is expressed in following formula.

$$V = -80 + ((t - t0) \bullet 0.16)$$

Equation 1: Equation for time to voltage conversion

Voltage ramp over 1 seconds raised membrane potential from -80mV to +80mV. The membrane voltage at any given time is proportional to time (t) minus time of voltage ramp start (t0) multiple by 0.16 and minus 80.

After membrane voltage is determined, IV curves are constructed by plotting voltage (mV) in the x-axis and corresponding current (nA) in the y-axis.

c. Analysis of tail current

Instantaneous tail current is used to measure the apparent open probability of the channel. I_{tail} is determined by fitting tail current measured to exponential decay function shown below.

$$f(x) = f_0 e^{-t/\tau}$$

Equation 2: Exponential decay function

The exponential decay function is used to determine the instantaneous tail current (I_{tail}). Tail current at any given time denoted f(x) is calculated by multiplying $e^{-t/\tau}$ to tail current at the change of voltage (equals to instantaneous tail current, I_{tail}). e is Euler's number, t is the time of measurement and τ is the time constant of decay function.

I_{tail}-V curve is constructed by plotting I_{tail} (y-axis) across varying step voltage (x-axis), and then the I_{tail}-V curve is fitted to Boltzmann equation shown below.

$$I_{tail} = \frac{(I_{tail\ max}) - (I_{tail\ min})}{1 + e^{V - \frac{V_{0.5}}{dx}}} + I_{tail\ min}$$

Equation 3: Boltzmann equation

Boltzmann fit to I_{tail}-V relations is used to describe voltage needed to achieve 50% of the maximum tail current ($V_{0.5}$) and slope factor (dx). $I_{tail\ max}$ is the largest instantaneous tail current measured and $I_{tail\ min}$ is the smallest instantaneous tail current measured. V denote step voltage and e is Euler's number.

d. Single channel recording analysis

Single channel recording is processed and analyzed by Clampfit 10 software (Molecular devices) and Origin 6.0 (Origin Lab). For samples with large noise, inside-out patch clamp data were subjected to offline digital low-pass filtering (500 Hz) for analysis and presentation. Subsequently, the leak current is subtracted by subtracting the average of 10-20 seconds of the control current from all recorded currents. In experiments where leak current is changing, further leak subtraction is performed manually. Once current are normalized to control, the data are presented as in form of i-t curve where time is plotted in the x-axis and current response plotted in the y-axis. In addition to the i-t plot, following analysis are performed using normalized single channel recording.

e. Construction of all point histogram and unitary conductance measurement

The all point histogram are used to summarize the channel activity and measures the unitary current of TRPV channels. Raw current recording across 18 seconds (unless otherwise indicated) are summarized into all point histogram with the x-axis plots current and the y-axis plots the event count. The histogram is then fitted by multiple Gaussian curves shown below.

$$y = y_0 + \frac{A}{w\sqrt{\pi/2}} e^{-\frac{(x-xc)^2}{w^2}}$$

Equation 4: Gaussian equation

Gaussian fit to all point histogram is used to describe numbers of open channel event (y) at any given current (x). y_0 is the base of the Gaussian curve, A is the area under the Gaussian curve, w is the width of the Gaussian curve, xc describe the center of the Gaussian curve, π is circle constant and e is Euler's number. The unitary current (i) is described by xc of open channel peaks.

The histogram is normalized to close channel by subtracting center of the Gaussian curve of the closed channel (xc closed) from all Gaussian fits, making the center of xc closed always equal zero. The center of the Gaussian curve of open channel (xc open) is measured to determine unitary current of the TRPV channels. In order to compare the unitary current between different voltage steps, unitary conductance is calculated as follow.

$$i = \gamma \cdot (V_M - E_{REV})$$

Equation 5: Equation for unitary conductance

Unitary current (i) is proportional to unitary conductance (γ) by the driving force, which depends on membrane potential (V_M) and the 'reversal' potential (E_{REV}) of current flowing through the open channel. The symmetrical solution is used to measure single channel activity and E_{REV} is expected to be 0.

f. Single channel event detection

The current measured in whole cell voltage clamp electrophysiology can be denoted as

$$I = N \cdot i \cdot P_O$$

Equation 6: Whole cell current

Whole cell currents (I) is proportional to the product of the number of functional channels in the cell membrane (N), the amplitude of unitary current (i), and P_O.

To better understand TRPV2 channel gating properties, it is important to measure both *i* and PO. The channel open probability (P_O) are detected using single channel search function (Clampfit 10, Molecular Devices) after the unitary current is determined by the Gaussian fit of all point histogram (see above). The single channel search function measures the fraction of time TRPV channels spends in open channel stated

compared to the time TRPV channel spend in closed channel states. First, a baseline for the level of current associated with the closed-channel state is manually defined. Next, events corresponding to channel openings of discrete, pre-defined amplitude (i.e., at +80 mV, $i \approx 6$ pA for TRPV1, $i \approx 6$ pA for TRPV2 and $i \approx 10$ pA for TRPV3; see Results) are automatically detected and counted. The investigator can manually include or exclude ambiguous events in the event count, and currents within ~10% of the expected amplitude are accepted as normal variability. To measure events associated with fully open channels, only channel openings lasting more than 0.1 ms are included in the event-based analysis. The single channel search in Clampfit 10 reports statistics associated with events detected in each recording, including mean open and closed times, average single channel amplitude, and the product of $N \cdot PO$ (NPo).

8. Statistical analysis

Statistical analysis is conducted by Origin 6.0 software or online statistical computation tools such as Verssarstat (www.verssarstat.net), or Graphpad website (http://www.graphpad.com).

Three statistical methods are used. The student t-test is used to compare two independent groups. Paired student t-test are used for statistical analysis of measurements between same cells. One-way ANOVA followed by Tukey's honest significance test are used for statistical analysis between more than three groups. Statistical significance is reached if the difference between groups reaches greater than 95% confidence interval. Results are presented in the form of mean ± standard error of the mean (SEM) unless otherwise noted.

Chapter III. Results

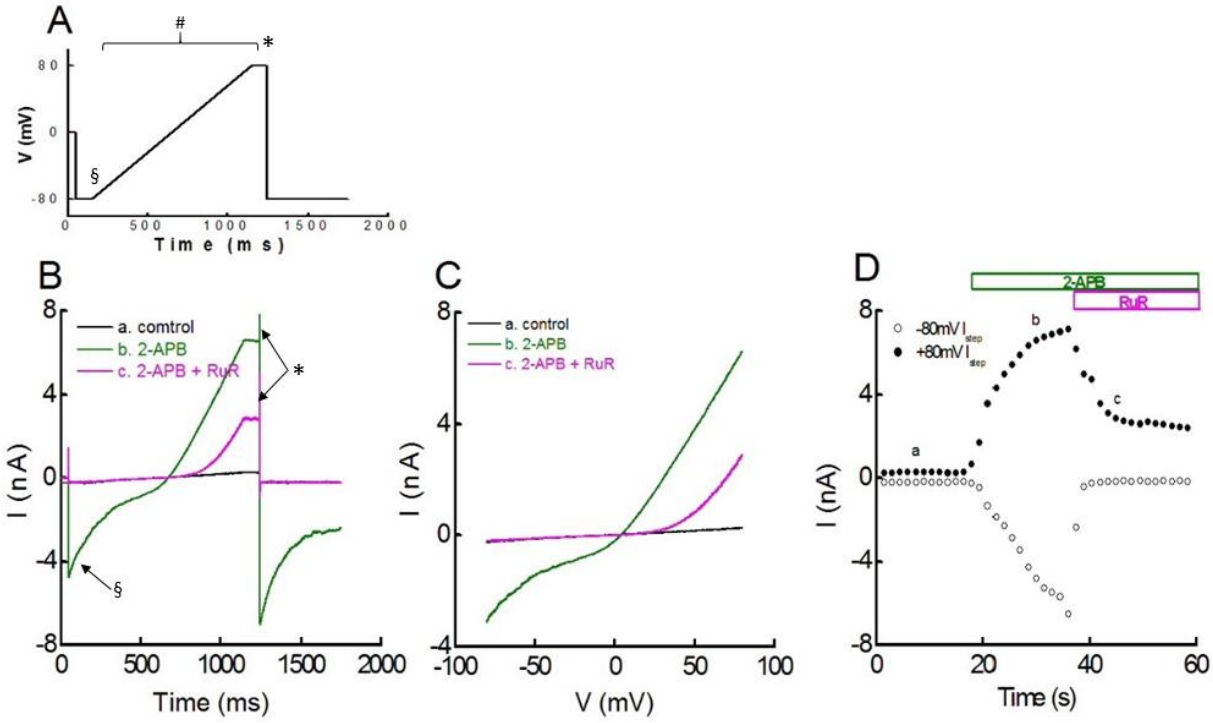

Figure 1: TRPV2 channels are activated by 2-APB and blocked by RuR.

A representative HEK-293 cell expressing EGFP-rTRPV2 is voltage clamped in the whole-cell mode and currents were elicited by voltage ramps (**A**) from -80 mV to +80 mV (1s duration, 0.25Hz). **B.** Currents elicited by the voltage protocol shown in **A** are measured in the absence (a. control, black line) or presence of 500 µM 2-APB (b., green line) or 500 µM 2-APB + 10 µM ruthenium red (RuR; c., magenta line). Letters refer to the time at which currents were measured (see panel **D**). Note that a prominent 'tail' current (§) is measured at -80 mV only in the presence of 2-APB. **C.** I-V relations determined during the linear portion of the voltage ramp protocol (indicated by # in panel **A**) are measured in the absence and presence of 2-APB and RuR (data from panel **B**) and plotted in function of membrane potential. **D.** Steady-state current (*; I_{step}, +80mV) and instantaneous tail current (§; I_{tail}, -80mV) elicited by voltage steps at the times indicated in panel **B** are measured over the duration of the experiment and plotted in function of time. Note that the time course of current activation by 2-APB is relatively slow, but appears to reach a steady-state after ~20 s, whereas RuR block of inward current is rapid. Letters indicate times at which the currents shown in panels **B** and C were measured: a., control; b., 2-APB; c., 2-APB + RuR.

1. Pharmacological property of the TRPV2 channel

TRP channels are characterized by their 'polymodal' sensitivity to multiple different stimuli[7,22]. TRPV2 is activated by heat, membrane depolarization, and organic compounds such as 2-APB[27,96], PBC[47], and

phytocannabinoids, including Δ^9-THC[44] and CBD[44,97]. To study gating properties of TRPV2, we use a combination of membrane depolarization and pharmacological stimulation. HEK-293 cells were transiently transfected with cDNA encoding an enhanced green fluorescent protein (EGFP)-rat TRPV2 (GFP-rTRPV2) fusion protein (Method 1) and subjected to whole cell voltage clamp (Method 6). A voltage ramp protocol from -80 mV to +80 mV (1 s duration) is repeatedly (20 kHz) delivered to the cell in the absence and presence of pharmacological agents applied by bath superfusion (Fig. 1A). A small background current is observed under control conditions (Fig. 1B, black line). As expected from previous studies[27,96] superfusion with the non-selective TRPV channel agonist 2-APB elicits a robust TRPV2 current (Fig. 1B, green line) that is voltage-dependently blocked by co-application of RuR together with 2-APB (Fig. 1B, magenta line). 2-APB is reported to activate rat TRPV2 (EC_{50} = ~130 μM) but not able to activate human TRPV2[32,96], and the large current observed in our studies is consistent with the hypothesis that rTRPV2 open probability (PO) is high under our experimental conditions. 2-APB activation of TRPV1-3 is also characterized by strong positive cooperativity, which is manifested as a steep Hill slope[27,43], and we also observe that a slightly lower concentration of 2-APB (100 μM) elicits small or undetectable TRPV2 currents (data not shown).

Voltage-dependent activation of rTRPV2 is fast, so currents elicited by slow voltage ramps can be used to generate quasi-steady-state current-voltage (I-V) relations (Fig. 1C). The amplitude of 2-APB activated currents in cells expressing TRPV1-3 varies with stimulus strength (i.e., agonist concentration, duration of agonist exposure and membrane potential)[25,98-100]. In the representative cell expressing rTRPV2 shown in Figure 4, 2-APB (500μM) elicits an I-V relation that exhibits weak outward rectification (Fig. 1C). Large 'tail' currents (measured at -80 mV instantaneously following the voltage steps to either 0 mV or +80 mV;

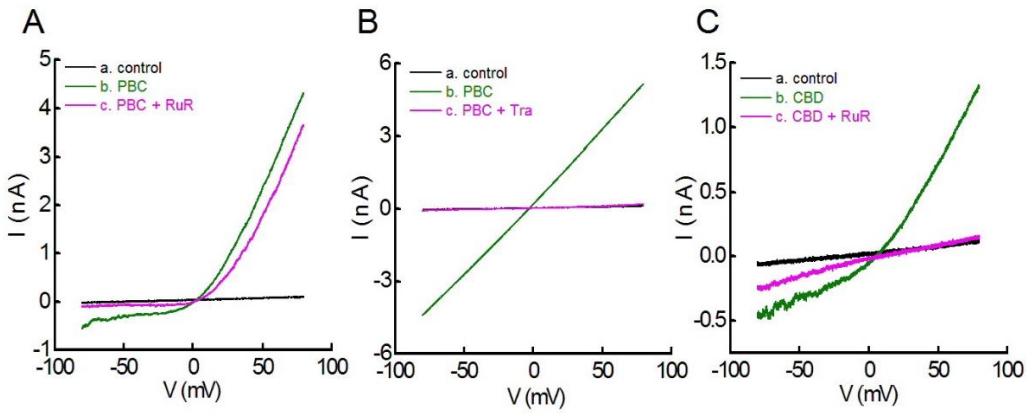

Figure 2: TRPV2 currents are activated by probenecid (PBC) and cannabidiol (CBD) and inhibited by tranilast.

Currents elicited by voltage ramps (see Fig. 1) are measured in a representative HEK-293 cell expressing EGFP-rTRPV2 and superfused with the indicated drugs. **A.** PBC (4 mM) induces an outwardly-rectifying current (green line) that is voltage-dependently blocked by co-application of RuR (10 μM) and PBC (magenta line). **B.** PBC (4 mM) induces a current with a linear I-V relation (green line) that is blocked by co-application of 1 μM Tranilast (magenta line). **C.** CBD (300 μM) induces an outwardly-rectifying current (green line) that is inhibited by 10μM RuR (magenta line). In **A**-**C**, black lines indicate current measured in the presence of vehicle alone (control).

Fig. 1B) are consistent with previous reports demonstrating depolarization-dependent activation of TRP channels[27,51].[48,101] Instantaneous tail current (I_{tail}) is observed in the presence of 2-APB, but not under control conditions (Fig. 1B), indicating that voltage-dependent gating is enhanced in the presence of a TRPV2 agonist. I_{tail} elicited by the initial hyperpolarization to -80 mV indicates that some TRPV2 channels are open at 0 mV; the larger inward tail current measured at -80 mV after a depolarizing voltage ramp and step to +80 mV is consistent with previous studies showing that PO is voltage-dependent[8,27]. The shape of the rTRPV2 ramp I-V relation (Fig. 1C) is thus attributed to voltage-dependent gating rather than pore rectification.

RuR functions as a voltage-dependent pore blocker in a number of different TRP channels[27], but RuR also has activity at other targets, including I_{CRAC}/Orai channels and IP_3 receptors[39]. Here we show that RuR (10 μM) fully blocks both I_{tail} and inward currents elicited by voltage ramps when co-applied together with 2-APB (Fig 1C). Consistent with previous reports[27], we find that concentration of extracellularly applied RuR which is sufficient to block inward current does not completely block outward currents at a (Fig 1C). Our data are therefore consistent with the hypothesis that RuR functions as a pore blocker in TRPV2 rather than as a gating modifier or antagonist, and the mechanism of action of RuR is thus distinct from 2-APB and other gating-modifier agonists and antagonists. We explore this phenomenon again later (Fig. 2B).

Activation of TRPV channels by chemical agonists is slow relative to the rates of voltage-dependent channel opening. Here we show that, as in previous studies, activation of rTRPV2 by 2-APB is relatively slow: under our recording conditions, superfusion of 2-APB (500 μM) for ~20 s is necessary to achieve apparent steady-state (Fig 1D). In contrast, apparent steady-state is reached within 100 ms after depolarization of cells expressing native (Fig. 33) or expressed TRPV2 channels (data not shown). The apparent rate of pharmacological activation by extracellularly applied 2-APB may depend on perfusion speed and/or availability of the drug to its binding site(s), which has not been unambiguously identified. We find that RuR (10 μM), which potently blocks TRPV channels [27], rapidly blocks inward TRPV2 current, arguing that superfusion speed under our experimental conditions is substantially faster than the rate of 2-APB current activation. The slow rate of TRPV2 current activation observed here and elsewhere is, therefore, consistent with the hypothesis that the 2-APB binding site is intracellular, and TRPV2 activation is temporally delayed by diffusion across the plasma membrane.

Among TRP channels, probenecid (PBC) is reported to selectively agonize TRPV2[47], however, PBC also acts at other molecular targets, including organic cation transporters. Here we show that superfusion of PBC (4 mM) elicits robust currents with an outwardly-rectifying I-V relation similar to 2-APB in cells expressing TRPV2 (Fig. 2A). Prolonged exposure to agonists such as 2-APB and PBC (4 mM) occasionally alters the shape of the I-V relation, which becomes linear after agonist superfusion (Fig. 2B). Our data

suggest that prolonged PBC exposure eliminates voltage-dependent gating in TRPV2. Previous reports showing that the duration of agonist exposure alters voltage-dependent gating in related TRPV1 and TRPV3 channels[25,98,99]. One possible explanation for the difference in current rectification is time dependent pore dilation, which has described for TRPV1 and TRPV3[25,98,99]. However, PI(4,5)P_2-dependence also appears to explain the conversion from voltage-dependent to voltage-independent gating in TRPV3[48]. One disadvantage to the use of PBC is its low potency, which could be a confounding factor in understanding its ability to modulate voltage-dependent gating. We have not explicitly tested whether ionic selectivity is altered in TRPV2 channels that exhibit voltage-dependent vs. voltage-dependent gating, and additional future experiments are therefore necessary to address the mechanism(s) by which agonists modulate TRPV channel gating and ion permeation.

As we observed previously when TRPV2 channels are activated by 2-APB, we find that RuR blocks a larger fraction of inward vs. outward PBC induced current (Fig 2A), indicating that the presumed mechanism of RuR action (voltage-dependent pore block) is likely to be similar. The anti-allergic drug tranilast (Rizuben) was previously reported to selectively inhibit TRPV2 channels[46,53], and here we show that tranilast (100 μM) completely antagonizes both inward and outward currents elicited by PBC (Fig. 2B). The data indicate that tranilast is likely to operate by a different mechanism from RuR, and we hypothesize that tranilast may act as a competitive antagonist rather than a pore blocker of TRPV2. Additional studies are needed to clarify the mechanism of tranilast action at TRPV2 and to identify amino acid residues that form the tranilast binding site.

Previous reports show that TRPV1-3 channels are non-selectively activated by both psychoactive (i.e., Δ^9-THC) and non-psychoactive (i.e., cannabidiol, CBD) phytocannabinoids in the micromolar concentration range[44,97]. Here we show here that TRPV2 is activated by CBD (300 μM), and that the outwardly-rectifying shape of the I-V relation is similar to short duration exposure of 2-APB or PBC (Fig. 2C). Although the cannabinoid binding site in TRPV is not known, mutagenesis and structural studies in TRPV1 and TRPV2 suggest that vanilloids (i.e., capsaicin and resiniferatoxin) share a common site that resides within the S1-

S4 ‘vestigial voltage sensor’ domain[43]. Because cannabinoids and vanilloids act as chemical agonists and are structurally similar, they may share common binding site, but additional studies are needed to specifically test this hypothesis. In summary, 2-APB, PBC, and CBD function as pharmacological activators (agonists) of TRPV2 that modulate voltage-dependent gating. Whereas 2-APB and CBD are non-selective TRPV1-3 agonists, PBC appears to be selective for TRPV2[47]. RuR behaves as voltage-dependent pore blocker and tranilast’s action is consistent with activity as a competitive antagonist[46,53-55]. These compounds establish a limited, but useful, pharmacopeia for selective activation and inhibition of TRPV2 channels.

2. TRPV2 channel is functionally expressed in microglia

TRPV2 channels are important in regulating phagocytes activities[64,66,68]. They are large conductance cation channels able to regulate calcium homeostasis in phagocytes[68]. Specifically, TRPV2 has been shown to regulate chemotaxis and cytokine production in macrophages[66,68]. However, TRPV channel functional expression in microglia is not well examined. To better understand TRP channel functional expression, immunocytochemistry and western blotting were used to determine TRP proteins, and whole cell voltage clamp is used to determine the presence of TRP current.

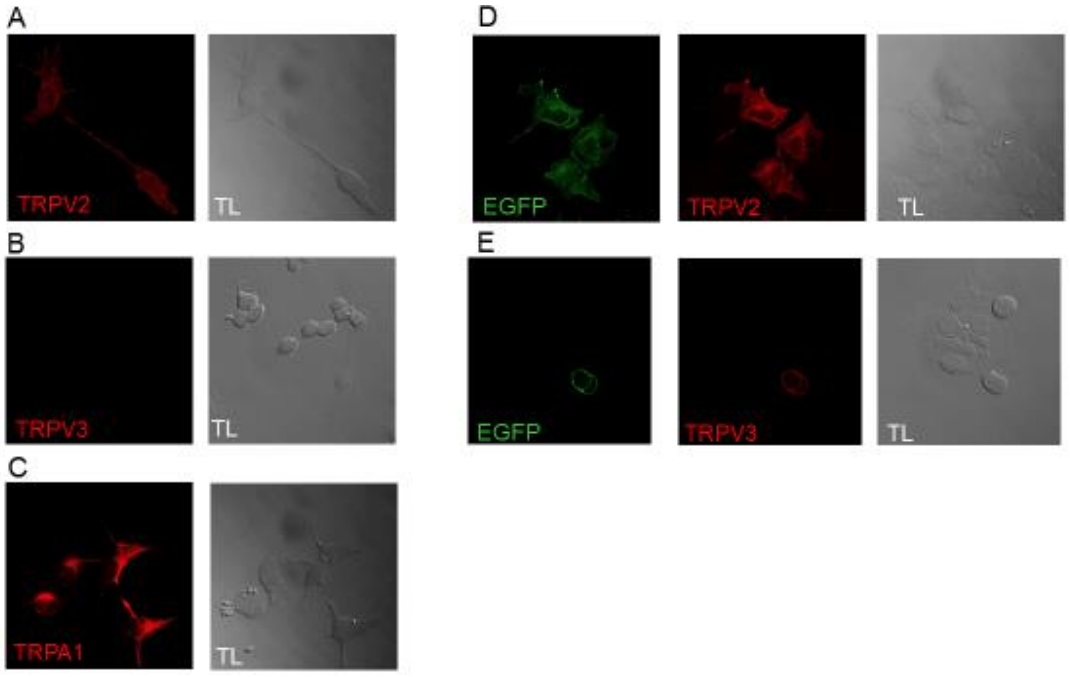

Figure 3: Immunocytochemical analysis of TRP channel in BV-2 microglia like cells.

BV-2 cells are fixed and incubated with **A.** rabbit-anti-mouse TRPV2 antibody (1:1000 dilution), **B.** rabbit-anti-human TRPV3 antibody (1:500 dilution), and **C.** mouse-anti-TRPA1 antibody (1:1000 dilution). Presence of TRPV2 (**A**) and TRPA1 channel proteins (**C**) are visualized by red immunofluorescence while TRPV3 channel protein is not detected (**B**). Positive control of TRPV2 and TRPV3 protein expression are prepared by transfecting **D.** EGFP tagged TRPV2 or **E.** EGFP tagged TRPV3 into HEK-293, and those cells are subjected to immunocytochemistry to rabbit-anti-mouse TRPV2 antibody (**D.** 1:1000 dilution) and rabbit-anti-human TRPV3 antibody (**E.** 1:500 dilution). The green fluorescence shows the presence of EGFP protein and successful transfection. The localization of EGFP is co-localized with red immunofluorescence indicating TRPV2 and TRPV3 antibody successfully recognizing transfected HEK-293 cells.

BV-2 cells are fixed, permeabilized, and then subjected to immunocytochemistry (see method 4). Expression of TRPV2 channel protein was confirmed by antibody recognition of TRPV2 protein in immunocytochemistry (Fig 3A. red immunofluorescence). On the other hand, TRPV3 channel proteins were not detected (Fig 3B). To examine whether hTRPV3 antibody are able to recognize TRPV3 protein, EGFP tagged-hTRPV3 transfected HEK-293 cells were subjected to immunocytochemistry as a positive control. Cells with successful transfection show green fluorescence, which was co-localized with red immunofluorescence indicating TRPV3 antibody binding (Fig 3E). TRPV3 antibody are able to detect hTRPV3 protein in transfected HEK-293 cells (Fig 28E). EGFP-tagged rTRPV2 transfected HEK-293 cells

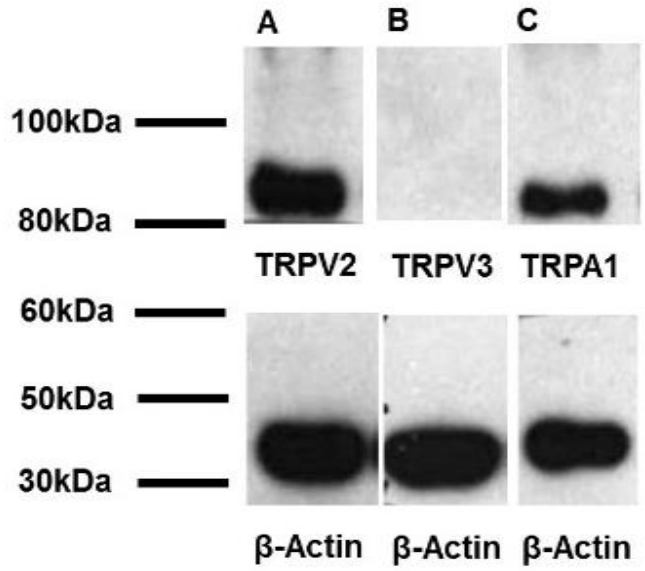

Figure 4: Functional expression of TRP channel in BV-2 microglia like cells.

Cultured BV-2 cells are subjected to total cell lysate and subjected to western blotting (see Method 5). Proteins of total cell lysate separated by 10% SDS-PAGE and blotted by **Lane A.** rabbit-anti-mouse TRPV2 antibody (1:1000 dilution), **Lane B.** rabbit-anti-human TRPV3 antibody (1:500 dilution), and **Lane C.** mouse-anti-TRPA1 antibody (1:1000 dilution). **Lane A.** TRPV2 protein band is visualized about 90kDa. The size of protein band matches with expected size of TRPV2 protein, confirming presence of TRPV2 protein in BV-2 cells. **Lane B.** No TRPV3 channel protein is detected at expected band of proximately 90kDa. **Lane C.** TRPA1 protein band is detected approximately 90kDa, size of the protein band matches with expected size of TRPA1. β–actin visualized by mouse-anti-Actin antibody (1:1000 dilution) is used as positive control. β–actin protein are present in all lanes at expected protein band size of 42kDa, confirming protein is loaded into and separated successfully by SDS-PAGE.

are used as positive control for the rTRPV2 antibody. The result shows red immunofluorescence of rTRPV2 antibody binding were co-localized with green fluorescence, indicating TRPV2 antibody is able to recognize its target (Fig 3D). TRPA1 proteins are also detected in BV-2 microglia (Fig 3C, red immunofluorescence). Those results show that TRPV2 and TRPA1 protein is expressed in BV-2 microglia like cells, but TRPV3 protein is not detected. It is possible that TRPV3 are expressed in low concentration, but current data suggest that BV-2 microglia like cells mainly express TRPV2 and TRPA1. To confirm protein expression, western blotting were used to determine the presence of selected TRP protein. Cultured BV-2 cells are subjected to SDS-PAGE and blotted against TRPV2, TRPV3, and TRPA1 antibody (see Method 5). Protein band was detected around 80-90kDa by the TRPV2 antibody, indicating the presence

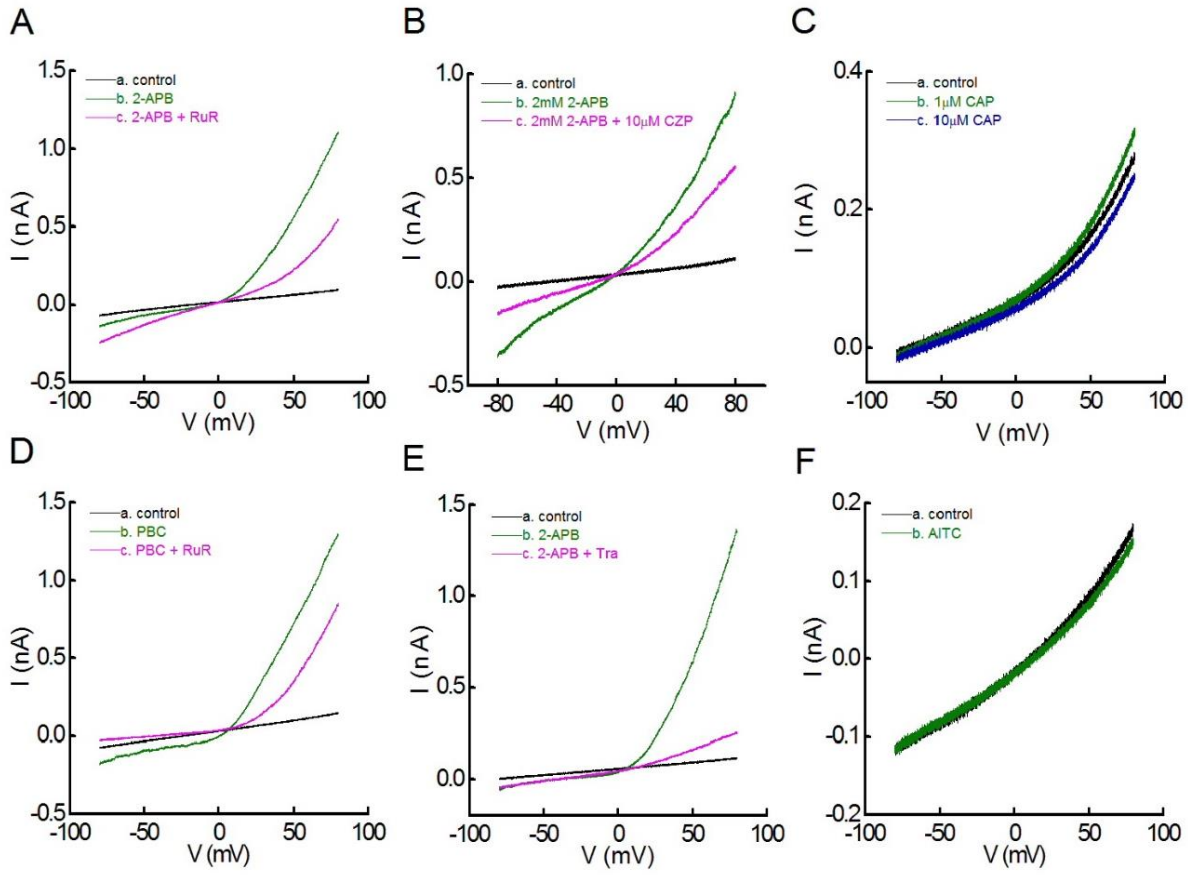

Figure 5: **Functional expression of TRP channel in BV-2 microglia-like cells.**

BV-2 cells are subjected to whole cell voltage clamp electrophysiology while TRPV channel agonist and antagonists are applied. A voltage ramp from -80 mV to +80 mV is repeatedly delivered to the cell to elicit currents, and the current result is plotted as I-V curve. **A.** Application of 2 mM 2-APB induces a robust outward rectified current in BV-2 cells which can be blocked by 10 μM RuR. **B.** However, application of TRPV1 antagonist 10 μM CZP did not fully inhibit the 2-APB current. **C.** Similarly, application of up to 10 μM CAP did not elicit any current, suggesting the current is not TRPV1 mediated. **D.** TRPV2 channel selective agonist 4 mM PBC induces outward rectified current which can be blocked by 10 μM RuR, and **E.** TRPV2 channel selective antagonist 1 μM Tranilast are able to inhibit 1mM 2-APB induced current in BV-2 cells. This suggests BV-2 contains functional TRPV2 channel. **F.** 20 μM AITC did not elicit any current, indicating no TRPA1 functional expression.

of TRPV2 protein (Fig 4A). The TRPV2 protein band size is matched with the reported size of TRPV2. Consistent with immunocytochemistry, TRPV3 protein is not detected (Fig 4B). TRPA1 protein is expected to have approximately 90kDa. TRPA1 protein bond was found approximately 80-90kDa (Fig 4C); conforming TRPA1 protein expression. The anti-β-actin antibody is used to visualize β-action protein for

loading control. The β-actin protein is detected in all experiments, confirming the lack of the TRPV3 protein band was not due to low protein loading (Fig 4 A-C).

The presence of proteins does not indicate the formation of functional channels in BV-2 microglia like cells. For example, TRPV1 channel is known to be expressed in the microglia, but no capsaicin current have been reported[61,102]. Whole cell voltage clamp electrophysiology was used to determine functional expression of selected TRP channels. Under control condition, only leak current was observed in BV-2 cells (Fig 5A-E, black line). A non-selective TRPV channel agonist 2 mM 2-APB elicit inward rectified current in BV-2 microglia like cells (Fig 5A, green line), which can be blocked by calcium channel blocker 10 μM RuR (Fig 5A, magenta line). This suggests the presence of TRPV1, TRPV2 or TRPV3 channel in BV-2 cells[27]. 2-APB induced current was not fully inhibited by TRPV1 channel selective antagonist 10 μM capsazepine (CZP), indicating the 2-APB current is not carried by TRPV1 (Fig 5B). As expected from published literature, up to 10 μM TRPV1 selective agonist capsaicin did not elicit an observable current in BV-2 (Fig 5C), confirming 2-APB current is not mediated by TRPV1. TRPV2 channel selective agonist 4 mM PBC induced outward rectified current similar to TRPV2 (Fig 5D, green line) which is blocked by 10 μM RuR (Fig 5D, magenta line). Furthermore, 1 mM 2-APB induced current (Fig 5E, green line) is inhibited by co-application of 1 mM 2-APB and 1 μM Tranilast (Fig 5E, magenta line). Those results indicate the functional expression of TRPV2 channel in BV-2 microglia. Lastly TRPA1 channel selective agonist 20 μM AITC did not induce currents in BV-2 (Fig 5F, green line). This result suggests a lack of functional expression of TRPA1 channel despite the presence of TRPA1 proteins. Together, whole cell voltage clamp indicates that TRPV2 but not TRPV1 or TRPA1 functionally expressed in BV-2 microglia like cells, and the TRPV2 is the main conductor of 2-APB induced currents.

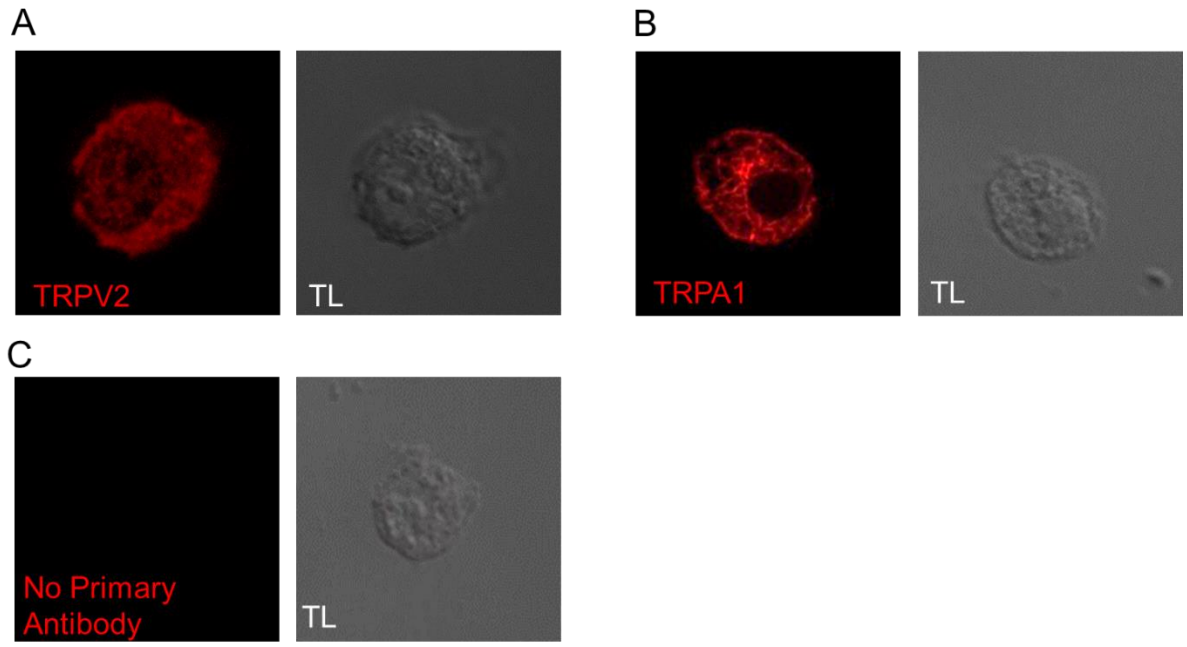

Figure 6: TRPV2 and TRPA1 channel expression in dissociated neonatal mouse primary microglia enriched culture.

Dissociated mouse neonatal primary microglia cells are fixed and incubated with **A.** rabbit-anti-mouse TRPV2 channel antibody (1:1000) and **B.** mouse-anti-TRPA1 channel antibody (1:1000). Red immunofluorescence indicate presence of TRPV2 (**A**) and TRPA1 (**B**) protein. **C.** Negative control where no primary antibody are applied. No background staining is detected in (**C**).

To confirm expression of TRPV2 and TRPA1 channel in native microglia, enriched microglia culture of neonatal mice is subjected to immunocytochemistry and whole cell electrophysiology. TRPV2 channel protein is shown to be present in mice neonatal enriched primary microglia culture (Fig 6A, red fluorescence). Also immunocytochemistry shows TRPA1 channel protein is expressed in mice neonatal enriched primary microglia (Fig 6B, red fluorescence). The red immunofluorescence is not due to none specific binding of secondary antibody since no red immunofluorescence is found in no primary antibody negative control (Fig 6C). Those result confirms TRPV2 and TRPA1 protein in dissociated neonatal mice primary microglia.

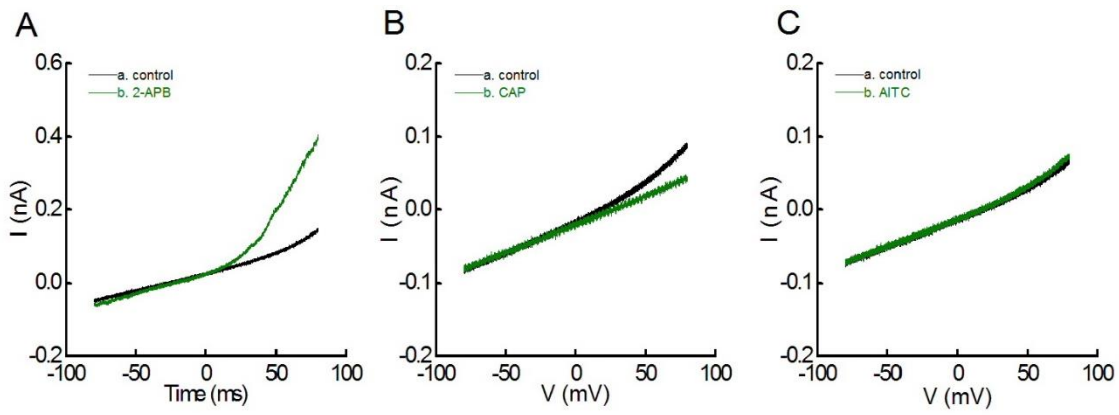

Figure 7: Functional expression of TRP channel in dissociated neonatal mouse primary microglia enriched culture.

Enriched mouse neonatal primary microglia cells are subjected to whole cell voltage clamp electrophysiology. **A.** Application of 1mM 2-APB induces a robust outward rectified current in BV-2 cell indicating the presence of TRPV1, TRPV2 or TRPV3 channel. **B.** Application of TRPV1 channel agonist 100 μM CAP did not induce a current response, suggesting the 2-APB current is not mediated by TRPV1. **C.** Application of TRPA1 channel agonist 20 μM AITC did not elicit any current suggesting that TRPA1 channel is not functionally expressed in dissociated mouse neonatal primary microglia.

To confirm functional expression of TRPV2 and TRPA1, dissociated neonatal mice primary microglia is subjected to whole cell voltage clamp. Voltage ramp protocol from -80 mV to +80 mV (1 s duration) is repeatedly delivered to the cell in the absence and presence of pharmacological agents applied by bath superfusion. Only small leak current is found under control condition (Fig 7A-C, black line). Application of 1 mM 2APB induces a rectified current in dissociated mice neonatal primary microglia (Fig 7A). This result indicates presence TRPV1 or TRPV2 channel in dissociated neonatal mice primary microglia[27]. However, TRPV1 channel selective agonist 100 μM CAP did not elicit current in mice neonatal primary microglia (Fig 7B). Also TRPA1 selective agonist 20 μM AITC did not induce current despite TRPA1 channel protein is detected (Fig 7C). This result suggests that the TRPA1 channel protein in microglia is not functional. From those results, it is suggested that TRPV2 channels are main TRPV channels mediate 2APB induced cation currents in microglia since TRPV3 channel protein is not detected and TRPV1 and TRPA1 channel agonist do not elicit current in microglia despite their protein are expressed.

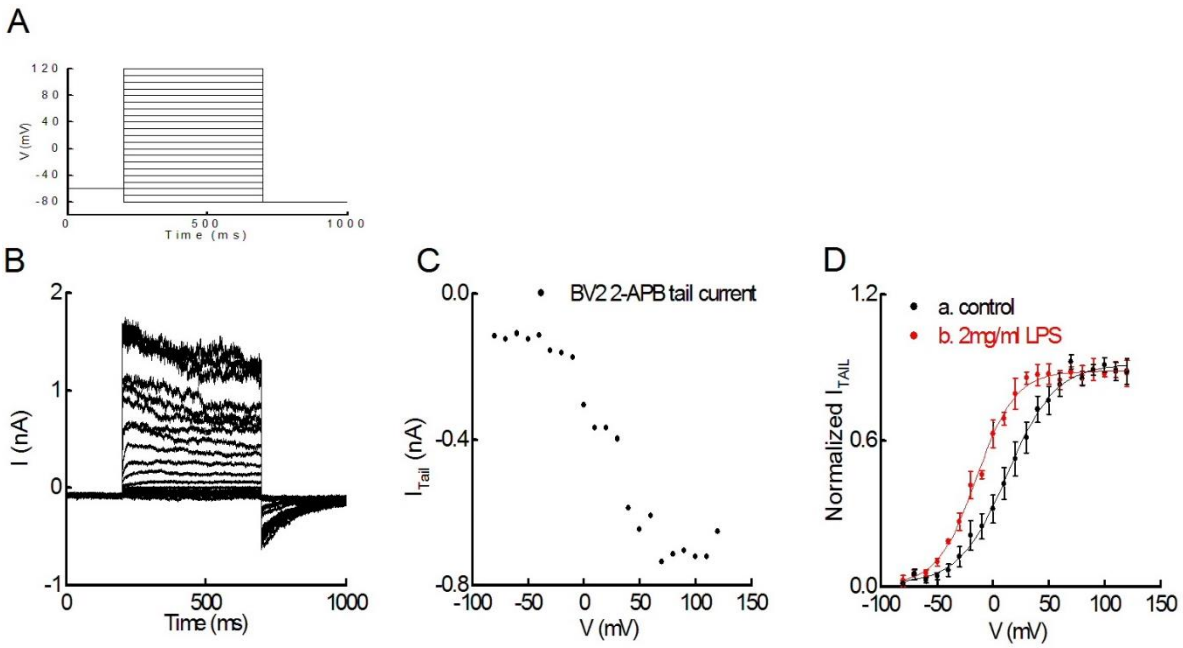

Figure 8: Pre-incubation of LPS alters TRPV2 gating in BV-2 cells.

The effect of LPS induction on TRPV2 gating is examined by whole cell voltage clamp. The tail current is measured during application of 1 mM 2-APB. **A.** A voltage step from -80mV to 120mV to measure the current response. Following voltage step, the membrane is stepped to -80mV to measure the instantaneous I_{tail}. **B.** 2-APB elicited BV-2 current response to voltage steps (**A**) is collected. The instantaneous I_{tail} is analyzed by fitting the current to an exponential decay function (equation 2). **C.** The tail current (Y axis) is plotted in relation to voltage step (X-axis). As membrane step increases I_{tail} become larger and the maximum current is reached about 70 mV. Because instantaneous I_{tail} informs the NPo of the channel, TRPV2 is thought to be activate starting -30 mV and reaching its maximum NPo at +70 mV. **D.** The instantaneous I_{tail} is then fitted to Boltzmann equation and normalized. The result is then plotted in Normalized I_{tail} – V plot. The result shows changes of tail current and apparent Po in response to changes in membrane voltage. Pre-incubation of BV-2 with 2 μg/ml of E.coli LPS for 30 minutes induced left shift of normalized I_{tail} – V curve compared to control media treated BV-2 cells.

To summarize TRPV2 and TRPA1 protein is present in both BV-2 microglia like cells and dissociated neonatal mice primary microglia. On the other hand, TRPV3 is not detected in BV-2. Of those channels, TRPV1 and TRPA1 currents are not found in BV-2 and dissociated neonatal mice primary microglia; making TRPV2 the main conducting channel for 2-APB induced currents.

3. LPS pre-administration enhances TRPV2 current in BV-2 microglia like cells.

Our studies have demonstrated that TRPV2 is the mediator of the 2-APB induced current in BV-2. Elevated H_2O_2 concentration is commonly observed in activated microglia and macrophages[75,76,103]. Administration of LPS is known to induce production of cytokine and phagocytosis in macrophage that is mediated by TRPV2. However, whether and how LPS activate TRPV2 is not known. LPS, a gram-negative bacteria outer wall glycoprotein, is commonly used in microglia research as a pro-inflammatory stimulation[75,76]. LPS application to microglia is known to induce production of H_2O_2 and cause pro-inflammatory activation of microglia. Given results in macrophage, LPS is likely to activate TRPV2. To test the hypothesis of activated microglia have enhanced TRPV2 activity, BV-2 cells are treated with control media or with 2 μg/ml of E.coli LPS for 30 minutes and then subjected to whole cell voltage clamp electrophysiology.

A voltage step from -80 mV to 120mV is applied to BV-2 to elicit the steady state current response at different voltages. Following voltage step, -80 mV membrane step is applied to measure the I_{tail} response (Fig 8A). Note that steady state current is archived during 500 ms of voltage step (Fig 8B). Following voltage step, -80 mV membrane step induced an instantaneous tail current of different size (Fig 8B). The instantaneous tail current is then analyzed for its relation to voltage step, time of decay, and maximum size (see method 7c). A representative tail current response plotted against voltage step is shown in Fig 33C. Tail current remains low during -80 to -20 mV membrane step, and gradually increase over -20 mV to 70 mV membrane step; reaching maximum tail current during -70 mV to 120 mV (Fig 8C). The tail current is directly proportional to the NPo, thus results indicate TRPV2 channel is opened over -20 to 70 mV membrane step and reaching maximum NPo at 70 mV. The I_{tail}-V curve is fitted to Boltzmann equation (equation 3) and normalized for analysis of half maximum Po ($V_{0.5}$), valance charge (z) and size of tail current. Normalized tail current – voltage curve (Normalized I_{tail}-V) is constructed (Fig 8D). Note that 30 minutes pretreatment of 2 μg LPS shifted the normalized Itail-V curve to the left (Fig 8D). In media pre-treated BV-2 cells, 1 mM 2-ABP increased apparent NPo starting -40mV, and apparent NPo

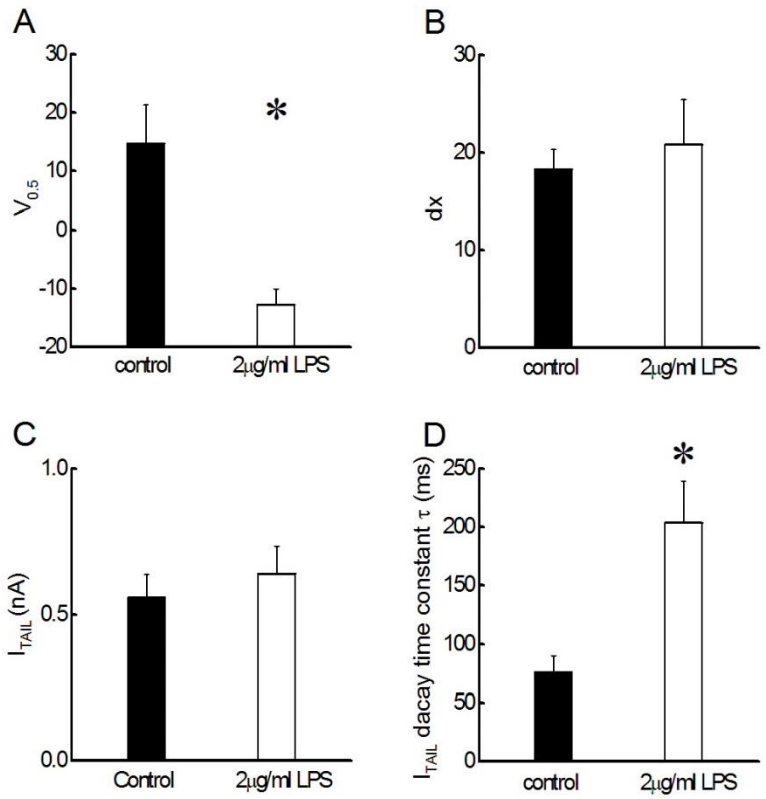

Figure 9: Analysis of LPS effect on TRPV2 gating in BV-2 cells.

Tail current of media treated and 2 μg/ml LPS treated BV-2 cells are analyzed. Cultured BV-2 cells are treated with no-LPS containing media or 2 μg/ml LPS containing media for 30 minutes in 37°C, and subjected to whole cell voltage clamp. **A.** Half maximum open probability ($V_{0.5}$) is calculated by measuring membrane voltage required to elicit 50% of maximum voltage under 1 mM 2-APB condition in BV-2 cells. In control media treated cells 14.7 ± 6.7 mV (n = 7) is required to reach $V_{0.5}$ compared to -12.7 ± 2.7 mV (n = 6) required for $V_{0.5}$ in 2 μg/ml LPS pretreated BV-2 cells. The result shows a statistically significant reduction of $V_{0.5}$ in cell pretreated by 2 μg/ml LPS (p = 0.004). **B.** The slope factor (dx) are determined by fitting normalized tail current to voltage curve to Boltzmann equation (equation 3). In control media treated cells dx is 18.3 ± 2.0 C/(J*mol, n = 7), and dx is 20.8 ± 4.6 C/(J*mol) in BV-2 cells pretreated with 2 μg/ml LPS (n = 6). No statistically significant difference is found between two groups (p = 0.61). **C.** I_{tail} current is determined by subtracting baseline current (minimum tail current) from the maximum tail current. The tail current is 0.6 ± 0.1 nA under control condition (n = 7) and 0.6 ± 0.1 nA in 2 μg/ml LPS pretreated condition (n = 6). No statistically significant difference is the found (p = 0.52). **D.** I_{TAIL} decay time (τ) is measured by fitting instantaneous I_{tail} following +80 to +120 mV step to exponential decay function (equation 2). Tail current decay time is 76.3 ± 13.8 ms (n = 7) under control condition, and tail current decay time is 203.7 ± 35.8 ms (n = 5) in 2 μg/ml LPS pretreated BV-2. Tail current decay time in 2 μg/ml LPS pretreated BV-2 is significantly increased compared to control media treated BV-2 cells (p = 0.003). Statics is analyzed by student t-test and results are considered significantly different if $\alpha<0.05$.

reached the maximum around 70 mV (Fig 8D, black line). In 2 μM LPS pre-treated BV-2 cells, 1 mM 2-ABP increased apparent NPo starting -50 mV, and apparent NPo reached the maximum around 30 mV

(Fig 8D, green line). The $V_{0.5}$ in media treated BV-2 cells are 13.1 ± 1.5 mV while $V_{0.5}$ in 2μg/ml LPS pre-treated BV-2 cells are -14.8 ± 1.3mV. This result suggests that the TRPV2 channel is more easily activated following LPS stimulation.

Statistical analysis shows that $V_{0.5}$ is significantly different between control media treated BV-2 cells and 2 μg/ml LPS treated BV-2 cells ($p = 0.004$, Fig 9A). $V_{0.5}$ in control media treated cells are 14.7 ± 6.7 mV ($n = 7$) and $V_{0.5}$ in 2 μg/ml LPS pretreated BV-2 cells -12.7 ± 2.7 mV ($n = 6$, Fig 9A). This result indicates TRPV2 require less membrane depolarization to be activated if BV-2 microglia like cells is pre-treated with LPS. The slope factor (dx), did not change between control media pre-treated and LPS pre-treated BV-2 cells ($p = 0.61$, Fig 9B). In control media treated cells dx is 18.3 ± 2.0 C/ (J*mol, $n = 7$), and dx is 20.8 ± 4.6 C/ (J*mol) in 2 μg/ml LPS pre-treated BV-2 cells ($n = 6$, Fig 9B). Also, the size of tail current did not change between two groups ($p = 0.52$, Fig 9C). The tail current is 0.56 ± 0.08 nA in control media pre-treated cells ($n = 7$) and 0.6 ± 0.1 nA in 2μg/ml LPS pretreated BV-2 cells ($n = 6$). This result indicates that despite the shift in $V_{0.5}$, the maximum NPo of TRPV2 does not change if the membrane is fully depolarized. Finally, tail current decay time (τ) is measured by fitting +80 to +120mV step induced tail current to exponential decay function (equation 2). The tail current decay time is 76.3 ± 13.8 ms ($n = 7$) in control media pre-treated BV-2 cells and 203.7 ± 35.8 ms ($n = 5$) in 2 μg/ml LPS pretreated BV-2. The tail current decay time in 2 μg/ml LPS pretreated BV-2 is significantly increased compared to control media treated BV-2 cells ($p = 0.003$). This result indicates that TRPV2 favors open state more if BV-2 cells are pre-treated with LPS.

Our results indicate that LPS stimulation of BV-2 microglia-like cells make TRPV2 open at a more negative membrane potential and make TRPV2 close slower once they are activated. In turn, those results imply that TRPV2 become easier to open in pro-inflammatory activated microglia, and TRPV2 channel will have enhanced activity when microglia is activated.

4. TRPV2 single channel properties

Although macroscopic whole-cell currents yield valuable information about TRPV2 biophysical properties, determining additional discriminative properties (i.e., single channel conductance, γ) requires additional experimental techniques. Classical ion channel theory hypothesizes that macroscopic currents (I) are proportional to the product of the number of functional channels in the cell membrane (N), the amplitude of unitary current (*i*), and P_O (see Method 7f, equation 6):

$$I = N \cdot i \cdot P_{OPEN}.$$

Unitary current (*i*) is proportional to unitary conductance (γ) by the driving force, which depends on membrane potential (V_M) and the 'reversal' potential (E_{REV}) of current flowing through the open channel by (see Method 7e, equation 5):

$$i = \gamma \cdot (V_M - E_{REV})$$

Despite its potential utility in discriminating between otherwise biophysically similar channels, the single channel conductance of TRPV2 has not previously been reported[35,43,70,104]. Furthermore, it is not known whether different channel agonists alter γ in TRPV2. We, therefore, sought to measure TRPV2 unitary

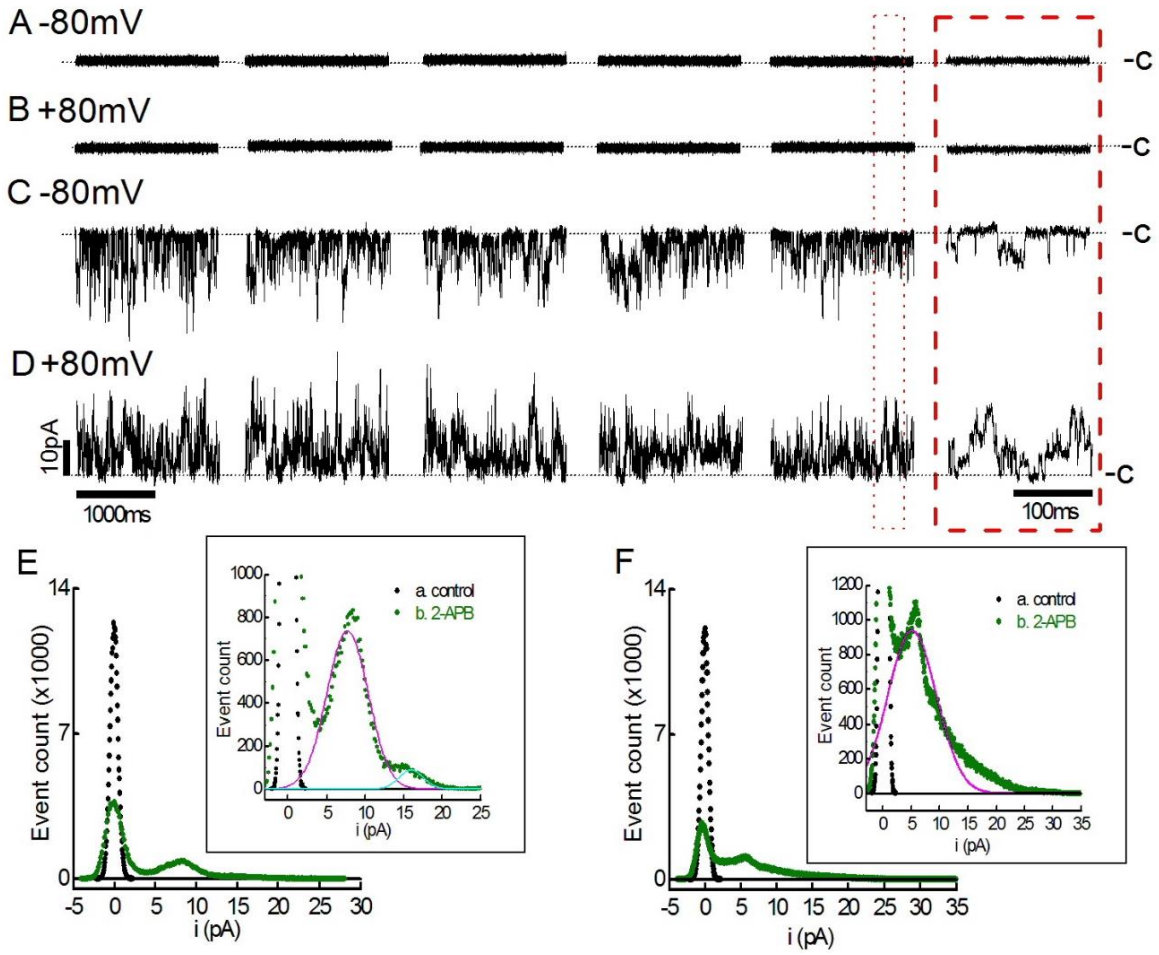

Figure 10: 2-APB elicits single TRPV2 channel activity in excised membrane patches.

Excised inside-out patches were pulled from HEK-293 cells expressing GFP-rTRPV2 and subjected to voltage clamp (Methods). **A, B.** Currents recorded at 5 different time intervals in a representative patch at -80mV (**A**) or +80 mV (**B**) under control conditions are shown. Note that no channel openings are observed. **C, D.** Addition of 2-APB (50 μM) to the bath solution (i.e., cytosolic face of the patch) elicits channel activity at both -80 mV (**C**) and +80 mV (**D**). Red box shows enlarged view of single channel activity across 200 ms. In **A**-**D**, dashed lines indicate the leak-subtracted zero current amplitude, which corresponds to the closed channel state (c). **E, F.** All-points histograms of the data shown in panels **A-D** in the absence (control, black circles) and presence (green circles) of 2-APB (50 μM) measured at +80 mV (**E**) or -80 mV (**F**) are shown. Lines represent fits of the data to the sum of several Gaussian functions (see Methods); the positions of peaks determined from Gaussian fits are used to determine unitary current amplitude (-7.7 pA at -80 mV and 5.3 pA at +80 mV, magenta lines). ***Insets*** show expanded views of the data in panels **E** and **F**. Patches in which several channels are simultaneously open generate addition peaks with amplitudes that are approximately multiples of the first peak (-16.0 pA at -80mV, cyan line). Current noise and the possible existence of sub-conductance states preclude unambiguous determination of additional open-state current amplitudes at +80 mV.

current amplitudes in inside-out patches excised from HEK-293 cells expressing rTRPV2. Such measurements could also be useful for directly determining Po under defined experimental conditions.

Consistent with a previous report, we find that TRPV2 exhibits a low open probability when no agonist is present [43]: no channel openings are observed in 5 representative recordings at either +80 mV or -80 mV (Fig. 10A, B). Gaussian fits of all-points histograms of excised patch currents measured over a total of 18 s at either -80mV membrane step or +80mV yield a single large peak centered at ~0 pA corresponding to the closed-channel state (Fig. 10E, F). Our excised patch data is consistent with whole-cell recording, where membrane depolarization alone was insufficient to elicit measurable TRPV2 current (Fig. 1). The apparent voltage-insensitivity of TRPV2 in the absence of agonist contrasts with the behavior of expressed rTRPV1 and hTRPV3 channels, for which depolarization alone is sufficient to cause channels to open (Figs. 6A and 8A).

Superfusion of 2-APB (50 μM) in the bath solution (i.e., to the cytosolic face of the membrane and intracellular side of the channel) induces a marked increase in TRPV2 channel activity, and channel openings are detected at both -80mV and +80mV (Fig 10C, D). In contrast to TRPV1 (Fig. 6) and hTRPV3 (Fig. 9), TRPV2 current records are characterized by 'erratic' TRPV2 channel activity (Fig 10C, 10D). TRPV2 channels under our recording conditions are characterized by brief openings and appear to manifest sub-conductance states (Figs. 10C and 10D, 11D, 15B, and 15C). Previous studies report similar 'erratic' gating phenomena and sub-conductance states in a mutant TRPV2 channel[35,43], but single channel currents in WT TRPV2 were not measured. All-points histograms generated from our excised patch data indicate the existence of two or more main open channels ($i \approx$ -8 pA at -80 mV; Fig. 10E). Broad Gaussian fits to the main open states suggest the possibility that we also measure other, more rarely populated sub-conductance states (Fig 10E, 10F). Additional peaks are fitted to Gaussian curve and their location to closed channel peak is measured to estimate unitary current of TRPV2 (see method 7e). The potential existence of sub-conductance states could interfere with our ability to resolve the main vs. sub-conductance unitary TRPV2 current amplitudes, particularly at voltages where apparent Po is higher (i.e., +80mV). The unitary current amplitude estimated from the peak of a Gaussian fit to the data (5.3 pA; Fig. 10F) is smaller than expected based on our estimate of *i* at -80 mV. In summary, TRPV2 channels exhibit rapid gating and sub-

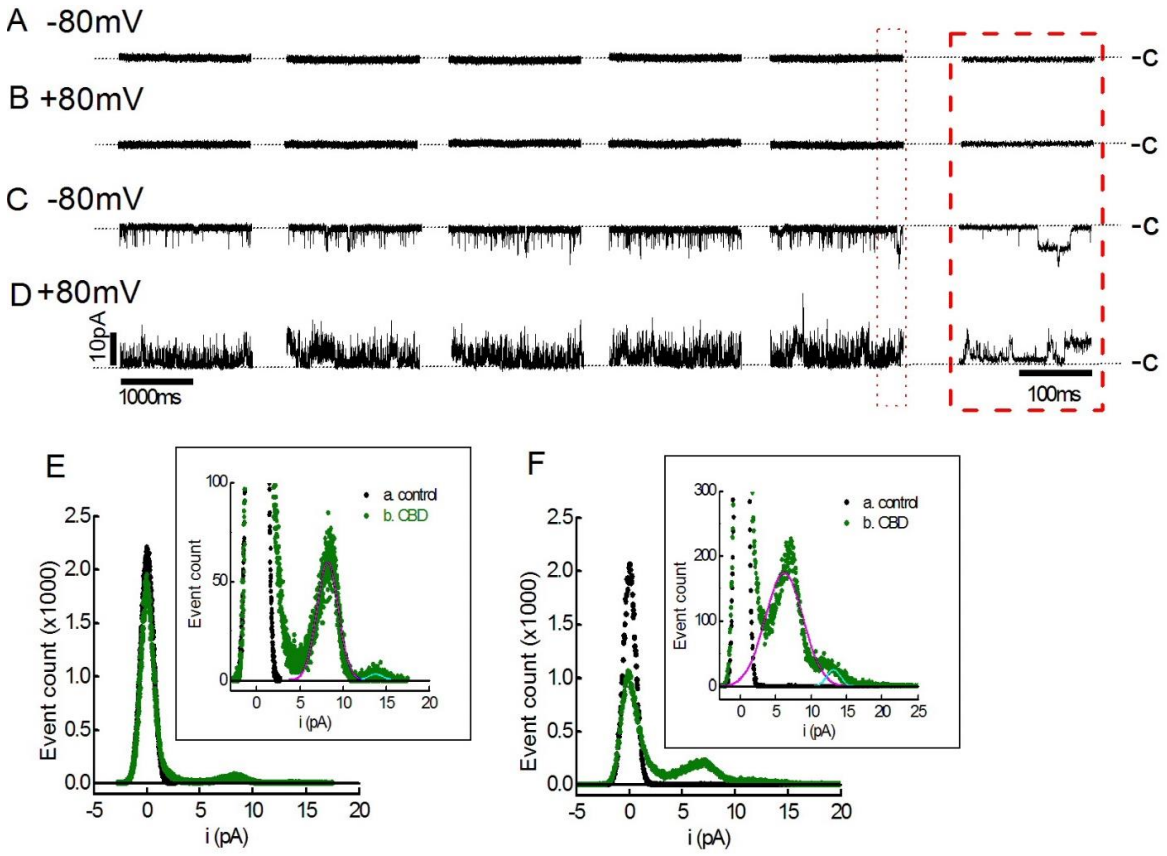

Figure 11: CBD elicits single TRPV2 channel activity in excised membrane patches.

Excised inside-out patches were pulled from HEK-293 cells expressing GFP-rTRPV2 and subjected to voltage clamp at -80mV or +80mV. **A, B.** No channel openings are observed at 5 different time intervals in a representative patch at -80mV (**A**) or +80 mV (**B**) under control conditions. **C, D.** Addition of CBD (300 μM) to the cytosolic face of the patch elicits channel activity at both -80 mV (**C**) and +80 mV (**D**). In **A**-**D**, leak-subtracted closed-channel (c) amplitudes are presented are indicated by dashed lines. Red box shows enlarged view of single channel activity across 200 ms. **E, F.** All-points histograms of the data shown in panels **A**-**D** in the absence (control, black circles) and presence (green circles) of CBD measured at +80 mV (**E**) or -80 mV (**F**). Lines represent fits of the data to the sum of three Gaussians (only fits to open-channel amplitude histograms are shown). ***Insets*** shows expanded views of the data in panels **E** and **F**. Unitary current amplitudes of CBD activated channels determined from Gaussian fits are -8.1 pA (**E**: -80 mV, magenta line) and 6.0 pA (**F**: +80 mV, magenta line). Gaussian fits to second peaks (cyan lines in **E** and **F**) have amplitudes that are approximately double the size of the first peak (magenta lines).

conductance states that make it difficult to unambiguously determine the amplitude of the single channel current. Nonetheless, we estimate that the main conducting state of rTRPV2 is likely to be ~ -8 pA at -80 mV, which is consistent with a previous report[43]. We revisit this interpretation in subsequent experiments.

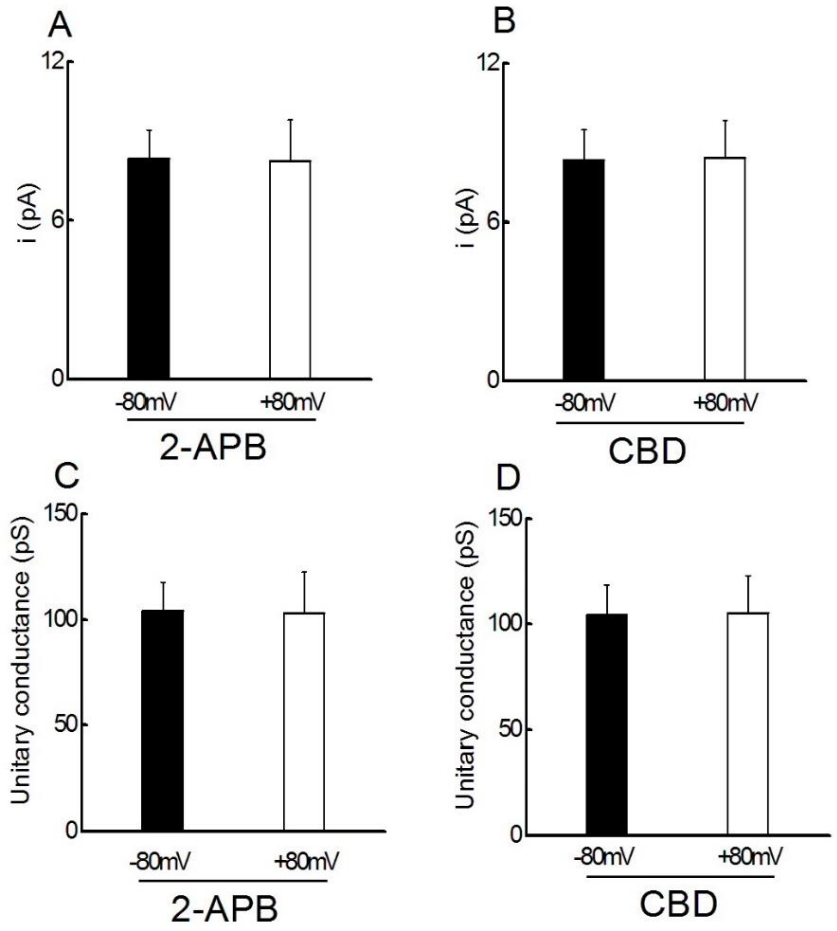

Figure 12: Unitary currents and conductance of TRPV2 at +80 mV and -80 mV.

Gaussian fits of all-points histograms were used to determine unitary current amplitudes (*i*) and unitary conductance (γ) is calculated ($\gamma = i/(V - E_{REV})$). **A.** Mean 2-APB (concentration?) activated unitary TRPV2 current amplitudes are -8.32 pA at -80mV and 8.24 pA at +80mV (n = 7 patches each). **B.** Mean CBD (concentration?) activated unitary TRPV2 current amplitudes are 8.3 pA at -80mV and 8.4 pA at +80mV (n = 4 patches each). **C.** Mean unitary conductance of 2-APB activated TRPV2 are 103.8 pS at -80 mV and 93.5 pS at +80 mV (n = 7 patches each). **D.** CBD activated TRPV2 channels exhibit unitary conductance of 104.3 pS at -80mV and 105.4 pS at +80 mV (n = 4 patches each). Differences in unitary conductance at -80mV vs. +80mV step and in presence of 2-APB vs. do not reach statistical significance ($p > 0.05$ by Student's unpaired t-test).

Similar to 2-APB, CBD (300 μM) activates TRPV2 channel activity in inside-out patches (Fig. 11). CBD appears to cause TRPV2 channels to open only briefly (flicker) like 2-APB (Fig 11C, 11D). All-points

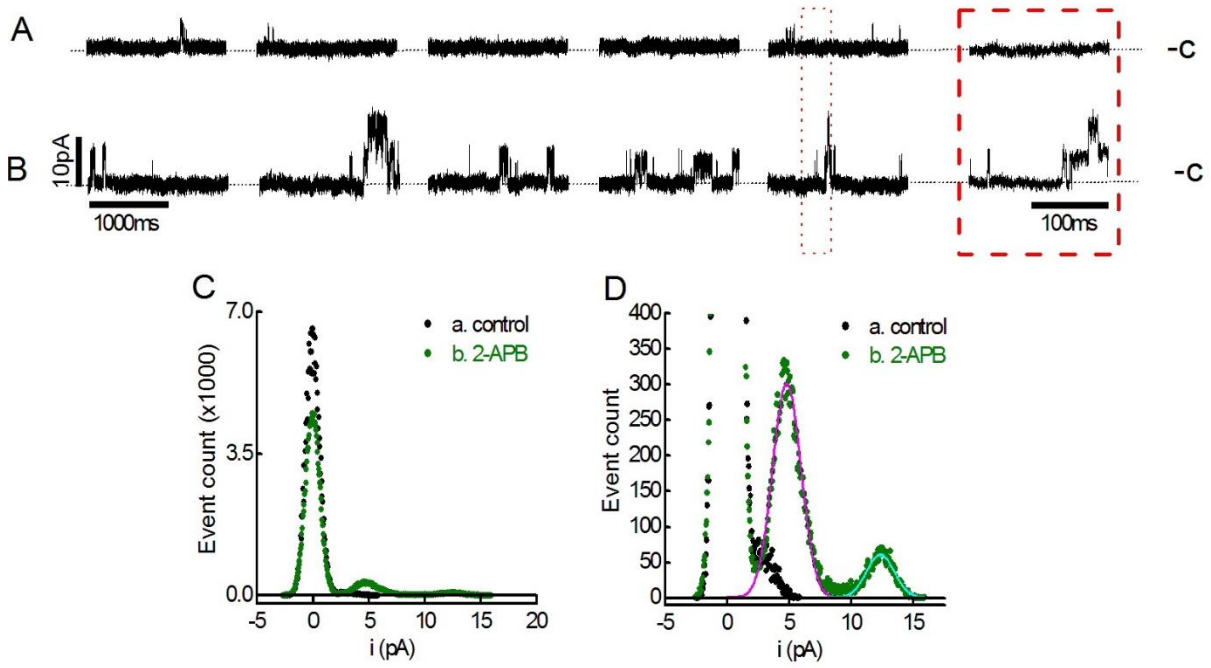

Figure 13: 2-APB induced TRPV1 single channel currents in excised membrane patches.

Excised inside-out patches were pulled from HEK-293 cells expressing GFP-rTRPV1 and subjected to voltage clamp at +80mV. **A.** 5 different time intervals in a representative patch in control conditions are shown; unlike TRPV2, occasional TRPV1 channel openings are observed +80mV in the absence of 2-APB. **B.** Addition of 2-APB (50 μM) to the cytosolic face of the patch elicits an increase in TRPV1 channel activity observed over 5 different time intervals. In **A** and **B**, leak-subtracted closed-channel (c) amplitudes are presented are indicated by dashed lines. Red box shows enlarged view of single channel activity across 200 ms. **C.** All-points histograms of the data shown in panels **A** and **B** in the absence (control, black circles) and presence (green circles) of 2-APB (50 μM) are shown. **D.** An expanded view of the data in panel **C** is shown. Gaussians fits to open-channel histograms yields a unitary current amplitude of 4.8 pA (magenta line); a second open-channel peak is located at 12.4 pA (cyan line).

histograms of currents measured over 18 s in a representative patch are more clearly fit Gaussian functions with peaks at -8.1 pA (-80 mV, Fig 11E) and 5.9 pA (-80 mV, Fig 11F).

Experiments conducted in a number of different patches allow us to estimate 2-APB and CBD activated TRPV2 single channel current amplitudes at +80 mV and -80 mV (Fig. 12A, 12B). Fig. 12A shows that the mean 2-APB activated unitary current amplitude at +80 mV (8.2 ± 1.6 pA) vs. -80mV (i = -8.3 ± 1.1 pA) is not different (p = 0.87 by Student's unpaired t-test). Similarly, no difference between mean CBD induced unitary current at -80 mV (-8.3 ± 1.2pA) vs. +80 mV (8.4 ± 1.4 pA) is observed (Fig. 12B). Our results compare well to the estimated unitary conductance in the rTRPV2 quadruple (F472S, L507M, S510T,

Q530E) mutant, for which γ = 101 pS[43]. Unitary TRPV2 conductance calculated from our data (Fig. 12C) reveal no significant difference (p = 0.87) between 2-APB activated γ measured at -80 mV (γ = 103.8 ± 18.9 pS) vs. +80 mV (γ = 93.5 ± 24.1 pS). Unitary conductance in CBD activated TRPV2 channels are also the same at -80mV (γ = 104.3 ± 14.4 pS) and +80 mV (γ = 105.4 ± 17.7pS; p = 0.96) and not different (p = 0.99) from 2-APB activated channels (Fig. 12C, D). Although macroscopic TRPV2 currents exhibit outward rectification (Figs. 1, 2), it was not previously clear whether the differences in inward vs. outward current amplitudes were caused by differences in gating (i.e., Po) or intrinsic pore rectification[27]. Our results in excised patches (Fig. 12) indicate that macroscopic current rectification in TRPV2 is attributable to voltage-dependent gating.

Unlike TRPV2, the single channel activity of TRPV1 and TRPV3 does not exhibit 'erratic' behavior. Under control conditions and at +80 mV, TRPV1 channels open occasionally, TRPV1 channel openings are rarely observed, indicating that apparent N·Po is low (Fig. 13A, C). Bath superfusion of 2-APB (50μM) increases channel activity (Fig 13B), and an all-points histogram assembled from a representative patch recording shows that 2-APB induced TRPV1 single channel has a current amplitude of ~5 pA (+80 mV; Fig 13C). The mean unitary conductance measured in several patches pulled from cells expressing rTRPV1 is 81.0 ± 14.3 pS at +80 mV (Fig. 14). In contrast to TRPV1 and TRPV2, TRPV3 is reported to mediate large unitary currents (γ = 185 – 206 pS, depending on cell type)[9,48,105]. 2-APB (10 μM) elicits channel activity (Fig 16B) in patches pulled from HEK-293 cells expressing hTRPV3 and a Gaussian fit to the representative all-points histogram (*i* = 14.3 pA; γ =175.3 ± 16.5 pS; Figs. 14, 16) yields a similar value to previously reports[9,48,105]. TRPV1 and TRPV3 (Figs. 13, 16) also exhibit 'well-behaved' single channel activity with open times that are sufficiently long to allow for unambiguously determination of single channel currents from visual inspection of our experimental data, consistent with previous reports [48,105-107].

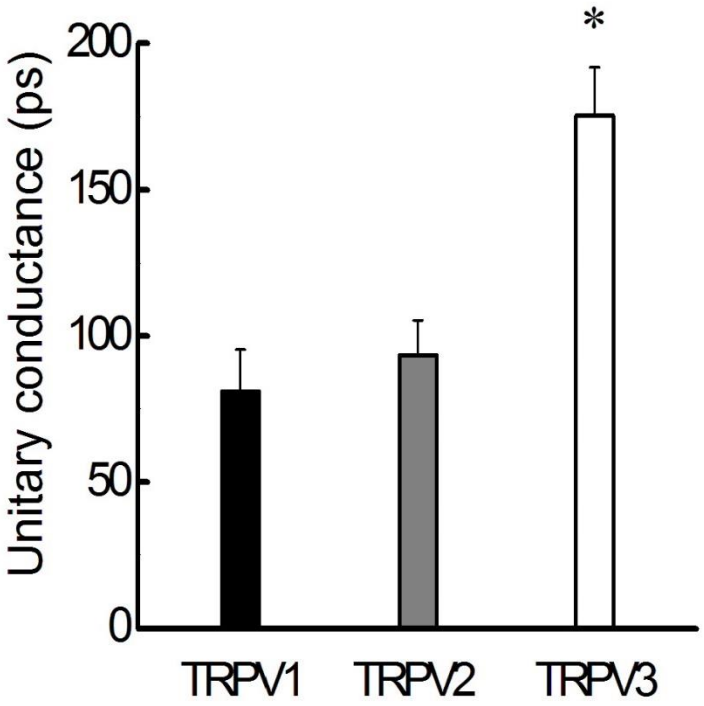

Figure 14: Comparison of unitary conductance in TRPV1, TRPV2 and TRPV3.

Unitary currents for TRPV1, TRPV2 and TRPV3 channels were determined from currents measured at +80 mV in inside-out patches excised from HEK-293 cells, as shown in Figs. 6-9 and 12. Mean peak values from Gaussian fits all-points histograms are: TRPV1, 81.0 ± 14.3 pS (n = 3); TRPV2, 93.4 ± 12.0 pS (n = 7); TRPV3, 175.3 ± 16.5 pS (n = 4). * Indicates TRPV3 unitary conductance is significantly different compared to TRPV1 and TRPV2 by one-way ANOVA with $\alpha < 0.05$.

The TRPV2 channel unitary conductance estimated here is more similar to TRPV1 (80-100 pS)[106,107] than TRPV3. TRPV1 channel unitary conductance is reported to be and TRPV3 unitary conductance is reported to be approximately 150 pS[48,105], consistent with our results. Our estimate of the TRPV2 unitary conductance is approximately midway between the value reported for native mechanosensitive currents in Jurkat cells (~40 pS) and purified, reconstituted TRPV2 channels in proteoliposomes (304 pS)[35,70]. The reasons for such discrepancies remain unclear, and additional experiments are needed to determine if TRPV2 unitary conductance is variable like other TRPV channels and whether differences between experimental conditions used here and elsewhere account for the variations in the unitary conductance[35,43,70].

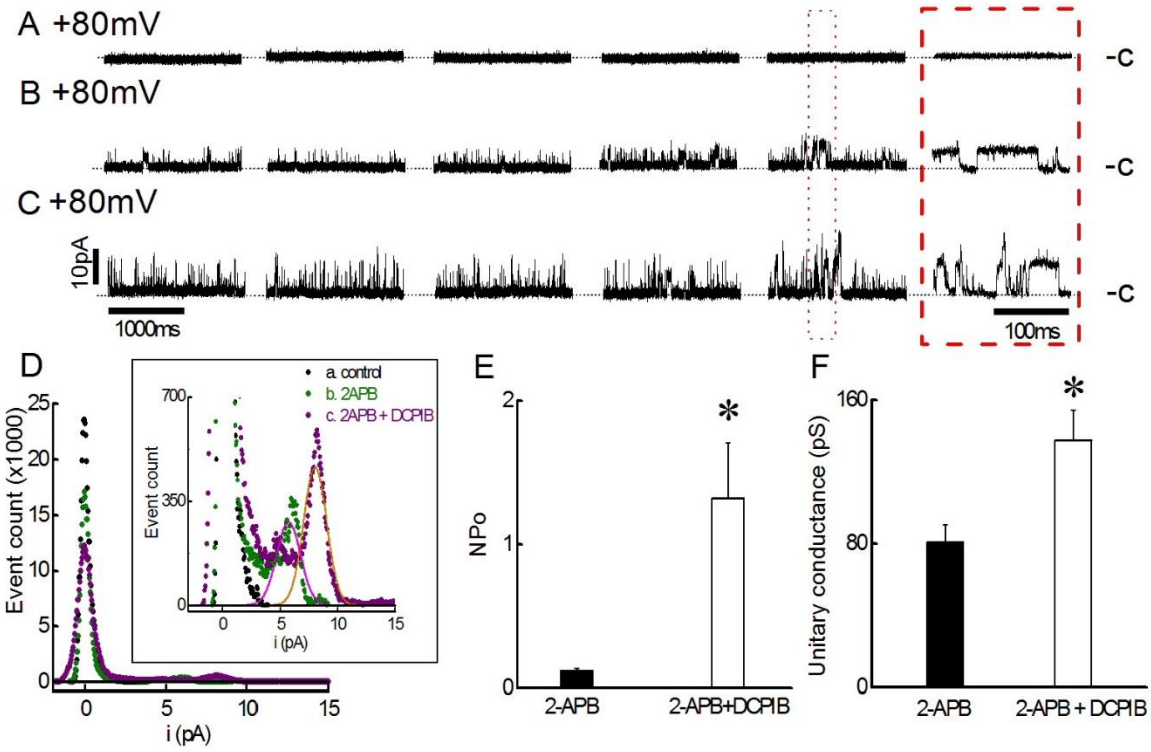

Figure 15: 2-APB and DCPIB induced TRPV2 activity in excised membrane patches.

Channel activity is measured in inside-out patches excised from HEK-293 cells expressing EGFP-rTRPV2 at +80 mV as described previously. Leak-subtracted zero current amplitudes are presented with closed channel state (c) indicated by dashed lines. **A.** No channel opening is measured under control conditions. **B.** Application of 2-APB (200 μM) to the bath solution increases TRPV2 channel activity. **C.** Application of DCPIB (10 μM) together with 2-APB (200 μM) further increases TRPV2 channel activity. In **A**-**C**, leak-subtracted closed-channel (c) amplitudes are presented are indicated by dashed lines. Red box shows enlarged view of single channel activity across 200 ms. **D.** All-points histograms of data in panels **A**-**C** are represented by black circles (control), green circles (2-APB alone) and purple circles (2-APB + DCPIB). ***Inset*** shows an expanded view of the data. Gaussian fits to the open-channel histogram data yield peak values of 5.83 pA (2-APB alone, magenta line) and 8.04 pA (2-APB + DCPIB, orange line). **E.** Open probability of the TRPV2 channel measured by Clampfit single channel detection program shows co-application of DCPIB significantly increases open probability of TRPV2 channel (NPo = 1.31 ± 0.39, n=3) compared to application of 2-APB alone (NPo = 0.12 ± 0.02, p = 0.03; n=3). **F.** Unitary current of TRPV2 channel is significantly increased if DCPIB is co-applied with 2-APB (11.00 ± 1.36 pA, p = 0.04; n=3) compared to 2-APB alone (6.45 ± 0.79 pA n=3). Unitary current is converted to unitary conductance (equation 5). Unitary conductance of 2-APB induced TRPV2 current is (80.6 ± 9.9 pS, n=3), and unitary conductance of TRPV2 is (137.6 ± 17.0 pS, p = 0.04; n=3) if DCPIB is co-applied with 2-APB. Statics is analyzed by paired student t-test with $\alpha<0.05$ for significance.

5. DCPIB alters TRPV2 unitary conductance

Erratic single channel activities of TRPV2 are partially caused by the presence of sub-conductance. Sub-conductance can be caused either by innate biophysical property of TRPV2 or by the presence of another channel. HEK-293 cells are known to contain swell activated chloride current, $I_{Cl,swell}$. $I_{Cl,swell}$ is mediated by a stretch and H_2O_2 activated channel that has a unitary conductance of approximately 10-20 pS[108]. $I_{Cl,swell}$ would induce 1-2pA current under -80mV or +80mV membrane step and could be responsible to sub-conductance observed. In order to confirm $I_{Cl,swell}$ is not causing sub-conductance, we used the $I_{Cl,swell}$ inhibitor DCPIB. Excised inside-out patch clamp recording of TRPV2 channel shows no channel activity under control conditions, while superfusion of 200 μM 2-APB induces channel opening of varying unitary conductance (Fig 15A, 15B). Superfusion of 10 μM DCPIB in addition to 200 μM 2-APB increases TRPV2 activity (Fig 15C). Note that small conductance still presents in the patch after addition of DCPIB (Fig 15C), suggesting sub-conductance states are an innate biophysical property of TRPV2, and not caused by the presence of $I_{Cl,swell}$ under our recording conditions. Furthermore, 2-APB is found to be an inhibitor of $I_{Cl,swell}$, as 100 μM of 2-APB inhibited $I_{Cl,swell}$[109]. These results suggest TRPV2 have more than one open state with different unitary conductance, or alternatively, modulation of TRPV2 such as phosphorylation or $PI(4,5)P_2$ binding induces a change in TRPV2 unitary conductance[18].

Interestingly DCPIB itself may change unitary conductance of TRPV2. Modulation of TRPV2 NPo and unitary current by DCPIB is confirmed in all point histogram. All point histogram shows that co-application of 2-APB and DCPIB caused a right shift of open channel peak, as well as increase the size open channel peak (Fig 15D). This result suggests DCPIB enhances both NPo and unitary current of 2-APB induced TRPV2 single channel activity. 2-APB induces NPo equal to 0.12 ± 0.02 and unitary conductance of 80.62 ± 9.9 pS at +80mV membrane step. Co-application of 2-APB and DCPIB induces NPo equals to 1.31 ± 0.39 and unitary conductance equals to 137.6 ± 17.0 pS at +80mV membrane step (Fig 15E, 15F). DCPIB

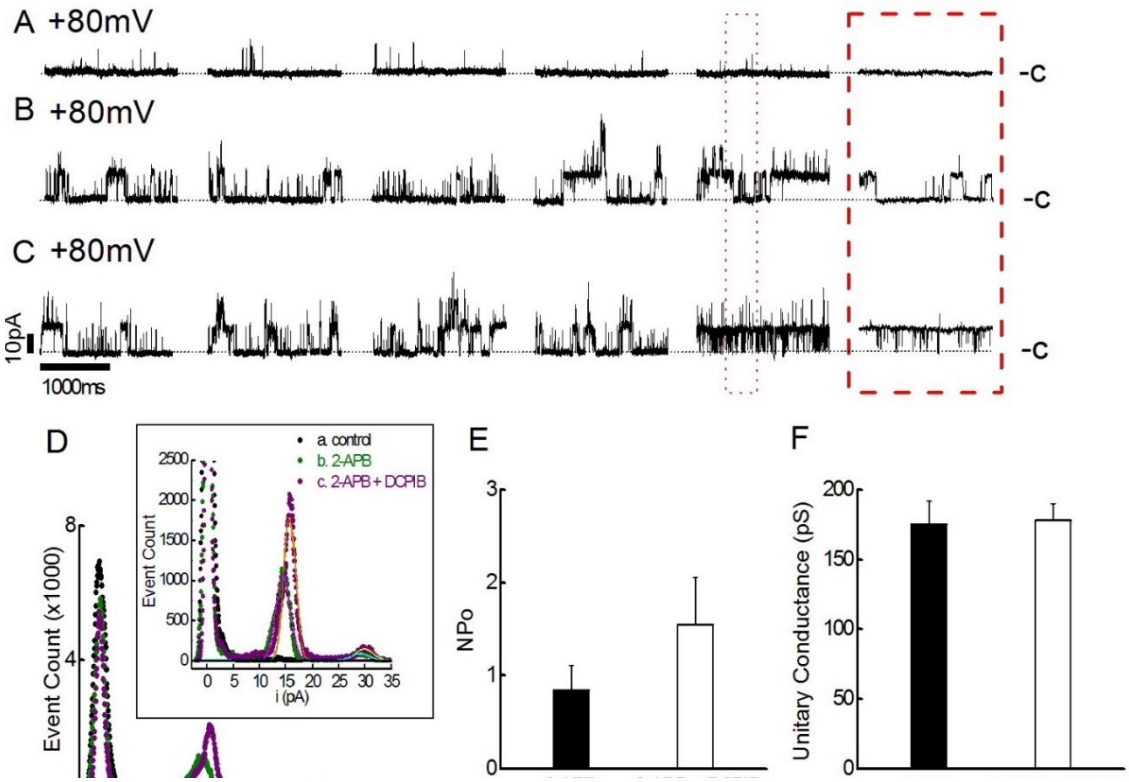

Figure 13: 2-APB and DCPIB induced TRPV3 activity in excised membrane patches.

EGFP-hTRPV3 channel transfected HEK-293 cells are subjected to excised inside-out patch clamp electrophysiology. Membrane potential is clamped to +80mV and the current response recorded. Leak-subtracted zero current amplitudes are presented with closed channel state (c) indicated by dashed lines. **A.** Low channel opening is detected under control condition in 5 different time intervals in a representative patch at +80mV. **B.** Application of 10μM 2-APB to the cytosolic face of the patch induces increases TRPV3 channel opening. **C.** Application of 10μM DCPIB in addition to 10μM 2-APB further increases channel opening of TRPV3 channel. The red box shows an enlarged view of single channel activity across 200 ms. **D.** Data in panel **A-C** are summarized in all point histogram. TRPV3 channel opening increased after 2-APB administration (green circle) compared to control state (black circle). ***Insets*** show expanded views of the data in panels **D**. Gaussian fit is used to determine unitary current of TRPV3 channel. Unlike TRPV2, the addition of DCPIB did not shift open channel peaks to right. 2-APB application induced first major peak with 14.31pA current (magenta line), and second major peak with 29.08pA current (cyan line). Co-application of 2-APB and DCPIB increased the amplitude of the first peak but does not induce a rightward shift of the first peak (purple circle). Application of 2-APB plus DCPIB induces single channel opening with the first peak equals to 15.57pA (orange line) and second peak equals to 29.82pA (yellow line). **E.** Open probability of the TRPV3 channel is measured by Clampfit single channel detection program. Application of 2-APB alone induced NPo=0.85 ± 0.26 (n=4). Co-application of 2-APB and DCPIB induces NPo=1.55 ± 0.51 (n=4). No statistically significant difference is found between two groups ($p = 0.07$). **F.** Unitary current and unitary conductance of TRPV3 channel do not change following the addition of DCPIB. 2-APB induces the unitary current of 14.02 ± 1.52pA while co-application of 2-APB and DCPIB induces the unitary current of 14.24 ± 1.10pA (n=4). The unitary conductance of 2-APB induced TRPV3 current is 175.3 ± 16.5 pS and unitary conductance of 2-APB and DCPIB induced current is 178.1 ± 12.0 pS. No statistical significant difference is found between two groups ($p=0.89$). Statics is analyzed by paired student t-test, and results are considered significant if $p<0.05$.

increases 2-APB induced TRPV2 channel NPo ($p = 0.03$) and unitary current ($p = 0.04$) significantly (Fig

15E, 15F).

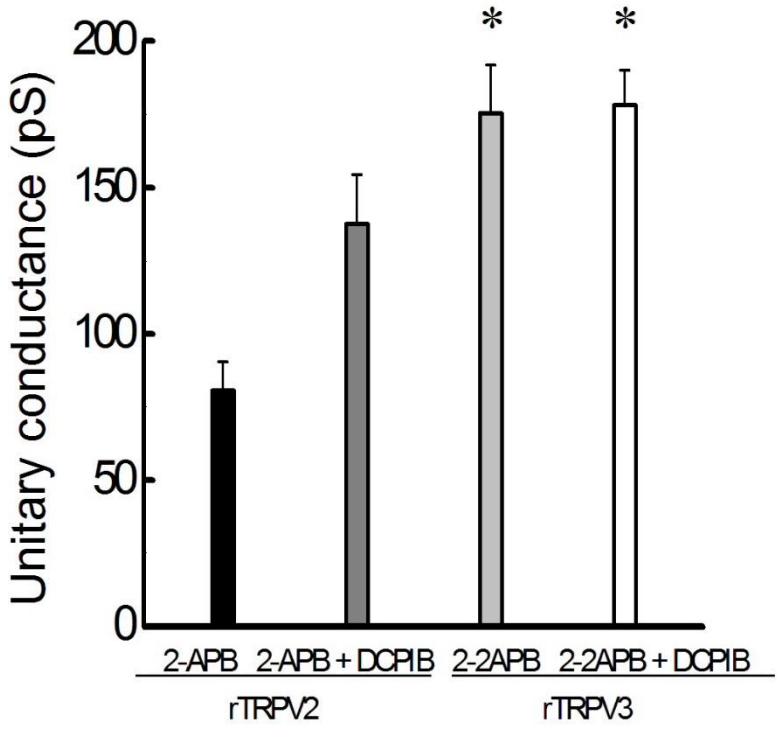

Figure 17: Statistical comparison of DCPIB effect on TRPV2 and TRPV3 unitary conductance.

The unitary current of TRPV2 and TRPV3 channels under DCPIB treated condition are measured by the Gaussian fitting of the all point histogram. The significant difference is found between unitary conductance of 2-APB induced TRPV2 current (80.6 ± 9.9 pS) and TRPV3 current (175.3 ± 16.5 pS). However, no difference in unitary conductance between co-application of 2-APB and DCPIB induced TRPV2 current (137.6 ± 17.0 pS) and TRPV3 current (178.1 ± 12.0 pS) is observed. * indicate a significant difference between TRPV3 channel unitary conductance compared to 2-APB induced TRPV2 unitary conductance. Statistics are measured by one-way ANOVA with the significance of regression coefficient of $\alpha<0.05$.

Unlike TRPV2, DCPIB did not alter the size TRPV3 channel unitary current. Under control condition representative current traces shows infrequent channel activity when the membrane voltage is stepped to +80mV (Fig 16A). Superfusion of 10 μM 2-APB to cytosolic face increases channel activity (Fig 16B), further superfusion of 10 μM DCPIB in addition to 10 μM 2-APB seems to enhance TRPV3 channel

activities (Fig 16C). All point histogram confirms DCPIB enhanced TRPV3 channel activity; 2-APB plus DCPIB have larger first and second open peak (Fig 16D, magenta circle) compared to 2-APB alone (Fig 16D, green circle). However, unlike TRPV2, all point histogram of TRPV3 did not show a right shift of open channel peak after co-application of 2-APB and DCPIB (Fig 16D). This result suggests DCPIB did not increase the unitary current of 2-APB induced TRPV3 current. In TRPV3 channel, 2-APB alone induces NPo equals to 0.84 ± 0.26 and unitary current equals to 175.3 ± 16.5 pS at +80mV step (Fig 16E, 16F). Co-application of 2-APB and DCPIB induces NPo equals to 1.55 ± 0.51 and unitary current equals to 178.1 ± 12.0 pS at +80mV step (Fig 16E, 16F). DCPIB did not induced significant change in NPo ($p=0.07$) or unitary current ($p=0.90$; Fig 16E, 16F). One-way ANOVA indicates that 2-APB induced TRPV2 unitary conductance and 2-APB induced TRPV3 unitary conductance was significantly different to each other ($p=0.003$; Fig 17). However, co-application of 2-APB and DCPIB induced a larger TRPV2 current which is no longer significantly different to TRPV3 unitary conductance (Fig 17). The result clearly shows DCPIB only increases TRPV2 channel NPo and unitary conductance but not that of TRPV3.

Pharmacological reagents are known to modulate TRPV2 Po; both 2-APB and CBD are thought to increase Po of TRPV2. However, in addition to increasing NPo of TRPV2, DCPIB was able to increase unitary conductance of TRPV2. This suggests DCPIB alters pore structure of TRPV2. Furthermore, the DCPIB effect is unique to TRPV2 but not to TRPV3, suggesting DCPIB may interacting or altering structure unique to TRPV2. DCPIB increases TRPV2 unitary current, essentially making TRPV2 more TRPV3 like.

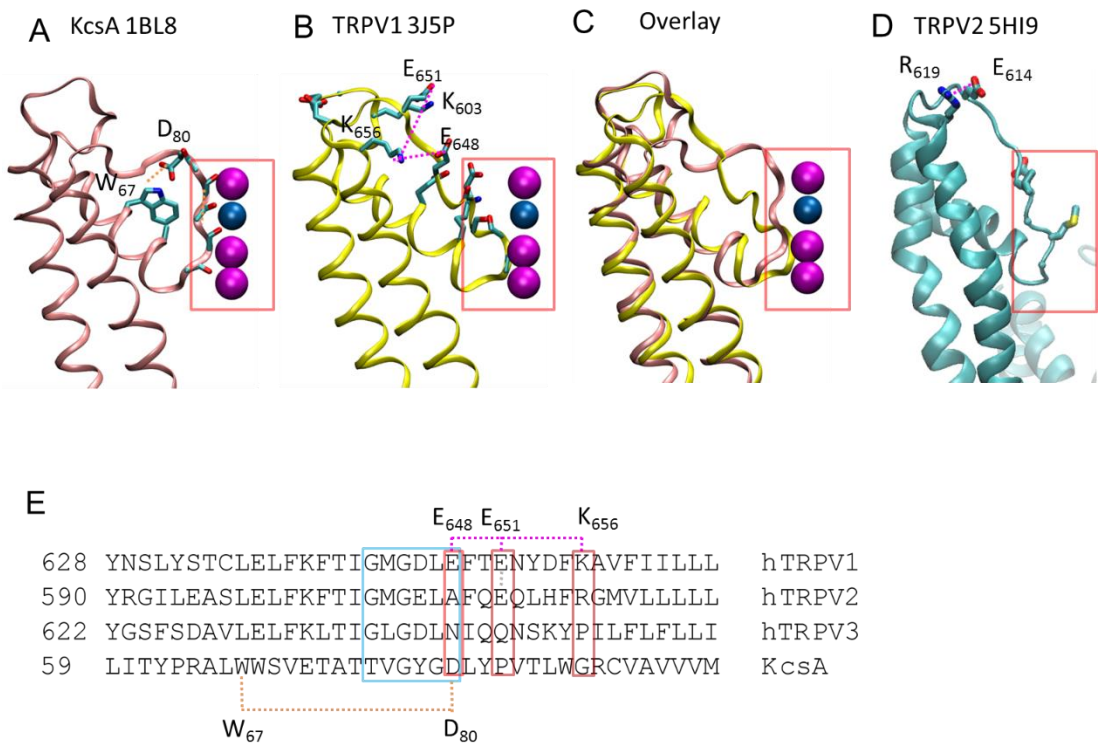

Figure 18: proposed residues regulate unitary conductance of TRPV channel.

TRPV have similar pore structure to KcsA. **A.** KcsA pore structure is shown in ribbon diagram (structure 1BL8: Doyle et al. 1998). The GYGVT amino acid sequence in the blue box forms the selectivity filter of pore of the KcsA. Two subunit near by the pore W67 and D80 are thought to form the ionic interactions that stabilizes pore. **B.** Structure of TRPV1 is shown in ribbon diagram (3J5P: Liao et al, 2013). The blue box indicate the GMGD amino acid sequence which forms selectivity filter of pore of TRPV1 channel. Similar to KcsA, TRPV1 contains two polar subunit near the pore E648 and K656. E648 and K656 on pore loop can also form electrostatic interactions that stabilize pore structure. **C.** Overlay of TRPV1 channel structure (yellow ribbon) and KcsA structure (pink ribbon) shows structural similarities of two channels. **D.** structure of TRPV2 is shown in ribbon diagram (5hi9: Huynh et al.). TRPV2 contains two polar units near pore loop, E614 and R619. **E.** Comparison of TRPV1, TRPV2, TRPV3 and KcsA reveals potential electrostatic interaction of E648, E651 and K656 in TRPV1. However this interaction cannot be formed in TRPV3. In TRPV3 channel, E648 position is replaced by N643, E651 is replaced with Q646 and K656 position is replaced by P651. In TRPV2 channel, E648 position is replaced by A611 but other two charged residues are conserved. E651 is conserved as E614 and a basic amino acid K656 position is replaced by another basic amino acid R619. This indicate TRPV3 do not have charged residue at S5-S6 pore loop to stabilize the pore structure. This may be cause of larger conductance in TRPV3. We hypothesized that lack of this electrostatic interaction may underlies difference in unitary conductance in TRPV1, TRPV2 and TRPV3 channel.

6. Charged residues in S5-S6 poor loop does not regulate unitary conductance of TRPV channels

The ability of DCPIB modulating TRPV2 unitary conductance suggest TRPV2 poor loop structure can be potentially altered by pharmacological reagents (Fig 15). This suggests that TRPV2 poor loop structure

may be flexible than initially expected. TRPV channel is thought to have a similar structure as Kv channels; they have similar six transmembrane domains, pore loop, and selectivity filter[7]. KcsA channel, a prokaryotic potassium channel, have similar pore structure compared to TRPV channels (Fig 18 A-C). Overlay of KcsA and TRPV1 shows two channel aligns closely in the S5 transmembrane domain, S5-S6 loop and the S6 transmembrane domain (Fig 18C); indicating two channel may have similar pore structure. Modulation of S5-S6 electrostatic interaction are reported to modulate KcsA gating property; Cordero-Morales reports that disruption of W67 – D80 hydrogen bonding result in a change of single channel NPo and KcsA inactivation process (Fig 18A)[110]. This demonstrates the electrostatic interaction between S5 and S6 loop can alter channel biophysical property.

Similar electrostatic interaction is conserved in TRPV1 (Fig 18B). In TRPV1 glutamic acid (E651) residue located in close proximity to lysine (K656) suggesting potential formation electrostatic interaction (Fig 18B). Same electrostatic interaction is conserved in TRPV2. E651 equivalent residue in TRPV1 is conserved (E614), and negatively charged K656 equivalent residue in TRPV1 is replaced by similarly charged arginine (R619; Fig 18E). This electrostatic interaction is not present in TRPV3 as E651 equivalent residue in TRPV1 is replaced by polar glutamine (Q646), and charged K656 equivalent residue in TRPV1 is replaced by hydrophobic proline (P651; Fig 18E). We hypothesized that formation of a potential interaction between E651 and K656 may configure pore structure in TRPV1 and TRPV2 to a small unitary conductance state, while the lack of electrostatic interaction may result in large unitary conductance in TRPV3. To examine this hypothesis, charged R619 residue in TRPV2 is mutated to proline in order to convert TRPV2 channel to TRPV3 like, and vice versa charged residues are introduced to TRPV3 by mutation of Q646 residue to glutamic acid and P651 residue to arginine to convert TRPV3 channel to TRPV2 like.

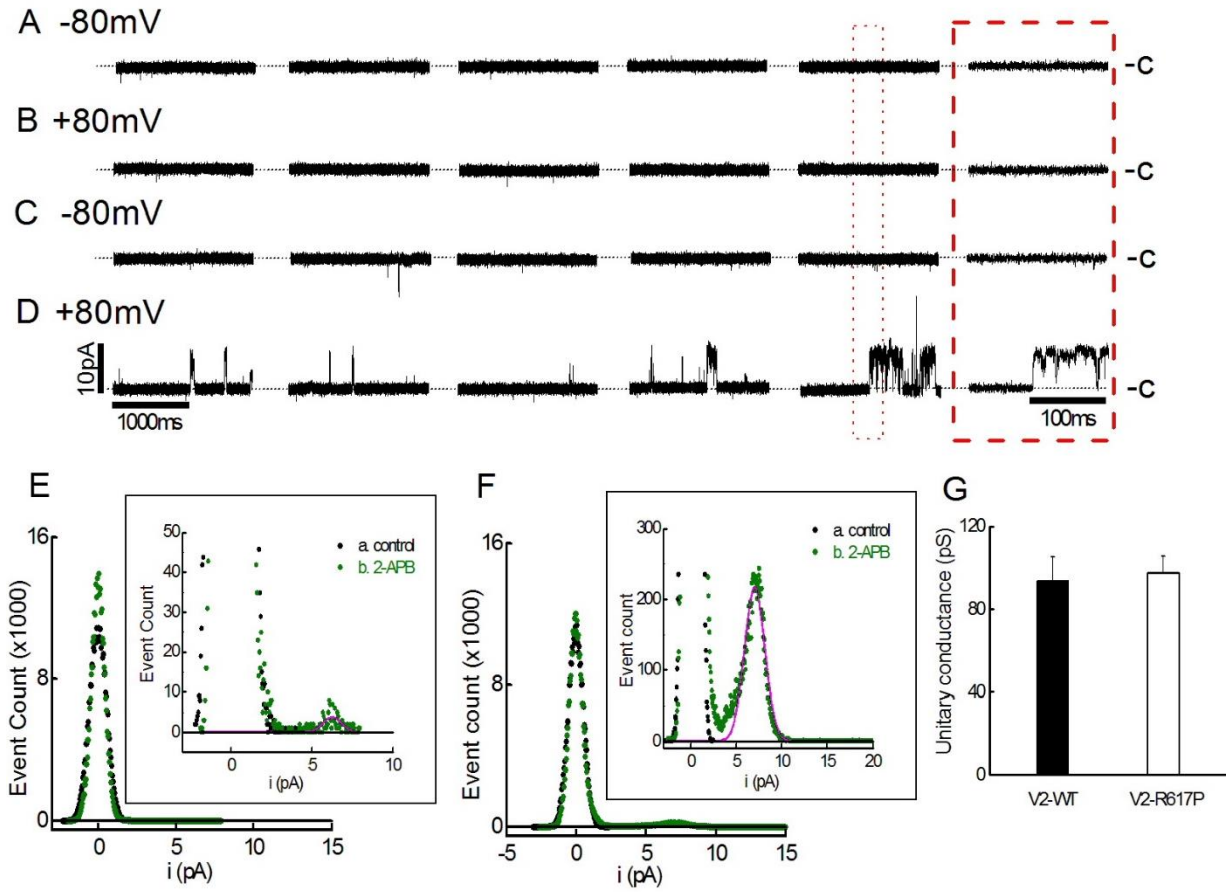

Figure 19: 2-APB induced R619P mutant TRPV2 activities in excised membrane patches.

HEK-293 cell is transfected with the EGFP-R619P-rTRPV2 mutant channel and subjected to excised inside-out patch clamp electrophysiology. The membrane is then stepped to -80 or +80 mV. Leak-subtracted zero current amplitudes are presented with closed channel state (c) indicated by dashed lines. **A, B.** Currents recorded at 5 different time intervals in a representative patch at -80 mV (**A**) or +80 mV (**B**) under control conditions are shown. Note that no channel openings are observed. **C, D.** Addition of 500 μM 2-APB to the bath (cytosolic face of the patch) elicits sporadic channel activity at -80 mV (**C**), while larger channel activity is observed in +80 mV (**D**). The red box shows an enlarged view of single channel activity across 200 ms. **E, F.** All-points histograms of the data shown in panels **A-D** in the absence (control, black circles) and presence (green circles) of 500 μM 2-APB measured at -80 mV (**E**) or +80 mV (**F**) are shown. ***Insets*** show expanded views of the data in panels **E** and **F**. Lines represent fits of the data to Gaussians; the position of the first major peak is 6.2 pA at -80 mV (**E,** magenta line) and 6.9 pA at +80 mV (**F,** magenta line). **G.** The unitary conductance is calculated from the unitary current by the equation 5. Compared to the wild-type rat TRPV2 channel, R619P mutant did not change unitary conductance. Wild-type TRPV2 channel has unitary conductance of 93.4 ± 12.0 pS (n = 7), while R619P mutant have 97.4 ± 8.2 pS (n = 4). No statistical difference is observed (p = 0.84). Statics is analyzed by student t-test with $\alpha<0.05$ for significance.

The mutagenesis is introduced to TRPV2 and TRPV3 respectively by PCR and cloned into EGFP vector.

The resulting EGFP-R619P-rTRPV2 protein is then expressed in HEK-293 cells and subjected to excised

inside-out patch clamp electrophysiology. Similar to wild-type TRPV2, no channel activity is observed under control condition (Fig 19A, 19B). TRPV2 and TRPV3 common activator 2-APB is then superfused to elicit current[27]. The addition of 500 μM 2-APB elicit sporadic channel activity when the membrane is stepped to -80mV, but 500 μM 2-APB elicit robust channel activity when the membrane is stepped to +80 mV (Fig 19C, 19D). Consistently with wild-type channel, larger NPo is observed when the membrane is stepped to +80 mV, however, the reason for sporadic channel activity in -80 mV is not clear (Fig 19C, 19D). Note that subconductance is still observed (Fig 19D). Also consistent with the wild-type TRPV2 channel, the Gaussian fit of all point histogram shows 2-APB induced unitary current is 6.2 pA at -80mV membrane step and 6.9 pA at +80 mV membrane step (Fig 19E, 19F). As expected from wild-type channel, no change in unitary current is observed (Fig 19E, 19F). Wild-type TRPV2 had unitary conductance of 93.4 ± 12.0 pS (n = 7), while R619P mutant have 97.4 ± 8.2 pS (n = 4). Student t-test shows there are no differences between unitary conductance of wild-type and R619P mutant channel. ($p = 0.84$). This result clearly shows abolishing charged residue at 619 position does not convert TRPV2 to TRPV3 like. However, the question remains whether if removal of both E614 and R619 residues convert TRPV2 to TRPV3 like.

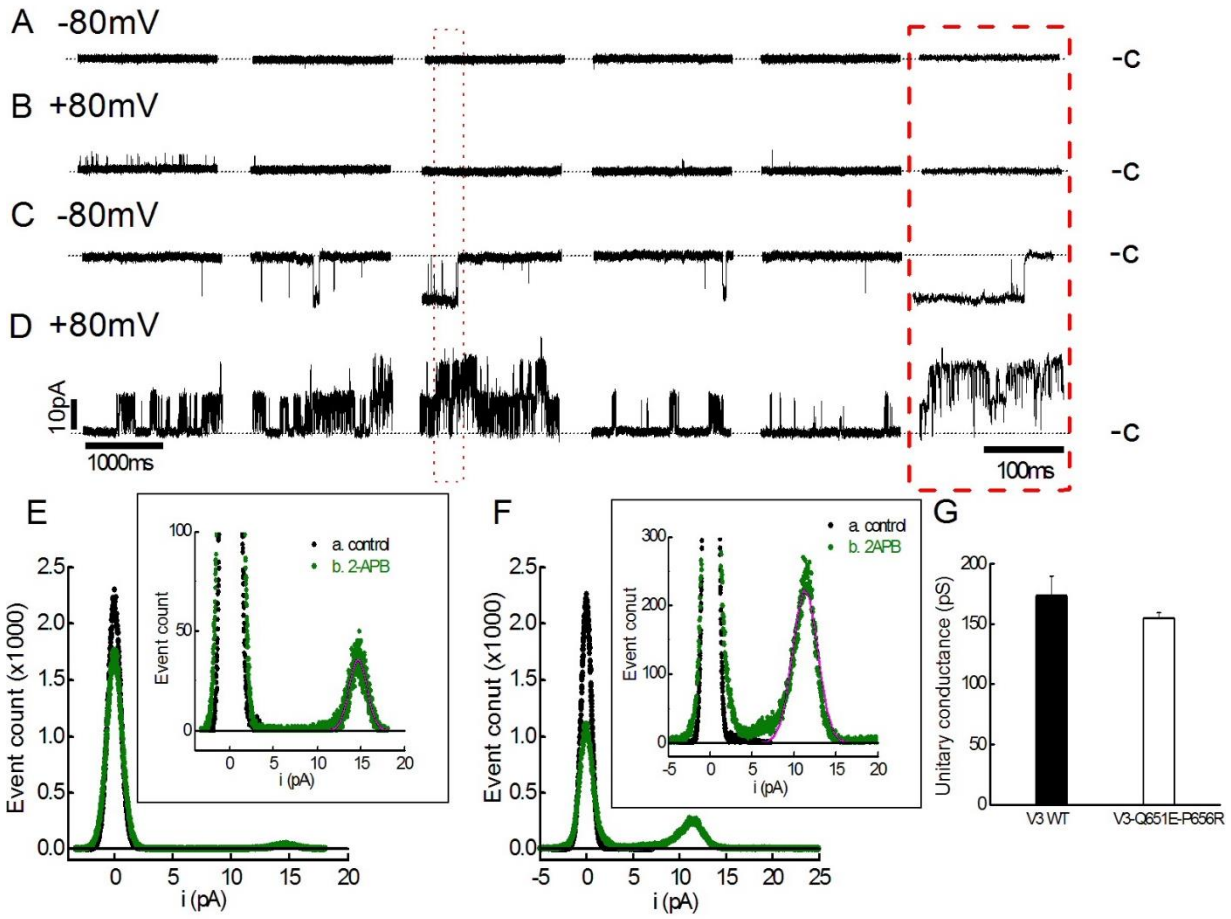

Figure 2014: 2-APB induced Q651E-P656R mutant TRPV3 activities in excised membrane patches.

HEK-293 cell is transfected with the EGFP-Q651E-P656R-hTRPV3 mutant channel and subjected to excised inside-out patch clamp electrophysiology. Membrane potential is clamped to -80 mV **(A)** and +80 mV **(B)**, and 5 different time intervals in a representative patch is shown. Leak-subtracted zero current amplitudes are presented with closed channel state (c) indicated by dashed lines. **A.** No channel openings are observed when the membrane potential is stepped to -80 mV under control condition. **B.** Occasional channel opening is found when the membrane potential is stepped to +80mV under control condition. **C, D.** Addition of 40μM 2-APB to the cytosolic face of the patch elicits channel activity at both -80 mV (**C**) and +80 mV (**D**). Consistently with wild-type channel, more channel activity is found in +80mV membrane step. The red box shows an enlarged view of single channel activity across 200 ms. **E, F.** All-points histograms of the data shown in panels **A**-**D** in the absence (control, black circles) and presence (green circles) of 40 μM 2-APB measured at -80 mV (**E**) or +80 mV (**F**) are shown. ***Insets*** show expanded views of the data in panels **E** and **F**. Lines represent fits of the data to Gaussians; the position of the first major peak is 14.6 pA at -80 mV (**E**, magenta line) and 11.2 pA at +80 mV (**F**, magenta line). **G.** The unitary conductance is calculated from the unitary current by formula G=I/V. Compared to the wild-type rat TRPV2 channel, Q651E-P656R-TRPV3 mutant did not change unitary conductance. Wild-type TRPV3 channel has a unitary conductance of 173.3 ± 16.5 pS (n = 4), while Q651E-P656R mutant has a unitary conductance of 154.6 ± 4.5 pS (n = 3). No statistical difference is observed (p = 0.34).

To address this question equivalent residues of hTRPV3 Q646 and P651 residues are mutated to glutamic acid and arginine, making hTRPV3 channels to TRPV2 like. EGFP-Q651E-P656R-hTRPV3 mutant channel is created by PCR mutagenesis and cloning. Then HEK-293 cells expressing EGFP-Q651E-P656R-hTRPV3 protein is subjected to excised inside-out patch clamp electrophysiology. Similar to the wild-type hTRPV3 sporadic channel openings are observed under control condition when the membrane is stepped to +80mV (Fig 20B), but no channel activities are observed when stepped to -80mV (Fig 20A). As expected superfusion of 40 μM 2-APB to cytosolic face elicit robust channel activity (Fig 20C, 20D). Note the single channel activities have a clearly definable open state similar to wild-type TRPV3 (Fig 20D). Gaussians fit of all point histogram reveals unitary current of 14.6 pA at -80 mV (Fig 20E, magenta line) and 11.2 pA at +80 mV (Fig 20F, magenta line). Q651E-P656R-hTRPV3 mutant channels have a unitary conductance of 154.6 ± 4.5 pS (n = 3) while wild-type TRPV3 channels have a unitary conductance of 173.3 ± 16.5 pS (Fig 20G, n = 4). There is no statistical difference between two groups ($p = 0.34$). Results clearly show the addition of charged amino acid at Q651 and P656 site does not reduce the size of the unitary conductance of TRPV3. The Q651E-P656R mutation did not significantly reduce TRPV3 channel unitary conductance, nor make TRPV3 single channel current flickering. Together with R619P-rTRPV2 mutant single channel activity we conclude, there is E651 and K656 residue does not regulate unitary conductance in TRPV channels. However, does E651 and K656 mutation cause further change in biophysical properties remains to be explored.

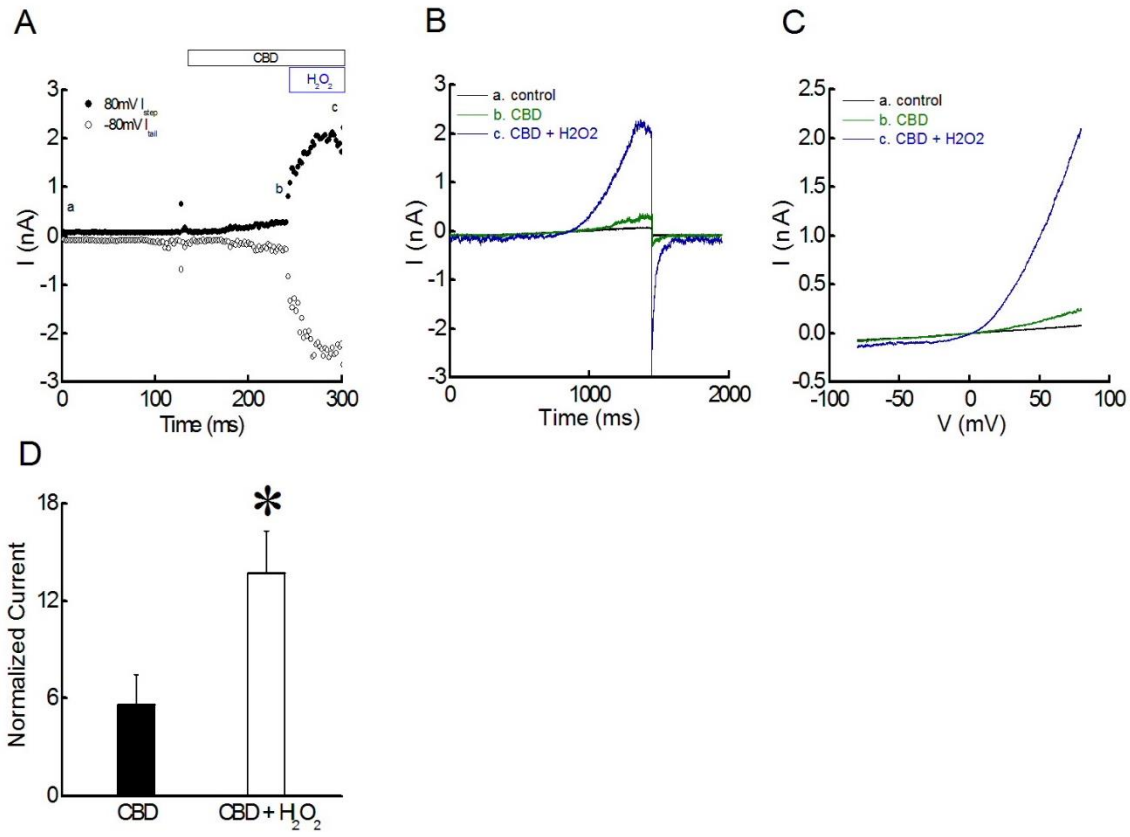

Figure21: CBD induced TRPV2 current is enhanced by H_2O_2.

A representative HEK-293 cell expressing EGFP-rTRPV2 is voltage clamped in the whole-cell mode to measure rTRPV2 current response to voltage ramp. **A.** Application of 300 µM CBD induces TRPV2 current slowly increase I_{step} (black circle) and I_{tail} measured (white circle). TRPV2 current is further increased by the addition of 1mM H_2O_2. Currents in panels B and C were measured at the times indicated by letters: a., control; b., 2-APB; c., 2-APB + RuR **B.** The representative current response to voltage ramp is shown under control (black line), 300 µM CBD (green line) and 300 µM CBD plus 1 mM H_2O_2 (blue line). H_2O_2 enhances both outward current and I_{tail} of rTRPV2 channels but did not increase in the inward current of TRPV2 channel. **C.** I-V relations measured in the absence and presence of CBD and H_2O_2 (data from panel B) are shown. I-V relation shows an increase of outward current in TRPV2 following the addition of H_2O_2. Currents in panels B and C were measured at the times in panel **A** indicated by letters: a., control; b., 2-APB; c., 2-APB + RuR. **D.** On average tail current of TRPV2 measures 0.8 ± 0.4 nA if CBD is applied and further increased to 1.9 ± 0.5 nA if CBD and H_2O_2 are applied together. Application of H_2O_2 and CBD (n=4) increase the normalized I_{tail} by 13.7 ± 2.6 times to that of control current while CBD alone (n=4) increased normalized I_{tail} to 5.6 ± 1.8 times of control. A significant difference is found between two groups ($p<0.05$; df = 6). * indicate the mean of normalized I_{tail} between CBD group and CBD + H_2O_2 group is significantly different measured by student t-test with $\alpha<0.05$ for a significant difference between groups.

7. Hydrogen peroxide enhances cannabidiol induced TRPVs current

TRPV2 channel is known to mediate pro-inflammatory activation of macrophages and leukocytes[64,66,68]. However, how do pro-inflammatory stimuli, such as LPS, alters TRPV2 channel gating is largely unknown. Activated microglia is known to produce ROS for signaling and bacterial killing. Furthermore, other TRP channels such as TRPV1 current is known to be enhanced by ROS such as H_2O_2[111,112]. Given their similarity, we hypothesized TRPV2 current may also enhance by H_2O_2.

To study the H_2O_2 effect on TRPV2, EGFP-tagged TRPV2 transfected HEK-293 cells are subjected to whole cell voltage clamp while a voltage ramp protocol from -80 mV to +80 mV (1 s duration) is repeatedly applied. As expected no TRPV2 current are detected under control condition (Fig 21A, 21B black line), and the addition of 300 μM cannabidiol to be bath (extracellular face) induces both +80mV step current and -80mV tail current (Fig 21A, 21B green line). Co-application of 1mM H_2O_2 and 300 μM CBD further increase both 80mV step current and -80mV tail current (Fig 21A, 21B blue line). I-V curve shows no current under control condition (Fig 21C black line), and 300μM CBD induces outward rectified current as expected (Fig 21C green line). The addition of 1 mM H_2O_2 increases the outward current but did not enhance the inward current (Fig 21C blue line). On average, 300 μM CBD induces a tail current of 0.84 ± 0.37 nA while co-application of 1mM H_2O_2 and 300 μM cannabidiol induces tail current equals to 1.9 ± 0.5 nA (Fig 21D). Our result shows H_2O_2 significantly increases CBD induced TRPV2 current ($p=0.04$; Fig 21D). As expected from published TRPV1 study H_2O_2 enhances TRPV2 channel sensitivity to agonist[111,112].

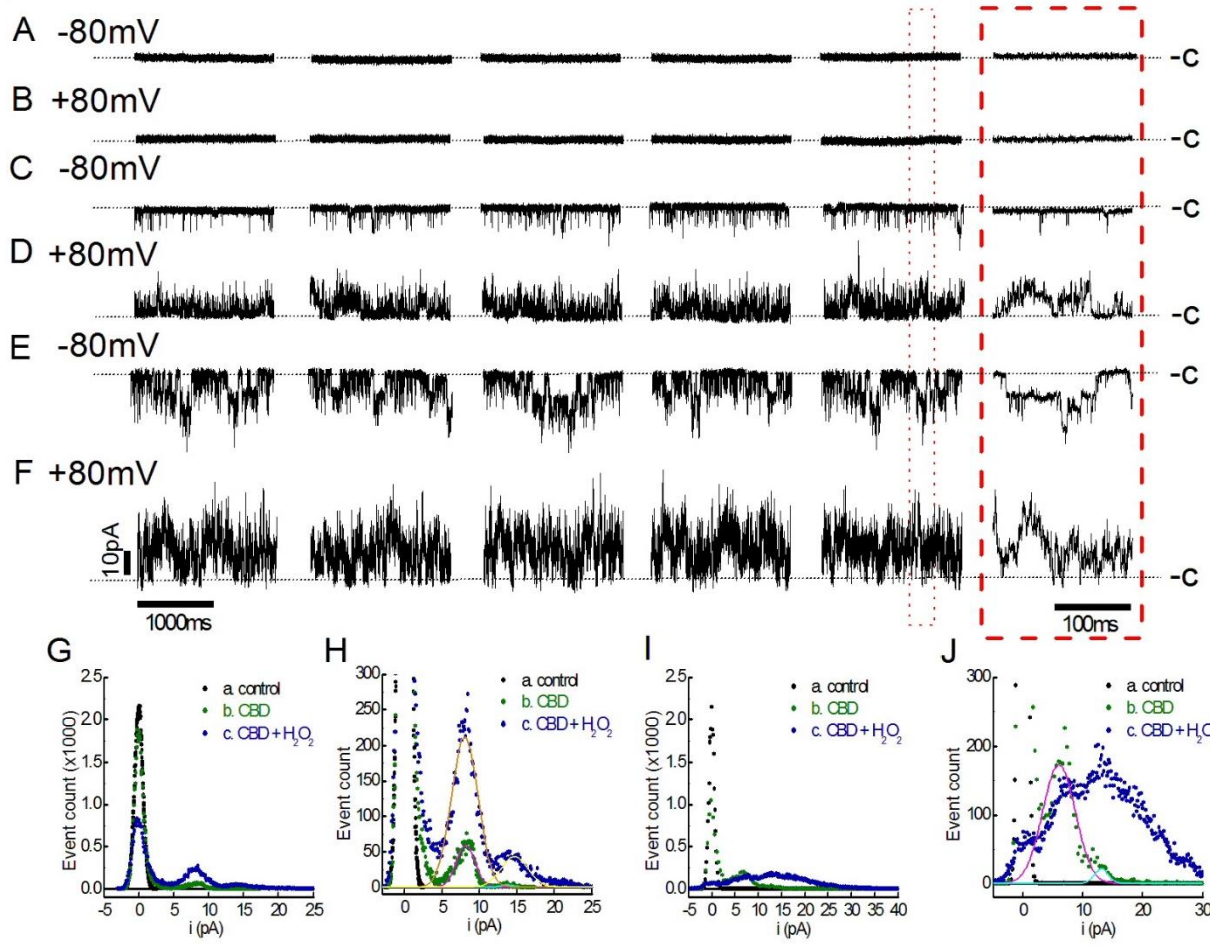

Figure 22: CBD and H_2O_2 induced TRPV2 activities in excised membrane patches.

HEK-293 cell is transfected with EGFP-rTRPV2 and subjected to excised inside-out patch clamp electrophysiology. Dash lines indicate leak-subtracted zero current amplitudes, which correspond to the closed channel state (c). **A, B.** No channel opening is observed under control condition whether the membrane is stepped to -80 mV (**A**), or to +80 mV (**B**). **C, D.** Application of 300 µM CBD to cytosolic face elicit TRPV2 opening in -80 mV (**C**), and +80 mV (**D**). Note the channel activity is larger in +80 mV step compared to -80 mV step. **E, F.** Addition of 1 mM H_2O_2 further increased channel opening compared to CBD alone in both -80 mV (**E**) and +80mV (**F**) steps. The highly erratic activity of TRPV2 channel is observed. The red box shows an enlarged view of single channel activity across 200 ms. **G.** All point histogram shows a current response to -80 mV membrane step measured across 20 seconds (data in **A, C, E**). **H.** Enlarged view of panel **G**. Only 0 current peak is found in control condition (black circle). The addition of CBD induces open channel peaks (green circle) and co-application of CBD and H_2O_2 further increased the size of open channel peaks (blue circle). The addition of H_2O_2 did not cause a shift of open channel peak compared to CBD alone. CBD induced unitary current first major peak equals to 8.1 pA and second major peak of equals to 13.7 pA. Co-application of CBD and H_2O_2 induces first major peak equals to 8.0 pA and second major peak equals 14.7 pA. **I.** All point histogram of the current response to +80mV membrane step measured across 20 seconds (data in **A** control black circle, **D** CBD green circle, and **F** CBD + H_2O_2 blue circle). **J.** Enlarged view of panel **I**. CBD induced TRPV2 current (green circle) has single TRPV2 channel opening with first major peak equals 5.9 pA and second major peak equals 13.4 pA. The addition of H_2O_2 to CBD induces highly erratic TRPV2 channel activity with possibly high channel noise and the existence of sub-conductance state at +80mV that precludes unambiguous determination of the single current amplitude (blue circle).

Whole cell current can be denoted by formula as *I=NiPo* (equation 6). To better understand whether H_2O_2 alters NPo or i, excised inside-out patch clamp electrophysiology were used to observe the effect of H_2O_2 on CBD induced current in EGFP-tagged TRPV2 expressing HEK-293 cells. Under control condition, no current was observed in representative records whether membrane potential was stepped to -80 mV (Fig 22A) or to +80 mV (Fig 22B). Application of 300 μM CBD induced TRPV2 channel activation at both -80mV membrane step (Fig 22C) and +80 mV membrane step (Fig 22D). Again higher single channel actives are observed in +80 mV membrane step compared to -80mV membrane step. Co-application of 1 mM H_2O_2 and 300 μM CBD further increased TRPV2 channel activates in both -80 mV and +80 mV step (Fig 22E, 22F). When membrane potential was stepped to +80 mV, co-application of H_2O_2 and CBD increased TRPV2 channel activity too high to discern closed channel state (Fig 22F). All point histogram shows that co-application of CBD and H_2O_2 did not change the unitary current of TRPV2 in -80 mV step (Fig 22G, 22H). As expected, no open channel peaks were observed under control condition in -80 mV membrane step (Fig 22G black circle) or +80 mV membrane step (Fig 22I, black circle). The addition of 300 μM CBD induced two major open channel peaks in -80 mV membrane step (Fig 15G, 15H green circle) and in +80mV membrane step (Fig 22G, 22H green circle). In -80 mV membrane step, the first major peak has a unitary current of 8.1pA (Fig 22H magenta line), and the second major peak has a unitary current of 13.7pA (Fig 22H cyan line). Co-application of CBD and H_2O_2 robustly increased the size of open channel peaks but did not change the unitary current of the open channel peaks (Fig 22H). Gaussian fit shows first major open channel peak have a unitary current of 8.0 pA (Fig 22H orange line), and second major open channel peak have a unitary current of 14.7 pA (Fig 22G, 22H). In +80mV membrane step, 300μM CBD induced two major open channel peaks in all point histogram (Fig 22I, 22J). First major peak has a unitary current of 5.9 pA (Fig 22J magenta line) and the second peak has the unitary current of 13.4pA (Fig 22J cyan line). At +80 mV membrane step, it was not able to measure the unitary current of CBD and H_2O_2 co-application as all point histogram was too flat and widespread for successful Gaussian fit (Fig 22I, 22J). This result highlight ability of H_2O_2 enhancing TRPV2 *Po*

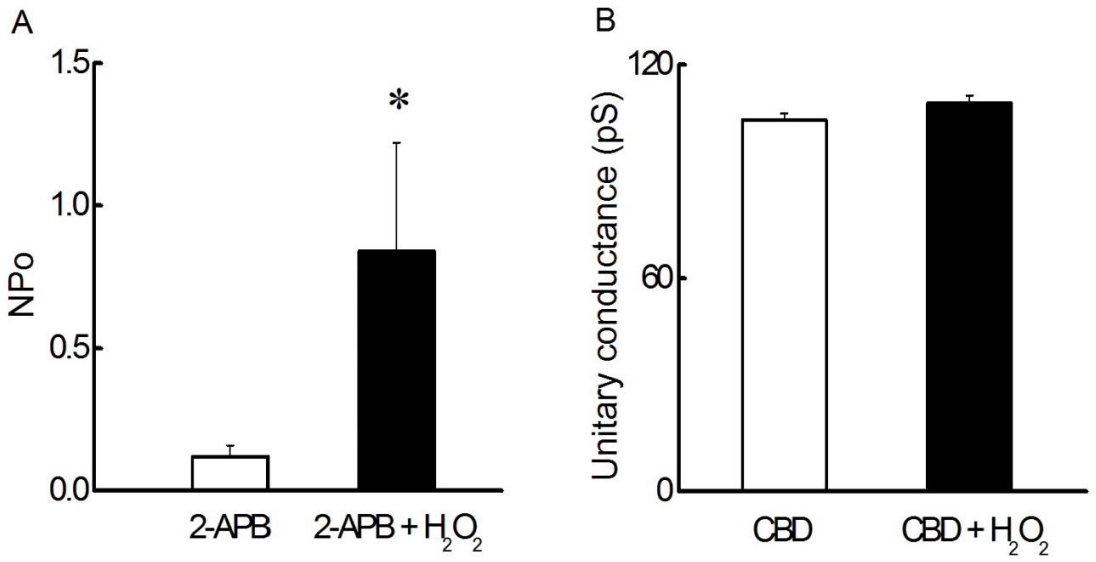

Figure 153: H_2O_2 effect on CBD induced TRPV2 unitary current.

NPo is measured by Clampfit single channel search program (see Method 7f) and unitary current are measured by Gaussian fit from the open channel peak of all point histogram. **A.** NPo of CBD induced TRPV2 activation is enhanced significantly by H_2O_2 ($p = 0.05$). NPo under CBD condition equals to 0.12 ± 0.04, and CBD + H_2O_2 equals 0.84 ± 0.38. **B.** Unlike NPo, unitary current did not change significantly with or without addition of H_2O_2 ($p = 0.15$). CBD induced unitary current equals to 8.4 ± 0.1pA and CBD plus H_2O induced unitary current of 8.7 ± 0.2. This result shows H_2O_2 enhances TRPV2 by increases its NPo. Statics is analyzed by student t-test with $\alpha<0.05$ for significance.

too high, converting the measurement of the single channel current to macroscopic current. Co-application of CBD and H_2O_2 significantly increased NPo of TRPV2 (NPo = 0.84 ± 0.38) compared to CBD alone (0.12 ± 0.04, p = 0.05, Fig 23A). However, no statistically significant difference were found between unitary conductance of CBD induced TRPV2 current (8.4 ± 0.1 pA) and CBD plus H_2O_2 induced TRPV2 current (8.7 ± 0.2 pA, p = 0.15, Fig 23B). This result confirms that H_2O_2 enhances NPo but not the unitary current of TRPV2.

The question remains whether if H_2O_2 enhances CBD effect on TRPV2, or CBD and H_2O_2 function separately to activate the TRPV2 channel. To examine whether H_2O_2 alone have the ability to activate TRPV2 channel, excised inside-out voltage clamp electrophysiology were used to measure the current response of EGFP-tagged-rTRPV2 channel to the H_2O_2 application. As expected no channel opening were found under control condition (Fig 24A, 24B). Application of 1 mM H_2O_2 (Fig 24C, 24D), or 10 mM H_2O_2

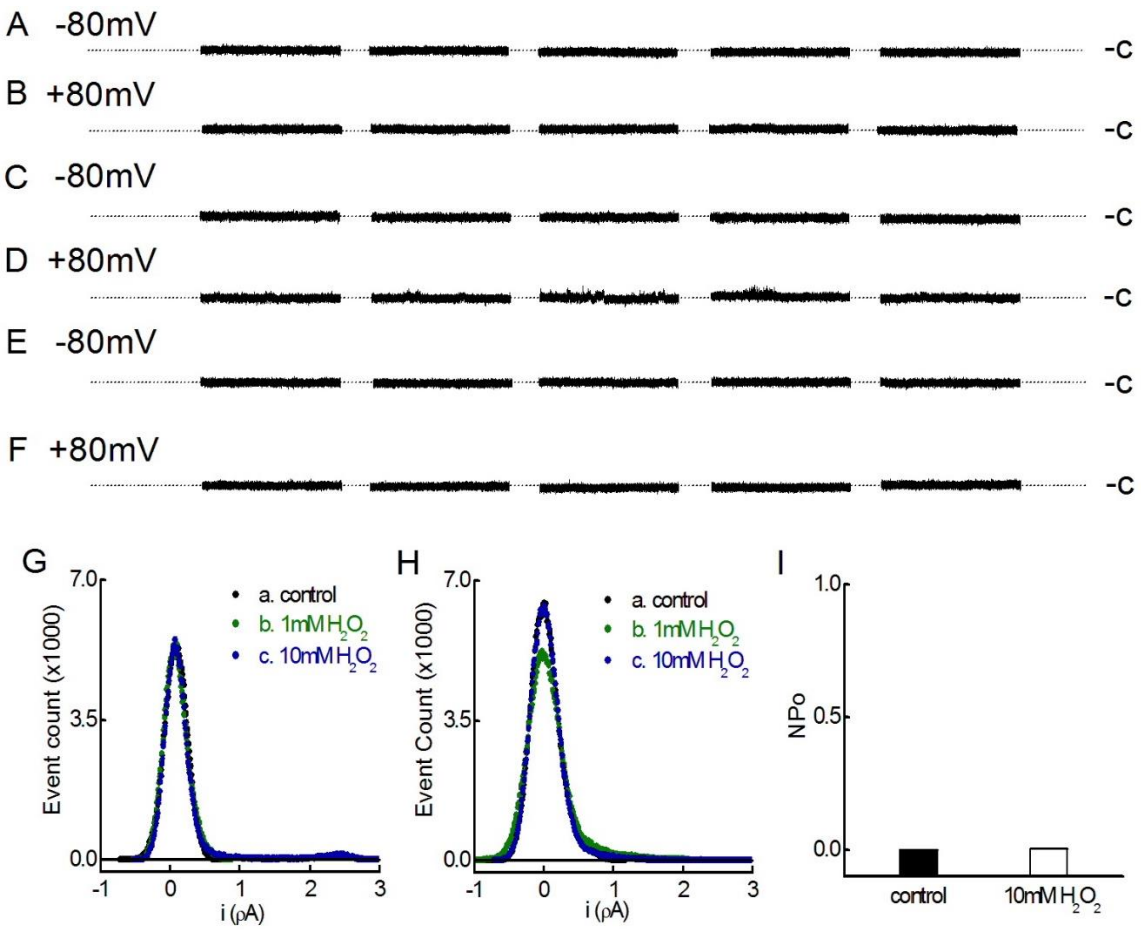

Figure 24: H_2O_2 alone does not activate TRPV2.

Currents recorded in a representative inside-out patch excised from a HEK-293 cell expressing EGFP-rTRPV2 are measured in the absence and presence of H_2O_2 (1 mM or 10 mM) at -80mV or +80mV. Dash lines indicate the leak-subtracted zero current amplitude, which corresponds to the closed-channel state (c). 5 representative time intervals are shown for each of following experimental conditions; control condition (no H_2O_2) at -80mV (**A**) or +80mV (**B**); 1 mM H_2O_2 at -80 mV (**C**) or +80 mV (**D**); 10mM H_2O_2 at -80 mV (**E**) or +80mV (**F**). Note that no channel openings are detected. **G.** All-points histograms of data shown in panels **A, C, E (**control, black circles; 1 mM H_2O_2, green circles; 10 mM H_2O_2, blue circles). **H.** All-points histograms of data shown in panels **B, D, F (**control, black circles; 1 mM H_2O_2, green circles; 10 mM H_2O_2, blue circles). Data in G and H represent 18 seconds of total recording time are shown. **I.** NP_O values are calculated from discrete event analysis of 18 s recordings under the conditions shown in A-F **(**Single Channel Search, Clampfit 10).

(Fig 24E, 24F) did not elicit channel activity in representative traces regardless -80 mV or +80 mV membrane steps. All point histogram confirms that no open channel peak is observed in 0 mM, 1 mM or 10 mM H_2O_2 application (Fig 24G, 24H). No channel opening was detected by single channel search

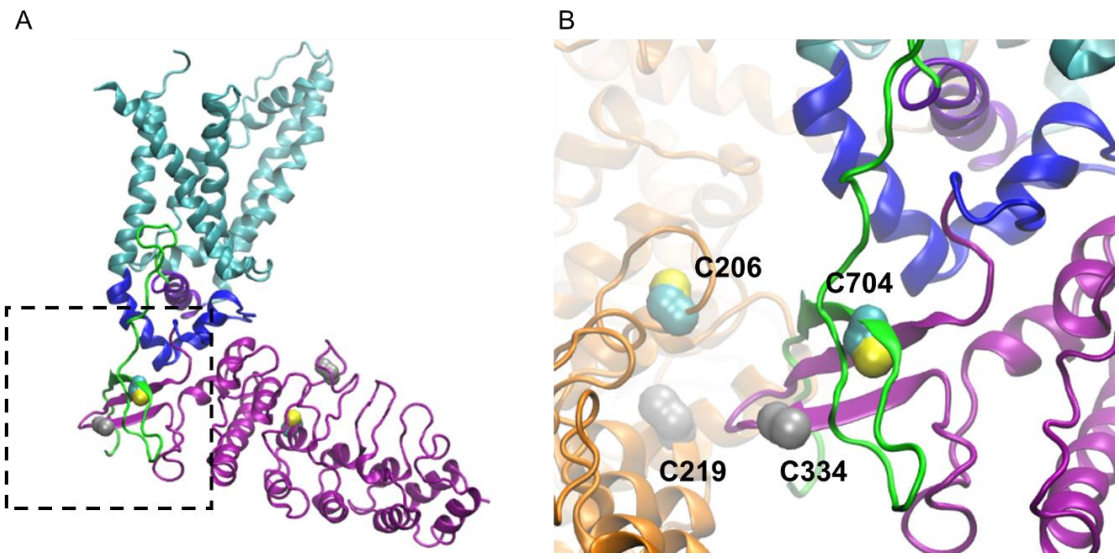

Figure 25: Locations of candidate Cys residues at the inter-subunit interface between ARDs in TRPV2.

A. Structure of one subunit in TRPV2 tetrameric channel is shown in ribbon representation. Four cysteine residues tested in this study are shown in space filling representation. Domains and motifs are individually colored for clarity: ARD, magenta; HLH linker, blue; S1-S6 TM domain, cyan; TRP helix, purple; CTD, green. The point of contact between ARDs in adjacent subunits is indicated by the black box, which is magnified in panel B. **B.** Selected Cys residues are shown in space filling representation (cyan, carbon; yellow, sulphur). C206 and C219 residues in one TRPV2 subunit (orange ribbons) are located close to C343 and C704 in the neighboring subunit (colored as in panel A). The proximity of these residues to one another suggests that inter-subunit disulfides bonds could form, and might constrain the relative positions of ARDs that favors an open-channel conformation. Representations shown here are based on the TRPV2 cryo-EM structure (pdb: 5hi9) determined by Huynh, et al. (2016)[1]. Graphical representations were created using VMD 1.9.3.

program of Clampfit software (Fig 24I). The result indicates H_2O_2 only have the ability to enhance CBD induced TRPV2 current but may not activate TRPV2 channel by itself.

To summarize, H_2O_2 enhances CBD induced TRPV2 channel activation, but may not activate TRPV2 channel by itself. Unlike DCPIB, H_2O_2 did not affect unitary conductance of TRPV2 but only affected NPo of TRPV2. H_2O_2 is commonly produced during immune cell activation[75]. This result indicates TRPV2 may be primed to activate in the environment with high inflammation and high ROS activity.

8. Cysteine residues in ARD domain is crucial for hydrogen peroxide sensitivity

The rotation of ARD in TRPV channels are thought to trigger TRPV channel activation. For example, the rotation of ARD during heating the environment is thought to drag transmembrane domains to induce conformational change leading to the opening of TRPV channel gate[29]. ARD domain in TRPV channels contains multiple cysteine residues which can serve as a site for H_2O_2 modulations. The cysteine residues in ARD are shown to form disulfide bonds with neighboring CTD in TRPV1[38]. The formation of disulfide connection can stabilize open channel state or closed channel state, and therefore promote opening or closing of TRPV channel[38]. TRPV2 channel contains four cysteine residues that locate closely to cysteine residues of neighboring subunits (Fig 25A). Cysteine 206 (C206) and cysteine 219 (C219) on ARD of one TRPV2 subunit are located near cysteine 334 (C334) on ARD and cysteine (C704) on CTD neighboring TRPV2 subunits (Fig 25B). Of those residues, C206 and C334 are unique to TRPV2 and not conserved in TRPV1 or TRPV3. The formation of inter-subunit or intra-subunit disulfide connections between ARD domains may lock the ARD domain to promote the open state. We hypothesize that mutation of those cysteine residues abolished H_2O_2 sensitivity in TRPV2 channels.

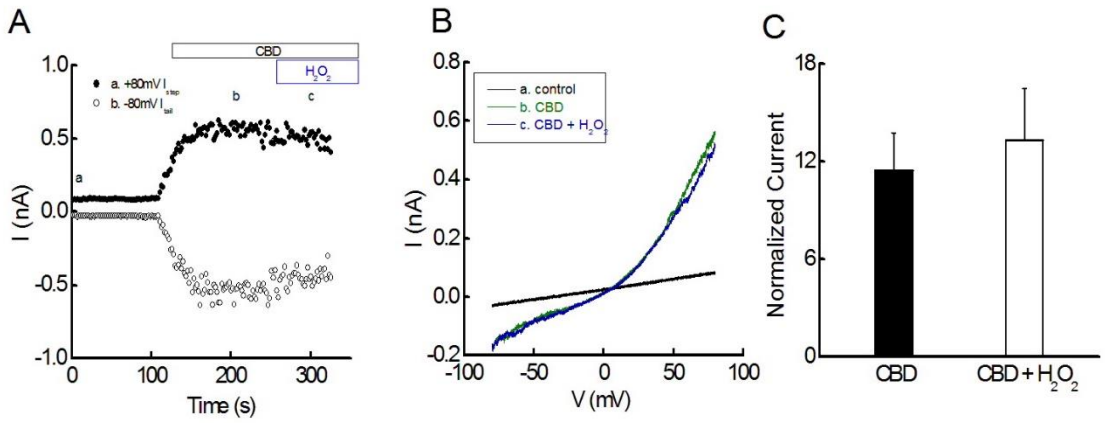

Figure 166: CBD induced current in TRPV2 C206A is not potentiated by H_2O_2.

Point mutation of C206A are introduced to TRPV2 channels using PCR. Then a representative HEK293 cell expressing GFP-C206A-rTRPV2 is voltage clamped in the whole-cell mode. **A.** I_{step} at +80mV and I_{tail} at -80mV are measured across time. Addition of 300 μM CBD to bath (extracellular face) elicits both I_{step} at +80mV and I_{tail} at -80mV, but co-application of 1mM H_2O_2 together with 300 μM CBD (CBD + H_2O_2) did not enhance current amplitude. **B.** Ramp I-V relations measured under control (a, black line), CBD (b, green line) and CBD + H_2O_2 (c. blue line) are shown. I-V curve of CBD induced current overlaps with the I-V curve in CBD + H_2O_2, indicating H_2O_2 did not enhance the CBD induced TRPV2 current at any voltage. Currents were measured at the times in panel **A** (a., control; b., CBD; c., CBD + H_2O_2). **C.** Mean normalized currents in the presence of CBD (black bar; 13.30 ± 3.19-fold increase compared to control) or CBD + H_2O_2 (open bar; 11.42 ± 2.32 fold increase compared to control)) are not different (P =0.48, df = 6, n = 4 each).

Mutation of four subunits was introduced into EGFP-tagged rTRPV2 by site-directed mutagenesis and then cloned mutant channel protein are transfected into HEK-293 cells (see Method 1 and 2). Then mutant channel expression HEK-293 cells were subjected to whole cell voltage clamp, and a voltage ramp protocol from -80 mV to +80 mV (1 s duration) is repeatedly delivered to the cell in the absence and presence of 300 μM CBD. C206 to alanine (C206A) mutation abolished the H_2O_2 sensitivity in TRPV2. No current are detected under control condition, while the addition of CBD to cytosolic face increased both +80mV steady state step (I_{step}) and -80mV instantaneous tail current (I_{tail}) in the C206A-TRPV2 mutant (Fig 26A). However, co-application of H_2O_2 with CBD did not enhance those currents (Fig 19A). CBD and H_2O_2 co-application induced current (Fig 26B black line) showed same I-V relation compared to CBD induced C206A-TRPV2 current (Fig 26B green line). To measure H_2O_2 induced current increase, -80mV I_{tail} are normalized to control. CBD alone increased -80mV I_{tail} by 11.42 ± 2.32 fold compared to control, while CBD plus H_2O_2 increased I_{tail} by 13.30 ± 3.19 fold compared to control (Fig 26C). No significant change is detected (p=0.48; Fig 19C), indicating removal of C206 abolished H_2O_2 effect on TRPV2.

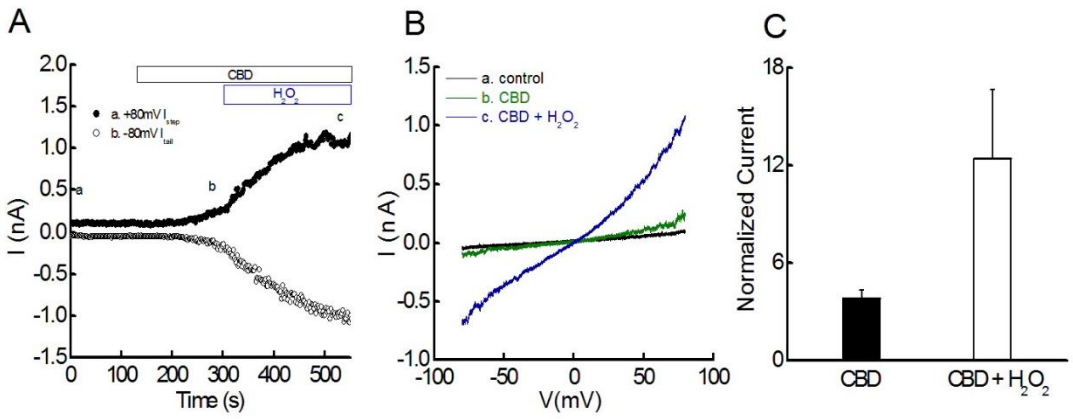

Figure 27: CBD induced C219A mutant TRPV2 current is enhanced by H_2O_2.

Point mutation of C219A is introduced to TRPV2 channels using PCR. The representative HEK-293 cell expressing EGFP-C219A-rTRPV2 is voltage clamped in the whole-cell mode. **A.** I_{step} at +80 mV and I_{tail} at -80 mV are measured over time under control (a), 300 µM CBD (b) and CBD plus H_2O_2 (c). The addition of CBD to extracellular side elicits both I_{step} and I_{tail}. The addition of 1mM H_2O_2 to 300µM CBD elicit larger I_{step} at +80 mV and I_{tail} at -80 mV. **B.** IV relation of representative traces of control (a, black line), CBD (b, green line) and CBD plus H_2O_2 (c. blue line) are shown. 300 µM CBD plus 1 mM H_2O_2 induces an increase in both inward and outward current compared to CBD alone. Currents in panels were measured at the times in panel **A** indicated by letters: a., control; b., CBD; c., CBD + H_2O_2. **C.** CBD increased current 3.8 ± 0.5 fold compared to control and CBD plus H_2O_2 increased TRPV2 current 12.4 ± 4.3 fold compared to control (P =0.12, df = 4, n = 3 each). No statistical difference are found between CBD and CBD plus H_2O_2 condition.

On the other hand, mutation of C219 residue to alanine (C219A) did not alter H_2O_2 sensitivity in TRPV2. As expected, no current are detected under control condition while application CBD increased both +80mV I_{step} and -80 mV I_{tail} in C219A mutant TRPV2 (Fig 27A). However, application of H_2O_2 still enhanced both +80 mV I_{step} and -80mV I_{tail} in C219A-rTRPV2 (Fig 27A). I-V relation of H_2O_2 plus CBD elicits larger inward current and outward current (Fig 27B blue line) compared to that of CBD induced current (Fig 27B green line). Normalized current shows that CBD application causes 3.8 ± 0.5 fold increase in I_{tail} compared to control while CBD plus H_2O_2 increased I_{tail} 12.4 ± 4.3 fold compared to control (Fig 27C). However, co-application of CBD plus H_2O_2 did not induce statistically significant current increase compared to CBD alone (P =0.12, n = 3 each; Fig 27C). Lack of statistical significance is thought to cause by high variability between groups. Increasing sample number may aid to elucidate effect on C219A mutant.

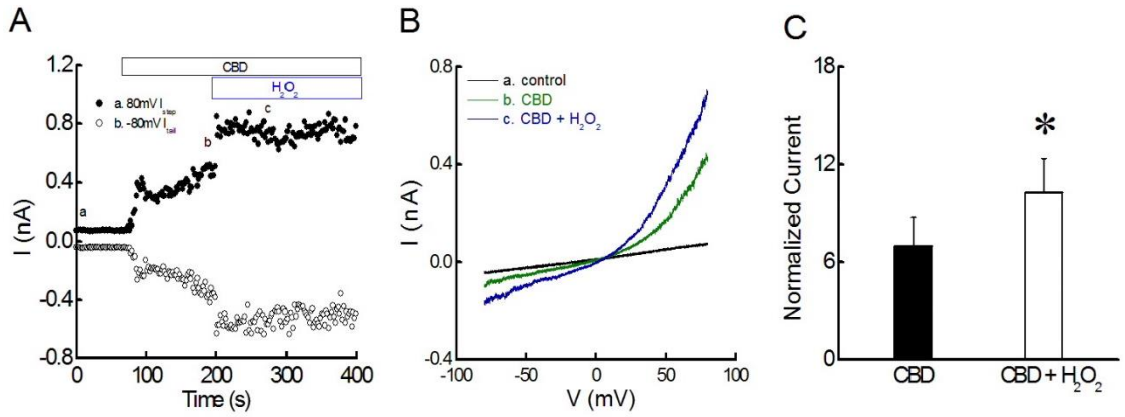

Figure 28: CBD induced C334A mutant TRPV2 current is enhanced by H_2O_2.

Point mutation of C334A is introduced to TRPV2 channels using PCR. The representative HEK-293 cell expressing EGFP-C334A-rTRPV2 is voltage clamped in the whole-cell mode. **A.** I_{step} at +80mV and I_{tail} at -80mV are measured over time under control (a), 300 µM CBD (b) and CBD plus H_2O_2 (c). The addition of CBD to extracellular face elicits both I_{step} and I_{tail} within 20 seconds. The addition of 1 mM H_2O_2 to 300 µM CBD elicit larger I_{step} at +80 mV and I_{tail} at -80 mV. **B.** IV relation of representative traces of control (a, black line), CBD (b, green line) and CBD plus H_2O_2 (c. blue line) are shown. 300 µM CBD plus 1 mM H_2O_2 induces an increase in both inward and outward current. Currents in panels were measured at the times in panel **A** indicated by letters: a., control; b., CBD; c., CBD + H_2O_2. **C.** H_2O_2 increased CBD increased current 7.96 ± 2.27 fold compared to control and CBD plus H_2O_2 increased TRPV2 current 11.3 ± 2.9 fold compared to control. The result shows significant difference between CBD condition current and CBD plus H_2O_2 condition (P =0.02, df = 5, n = 6 each).

Mutation of C334 to alanine (C334A) also did not abolish H_2O_2 effect on TRPV2. As expected, no current were detected under control condition while application CBD increased both +80mV I_{step} and -80mV I_{tail} in C219A mutant TRPV2 (Fig 28A). Both +80mV I_{step} and -80mV I_{tail} were further enhanced by co-application of H_2O_2 and CBD (Fig 28A). CBD induced rectified I-V curve (Fig 28B, green line), and co-application of H_2O_2 and CBD enhanced both inward and outward current (Fig 28B, blue line). Co-application of CBD and H_2O_2 induced a significantly larger normalized current (11.9 ± 2.9 fold increase compared to control) compared to CBD alone (8.0 ± 2.3 fold compared to control, p=0.02; Fig 28C). This result shows mutation of C334A has no effect on TRPV2 H_2O_2 sensitivity.

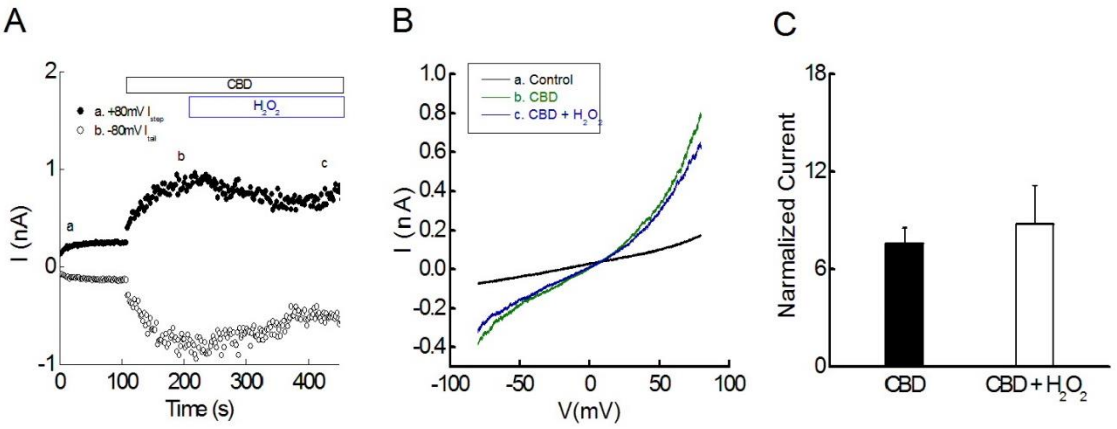

Figure 29: CBD induced C704A mutant TRPV2 current is not enhanced by H_2O_2.

Point mutation of C704A is introduced to TRPV2 channels using PCR. The representative HEK-293 cell expressing EGFP-C704A-rTRPV2 is voltage clamped in the whole-cell mode. **A.** I_{step} at +80mV and I_{tail} at -80mV are measured over time under control (a), 300μM CBD (b) and CBD plus H_2O_2 (c). The addition of CBD to extracellular face elicits both I_{step} and I_{tail}. Note the slow rise of the current. The addition of 1mM H_2O_2 to 300μM CBD did not elicit additional current. **B.** IV relation of representative traces of control (a, black line), CBD (b, green line) and CBD plus H_2O_2 (c. blue line) are shown. Application of 300μM CBD induced an increase in both inward and outward current, while co-application of 1mM H_2O_2 and 300μM CBD did not change the current response. Currents in panels were measured at the times in panel **A** indicated by letters: a., control; b., CBD; c., CBD + H_2O_2. **C.** CBD increased current 7.6 ± 1.0 compared to control and CBD plus H_2O_2 increased TRPV2 current 8.8 ± 2.4 times compared to control. The difference between two groups are significant (P =0.55, n = 3 each). Statistics are analyzed by paired t-test with result considered significantly different if $\alpha<0.05$.

Finally, mutation of C704 residue to alanine (C704A) abolished H_2O_2 sensitivity in TRPV2. No current were detected under control condition (Fig 29A). The addition of 300 μM CBD increased both +80 mV I_{step} and -80mV I_{tail} in the C704A-rTRPV2 mutant, but co-application of 1mM H_2O_2 and 300 μM CBD did not further increase those currents (Fig 29A). I-V curve also shows co-application of CBD and H_2O_2 (Fig 29B, blue line) have same I-V relationship compared to CBD alone (Fig 29B, green line). CBD alone increased -80mV normalized I_{tail} by 11.4 ± 2.3 fold compared to control while CBD plus H_2O_2 increased normalized I_{tail} by 13.3 ± 3.2 fold (Fig 29C). No significant change in normalized I_{tail} was detected (p=0.55; Fig 29C), indicating that C704A mutation abolishes TRPV2 sensitivity to H_2O_2. This result suggests C704 residue is a site for H_2O_2 modulation.

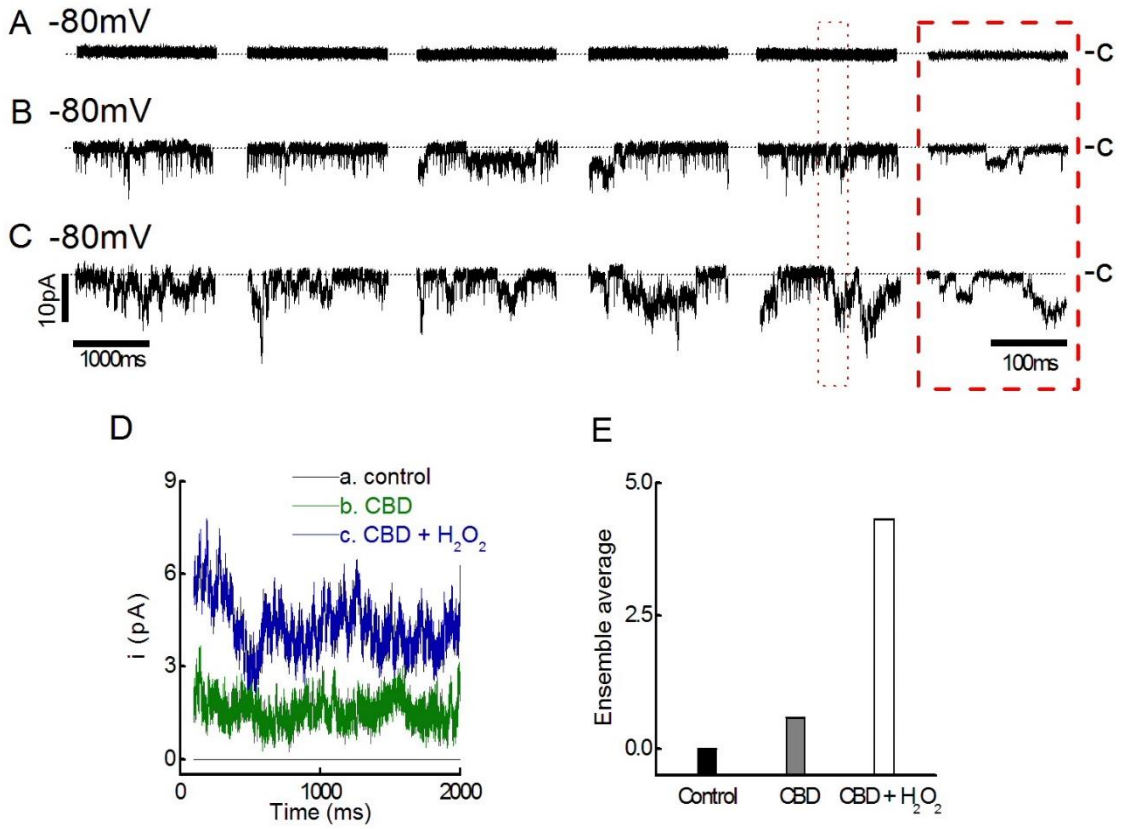

Figure 30: H_2O_2 enhance CBD induced TRPV2 activity in excised membrane patches.

HEK-293 cell is transfected with EGFP- rTRPV2 channel and subjected to excised inside-out patch clamp electrophysiology. The current response to -80 mV membrane potential step is measured. Representative current response across 5 time intervals under control condition (**A**), 300 µM CBD (**B**), and co-application of 300 µM CBD and 1 mM H_2O_2 (**C**) are shown. Dash lines indicate leak-subtracted zero current amplitudes corresponding to the closed channel state (c). **A.** Under control condition, no channel activity are observed. **B.** Application of 300 µM CBD induces the erratic activity of TRPV2 **C.** Addition of 1 mM H_2O_2 on top of 300 µM CBD enhanced TRPV2 activity. The red box shows an enlarged view of single channel activity across 200 ms. **D.** The current response to -80 mV is normalized to control and averaged across 10 sweeps to construct average current response (see Method). The addition of CBD induces current activity (green line) higher than control condition (black line). CBD and H_2O_2 co-application induced current (blue line) that is larger than CBD induced current (green line). **E.** Mean current response in **D** is further averaged to calculate ensemble average current response across 20 seconds of measurement. Co-application of CBD and H_2O_2 further increases channel opening compared to CBD alone.

Those result revealed that cysteine residue at 206 and 704 site is important in H_2O_2 modulation of TRPV2 channel opening. Mutation of either C206A or C704A was sufficient to abolish H_2O_2 sensitivity in TRPV2 channel. In order to confirm C704A mutant abolishes H_2O_2 sensitivity in rTRPV2, excised inside-out patch clamp electrophysiology was utilized. Since CBD and H_2O_2 induced high NPo when membrane step to

+80mV, the effect of CBD and H_2O_2 co-application during -80mV membrane step were used to quantify TRPV2 channel open probability. For control, EGFP-tagged rTRPV2 transfected HEK-293 were subjected to excised inside-out patch. As expected, -80 mV membrane step alone did not cause TRPV2 channel activation in representative traces (Fig 30A). Application of 300 μM CBD elicits rTRPV2 channel opening (Fig 30B). Further addition of 1 mM H_2O_2 induced higher channel activity as expected (Fig 30C). The current response across 18 seconds was collected (Fig 30D) and subjected to ensemble average quantification (Fig 23E). The average current across 10 sweeps are shown in Fig 26D. Co-application of CBD and H_2O_2 induced higher average current trance (Fig 30D, blue line) compared to CBD alone (Fig 30D, green line). Ensemble average shows CBD alone induced 0.6 pA, while co-application of CBD and H_2O_2 induced 4.3 pA current in average across 18 seconds (Fig 30D).

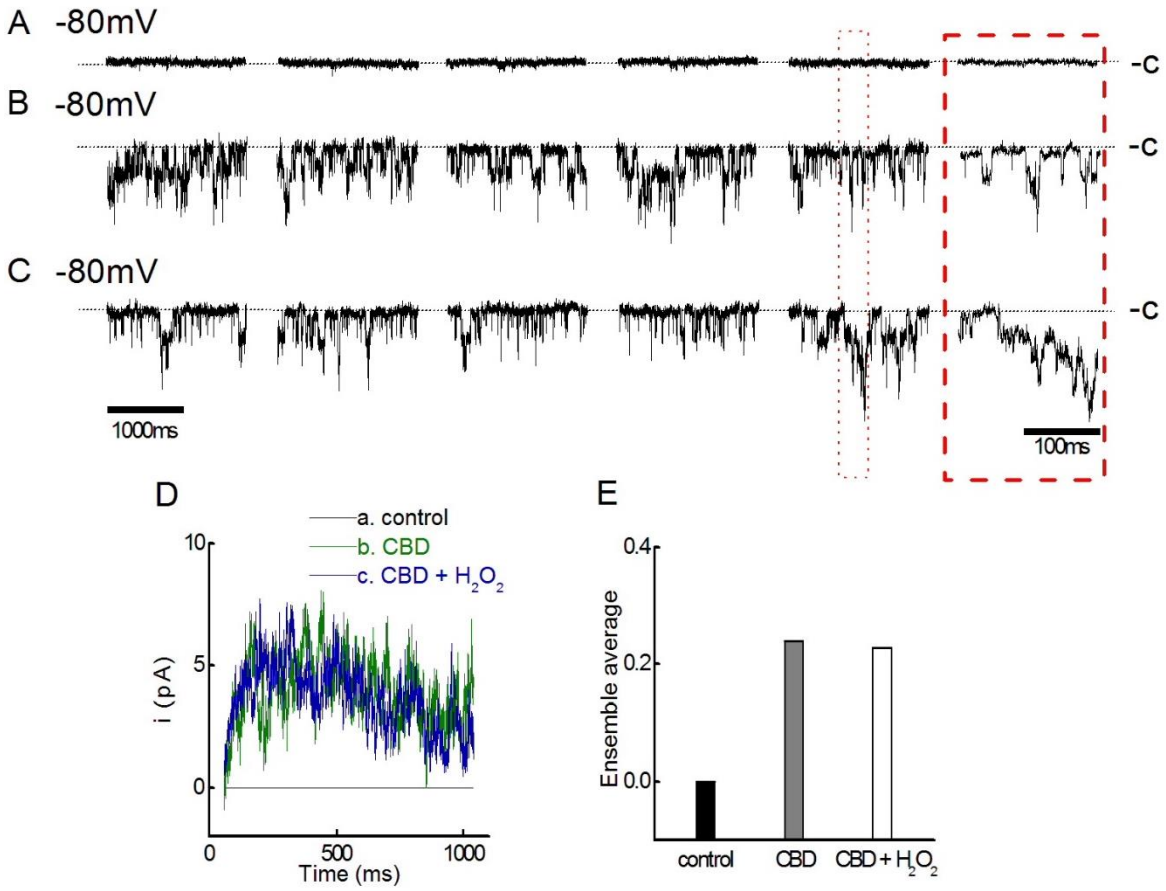

Figure 31: H_2O_2 does not enhance CBD induced C704-rTRPV2 activity in excised membrane patches.

HEK-293 cell is transfected with the C704R-mutatnt rTRPV2 channel and subjected to excised inside-out patch clamp electrophysiology. The current response to -80 mV membrane potential step is measured. Representative current response across 5 time intervals under control condition (**A**), 300 μM CBD (**B**), and co-application of 300 μM CBD and 1mM H_2O_2 (**C**) are shown. Dash lines indicate leak-subtracted zero current amplitudes corresponding to the closed channel state (c). **A.** Under control condition, no channel activity are observed. **B.** Application of 300 μM CBD induces the erratic activity of TRPV2 **C.** However, unlike wild-type TRPV2 channel addition of 1mM H_2O_2 on top of 300μM CBD did not enhance TRPV2 activity. The red box shows an enlarged view of single channel activity across 200 ms. **D.** The current responses to in **A-C** are normalized to control condition (A) and averaged across 10 sweeps to construct average current response (see Method). The addition of CBD induces current activity (green line) higher than control condition (black line). CBD and H_2O_2 co-application induced current (blue line) that is larger than control current but equal to CBD induced current (green line). **E.** Mean current response in **D** is further averaged to calculate ensemble average current response across 20 seconds of measurement. Co-application of CBD and H_2O_2 did not increase channel opening compared to CBD alone.

Next EGFP-tagged C704A-rTRPV2 are subjected to excised inside-out patch clamp electrophysiology to examine the effect of H_2O_2 sensitivity on C704A-rTRPV2. In the C704A-rTRPV2 mutant, H_2O_2 did not enhance single channel activity of CBD induced TRPV2 current consistent with the whole cell current

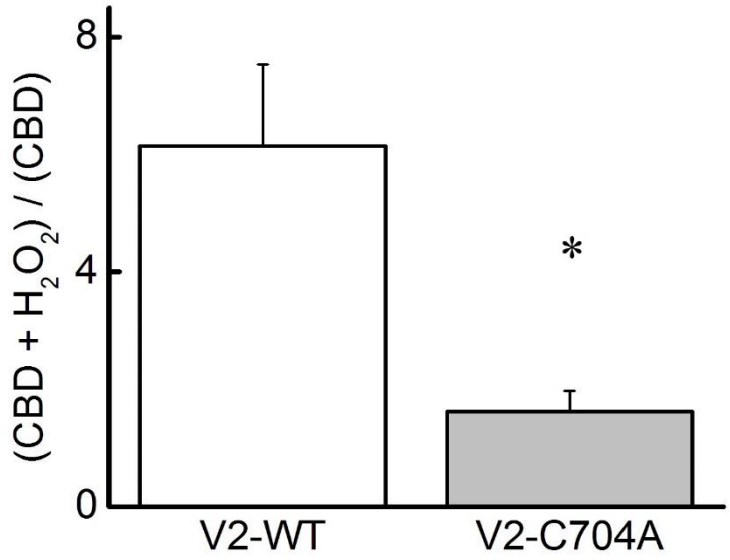

Figure 3217: Ensemble average analysis of H_2O_2 enhancement of CBD induced TRPV2 current.

Ensemble average result of CBD plus H_2O_2 is divided by CBD alone to calculate fold increase of H_2O_2 induced TRPV2 channel current potentiation. In wild-type TRPV2 channel 1 mM H_2O_2 are able to increase the 300 μM CBD induced TRPV2 current by 6.1 ± 1.4 folds. Application of 1 mM H_2O_2 to C704A mutant TRPV2 channel only increased 300μM CBD induced current by 1.6 ± 0.4 fold. C704A mutation significantly reduced H_2O_2 potentiation ($p = 0.03$, $n = 3$ each group).

record. Similar to wild-type TRPV2 channel, stepping membrane potential to -80mV alone did not activate C704A mutant TRPV2 channel (Fig 31A). Application of 300 μM CBD induced multiple TRPV2 opening (Fig 31B). However, unlike wild-type channel, the addition of 1 mM H_2O_2 did not enhance CBD induced C704A mutant TRPV2 channel activity (Fig 31C). Abolished TRPV2 channel H_2O_2 sensitivity is evident as averaged current traces of CBD plus H_2O_2 (Fig 31D, blue line) overlaps with averaged current trance of CBD alone (Fig 31D, green line). Ensemble average shows CBD alone induces 0.2 pA, while co-application of CBD and H_2O_2 induces 0.2 pA current on average (Fig 31D). In wild-type, TRPV2 channel addition of H_2O_2 increased CBD induced TRPV2 current by 6.1 ± 1.4 fold (n=3), while the addition of H_2O_2 to C704A mutant increased CBD induced TRPV2 current by 1.6 ± 0.4 fold (n=3; Fig 32). The effect of H2O2 enhancement of CBD induced TRPV2 current is significantly different in wild-type and C704A mutant

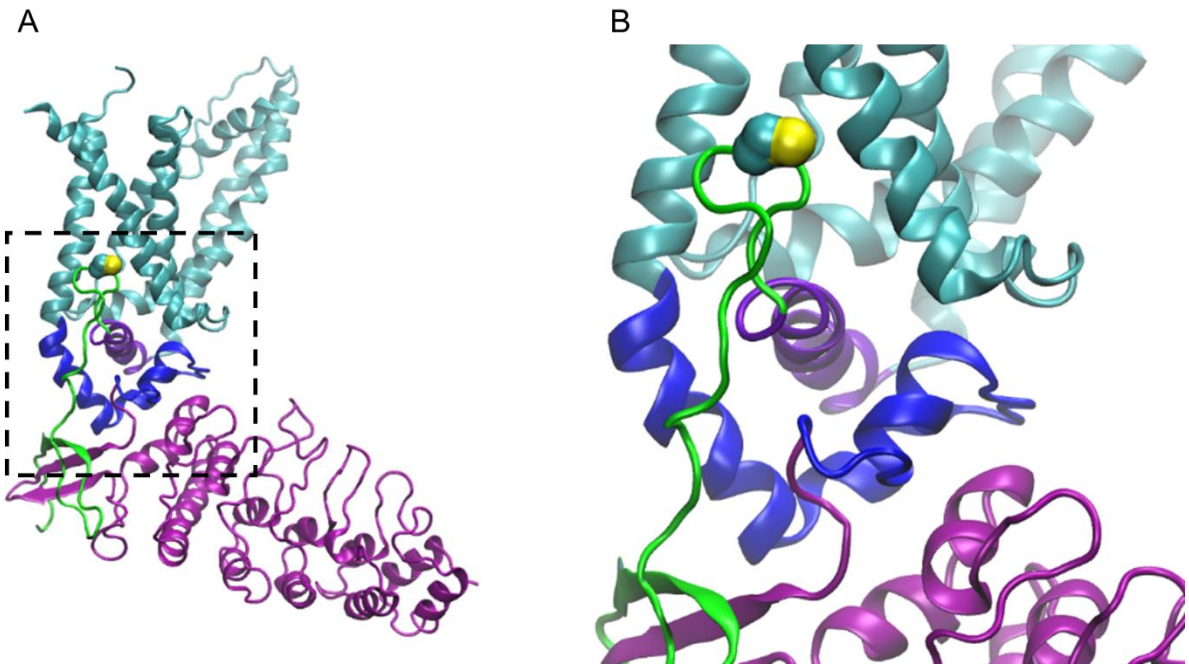

Figure 33: Cysteine 678 residue provide a potential site for H_2O_2 modulation.

A. Structure of one subunit in TRPV2 channel is shown in ribbon representation. The cysteine residue tested in this study are shown in space filling representation. Domains and motifs are individually colored for clarity: ARD, magenta; HLH linker, blue; S1-S6 TM domain, cyan; TRP helix, purple; CTD, green. The the hook structure is indicated by the black box, which is magnified in panel B. TRPV2 structure exhibits a unique 'hook' structure between the TRP helix and downstream CTD. The tip of the hook points toward the lipid bilayer. **B.** An enlarged view of the hook structure (dashed box in panel A) highlights the position of C678 (space filling representation: cyan, carbon; yellow, sulphur). Representations shown here are based on the TRPV2 cryo-EM structure (pdb: 5hi9) determined by Huynh, et al. (2016)[1]. Graphical representations were created using VMD 1.9.3.

(p=0.03; Fig 32). This confirms that H_2O_2 enhances CBD induced TRPV2 current, and C704A mutation abolished H_2O_2 sensitivity.

Additionally to ARD and CTD, TRPV2 also contains a hook structure connecting TRP domain to CTD (Fig 33A, 33B). This structure is unique to TRPV2 and not found in TRPV1. At the tip of hook structure, a cysteine at 678 position is found. Given this hook structure point toward extracellular matrix and come close proximity to the inner leaflet of plasma membrane, it is possible that this portion of TRPV2 channel may come to contact with lipid molecules. The importance of C678 is not known. To examine the C678 effect on H_2O_2 sensitivity, the C678 residue is mutated to arginine (C678R) and TRPV2 channel sensitivity to H_2O_2 was examined.

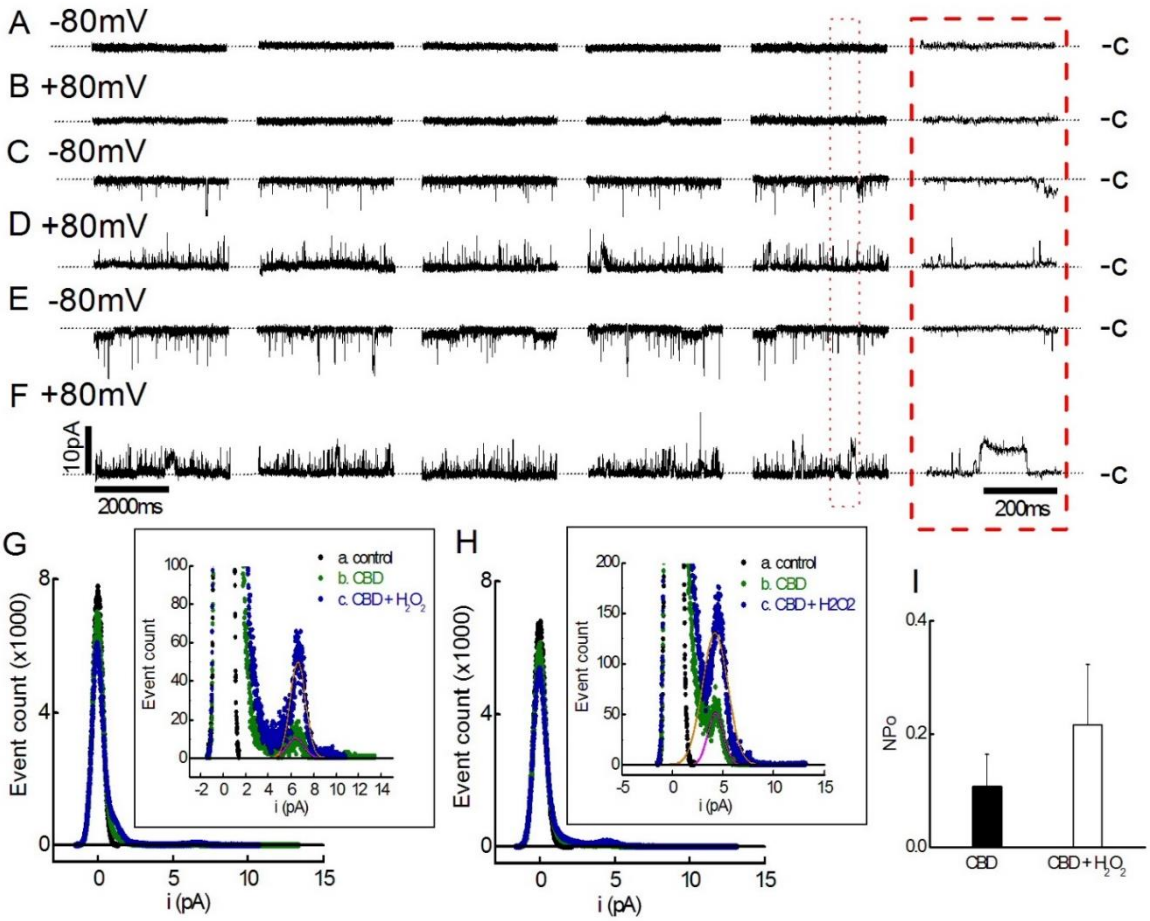

Figure 184: H_2O_2 enhances CBD induced C678R mutant TRPV2 activity in excised membrane patches.

C619R mutation is introduced by PCR and transfected into the HEK-293 cell. C619R-mutant rTRPV2 transfected HEK-293 are subjected to excised inside-out patch clamp electrophysiology. Dash lines indicate leak-subtracted zero current amplitudes, which correspond to the closed channel state (c). **A, B.** No channel opening is observed under control condition whether the membrane is stepped to -80 mV (**A**), or to +80 mV (**B**). **C, D.** Application of 300 µM CBD to cytosolic face elicit TRPV2 channel opening in -80 mV (**C**), and +80 mV (**D**). **E, F.** Addition of 1 mM H_2O_2 further increases channel opening compared to CBD alone in both -80 mV (**E**) and +80 mV (**F**) steps. The red box shows an enlarged view of single channel activity across 200 ms. **G.** All point histogram summarize the current response to -80 mV membrane step in control (**A**), 300 µM CBD **(C**) and 300 µM CBD plus 1 mM H_2O_2 (**E**). ***Insets*** show an enlarged view of panel **G**. Only 0 current peak is found in control condition (black circle). The addition of CBD induces open channel peaks (green circle) and co-application of CBD and H_2O_2 further increased the size of open channel peaks (blue circle) but did not cause a shift of open channel peak. CBD induced unitary current first peak equals to 6.3 pA. Co-application of CBD and H_2O_2 induces first peak measures 6.5 pA. **H.** All point histogram summarize the current response to +80 mV membrane step in control (**B**), 300 µM CBD **(D**) and 300 µM CBD plus 1 mM H_2O_2 (**F**). ***Insets*** show an enlarged view of panel **H**. Open channel peak is found after addition of CBD (green circle), and co-application of CBD and H_2O_2 further increased the size of open channel peaks (blue circle). The addition of H_2O_2 did not cause a shift of open channel peak. CBD induced current have the first peak equals to 4.2 pA, and co-application of CBD and H_2O_2 induced current has the first peak equals to 4.2 pA. **I.** Paired student t-test across three cells shows there is no statistically significant difference between CBD condition and CBD plus H_2O_2 condition. CBD induced NPo equals to 0.11 ± 0.06 and CBD plus H_2O_2 induced NPo equals to 0.22 ± 0.11. No statistical significant difference is found ($p = 0.32$, $n = 3$ each). Statistics are considered significant if $\alpha<0.05$.

EGFP-C678R-rTRPV2 expression HEK-293 cells were subjected to excised inside-out patch clamp electrophysiology. Similar to wild-type rTRPV2, no channel activity is observed in C678R-rTRPV2 under control condition (Fig 34A, 34B). The addition of 300 μM CBD to cytosolic face induced single channel activity in both -80mV membrane step and +80mV membrane step (Fig 34C, 34D). The result shows C678R-rTRPV2 retains CBD sensitivity. Note that fast flickering activity was found, similar to wild-type TRPV2. Co-application of 1 mM H_2O_2 and 300 μM CBD enhanced both -80mV and +80mV single channel activity (Fig 34G, 34H). However, note that the effect of H_2O_2 enhancement was not as prominent as in wild-type rTPRV2. Gaussian fits of all point histogram indicated that CBD induced unitary current have first major open channel peak equals to 6.3pA, and co-application of CBD and H_2O_2 induced first major open channel peak equals to 6.5 pA at -80mV membrane step (Fig 34G). At +80 mV membrane step, CBD induced current have first major open channel peak equals to 4.2 pA, and co-application of CBD and H_2O_2 induced current to have first major open channel peak equals to 4.2 pA (Fig 34H). Note that C619R mutation did not alter TRPV2 unitary conductance. The H_2O_2 application also did not change unitary conductance as expected (Fig 34G, 34H). C619R mutation is able to abolish the H_2O_2 effect of enhancing TRPV2 current. No statistically significant difference between CBD induced NPo (0.11 ± 0.06) and CBD plus H2O2 induced NPo (0.22 ± 0.11) were observed ($p = 0.32$). This result indicated that C678R mutation also reduces H_2O_2 sensitivity, but may not as strongly as C704A mutation.

To summarize, C206, C678, and C704 are expected to be the site regulate H_2O_2 sensitivity in TRPV2, as those residues are required for H_2O_2 enhancement of CBD induced TRPV2 current. However, C219 and C334 residues are less likely involved in H_2O_2 sensitivity. At current knowledge, whether TRPV2 forms intra-subunit disulfide bond between C206 and C704 residue is not known. Alternatively, C206 and C704 may form intra-subunit bonds with nearby cysteine residues. The intra-subunit disulfide bridge formation is possible as suggested by TRPV1 study, further experiments are required to draw conclusions[38]. Hook is

Chapter IV. Discussion

1. TRPV2 have fast flickering single channel activities with multiple conductance states

At the time of the study, TRPV2 single channel activity has not been fully demonstrated despite wide distribution of TRPV2 across the body and proposed roles in osmosensation, mechanosensation, cardiac cell function, innate immunity, and cancer cell migration[20,66,70,113-115]. In past three years, several studies have tried to examine single channel activity of TRPV2 under different experimental conditions. Pottosin et al and McGahon et al both used cell-attached patch clamp recording to examine native stretch-activated single channel current in Jarket cells and rat retinal arteriole cells respectively[70,104]. Those currents are believed to be TRPV2 related based on TRPV2 gene knockdown experiment[70,104]. The single channel activities of purified rTRPV2 reconstituted in preformed asolectin liposomes is observed by Huynh et al using excised inside-out patch clamp[35]. The reconstituted TRPV2 demonstrate functional PBC induced rTRPV2 current in the artificial lipid bilayer, but effects of removing TRPV2 from the cellular environment is unknown. Most recently, Zhang et al expressed resiniferatoxin (RTx) sensitive mutant TRPV2 (TRPV2-QM) in HEK-293 cells and measured RTx activated TRPV2 current in excised inside-out patch clamp configuration[43]. Despite efforts, results disagree with each other and interestingly no study have examined wild-type TRPV2 activity in mammalian cells. The goal of this study is to characterize wild-type TRPV2 single channel activity in the widely used experimental system. Utilizing commonly used TRPV2 agonist 2-APB and CBD, here we report wild-type rTRPV2 single channel activity in HEK-293 cells under excised inside-out patch clamp configuration.

Despite varieties of experimental conditions, all studies, including ours, reveal fast flickering activities of TRPV2[35,43,70,104]. Fast flickering activities are not due to experimental conditions as we demonstrate stable, long time opening of TRPV1 and TRPV3 under same experimental conditions, consistent with the previous publications[48,105-107]. Fast flickering activities are not agonist dependent as they are observed whether 2-APB, CBD, PBC[35], RTx[43] or membrane stretch[70,104] are used to activate TRPV2. Furthermore, fast flickering activities are also independent of membrane voltage step and conducting ions; the fast flickering

activities are observed regardless whether membrane potential is stepped to negative or positive and whether Na^+ or K^+ are used as conducting ion [35,43,70,104]. What accounts for the fast flickering nature of TRPV2 is unknown, but results suggest TRPV2 rarely remain in open states for a prolonged time.

Also, TRPV2 have low Po without agonist. Consistently with previous results, there is no TRPV2 channel opening detected without application of agonist[18,43,70,104]. Unlike TRPV1 and TRPV3 that have a low level of NPo without the addition of agonist, TRPV2 is not activated by voltage step alone. Membrane steps up to 120mV did not show single channel activity. This result is also shown in whole cell voltage clamp, no current is observed without agonist addition, confirming TRPV2 is not activated without agonist[27,32,97]. Those results suggest polymodal gating of TRPV2[7,22]. In addition to voltage agonists, temperature or membrane stretch may be required for activation of TRPV2.

Other than fast flickering activity, TRPV2 also show subconductance. Subconductance current is found to be approximately 10-20 pS. Interestingly subconductance is also observed in excised inside-out patch of TRPV2-QM mutant channel expressed in HEK-293 cells[43], but not prominent in purified TRPV2 reconstituted in liposome[35]. Those results suggest that subconductance may originate from channels endogenously expressed by HEK-293. HEK-293 cells are known to endogenously express voltage gated potassium[116], voltage gated calcium (i.e. L-type Ca_V)[66] and voltage gated sodium channels (i.e. $Na_V1.7$)[65] which may have unitary conductance approximately 10-20pS[10,68]. However, experimental conditions exclude the possibility of K^+, Ca^+ and Na^+ current. K^+ and Ca^{2+} are chelated from solution hence subconductance observed is not likely to originate from highly selective K^+ and Ca^{2+} channels. Also, $Na_V1.7$ is not likely since subconductance is no observed without application of 2-APB or CBD, indicating subconductance channel cannot be activated by voltage step alone and subconductance is 2-APB and CBD sensitive. Furthermore, TRPV2 current including subconductance is inhibited by addition of RuR to intracellular face of the excised inside-out patch, indicating subconductance is generated by a calcium conducting channel. HEK-293 also express numbers of chloride channels[117]. It is possible that subconductance originate from $I_{Cl,swell}$. However, this hypothesis is rejected as the application of DCPIB, a

potent Cl_{swell} blocker did not eliminate 2-APB induced subconductance current[118,119]. Furthermore, 2-APB is suggested to inhibit $I_{Cl,swell}$ current at concentrations above 100 μM[109], making $I_{Cl,swell}$ unlikely to present in our experimental condition. Together those results suggest subconductance is a part of the TRPV2 biophysical property; indicating TRPV2 may have more than one open state with different unitary conductance.

The flickering activity and subconductance states may represent dynamic pore. Given erratic and fast flickering nature of TRPV2 current, TRPV2 may not have a "fixed" open state, rather they may flickering between different open states. TRPV1 have shown to produce similar flickering single channel activities[120,121]. Compared to Kv channels, cryo-EM of TRPV1 reveals dynamic pore structure which may underlie flickering activity[4], which suggest a similar mechanism in highly similar TRPV2 pore[1,29]. Alternatively, two population of TRPV2 with two different unitary conductance may exist. For example, TRPA1 unitary conductance is modulated by a high concentration of $PI(4,5)P_2$[122]. Phosphoinositide interacting regulator of TRP, a two transmembrane protein, is also shown to modulate unitary conductance of TRPM8[123]. Mercado et al (2010) have shown $PI(4,5)P_2$ also modulates TRPV2 current in excised inside-out patch[18]. However, they were only able to observe macroscopic current, and it is not clear whether $PI(4,5)P_2$ affect NPo or unitary conductance of TRPV2[18]. Those results suggest TRPV2 unitary conductance may be modulated by the presence of auxiliary proteins and lipids.

Indeed our result shows that $I_{Cl,swell}$ inhibitor DCPIB increased NPo and unitary conductance of TRPV2, demonstrating TRPV2 unitary conductance can be modulated by pharmacological reagents. DCPIB is not known to alter TRP activities previously. Our data reveals a noble effect of DCPIB enhancing 2-APB induced TRPV2 and TRPV3 NPo in excised inside-out patch clamp electrophysiology. Interestingly, DCPIB also increases unitary conductance of TRPV2 but did not affect unitary conductance of TRPV3. The mechanism of DCPIB only alters TRPV2 unitary conductance is unknown. One hypothesis is that DCPIB may shift TRPV2 activation to "fully opened" state. It is possible that 2-APB does not induce full

opening of TRPV2 channel, and the addition of DCPIB promote the transition to the full opened state of TRPV2.

In the end, reports from multiple labs indicate TRPV2 have fast flickering current with possible subconductances, and we confirms same gating characteristic in wild-type TRPV2 activated by 2-APB and CBD. Furthermore, we demonstrate TRPV2 *NPo* and unitary conductance can be modulated by pharmacological reagents such as DCPIB, suggesting the potential of endogenous molecules modulating TRPV2 unitary conductance and *NPo*. In addition to describing characteristics of TRPV2, we further identified a pharmacological reagent that can act as TRPV2 co-agonist.

2. Rat TRPV2 have unitary conductance of approximately 100pS

Whole cell current (*I*) at any given time is the product of the number of functional channel in the membrane (*N*), the unitary current of the channel (*i*) and open probability of the channel (*Po;* see equation 6). Hence understanding unitary current and unitary conductance (*i*) is crucial for understanding biophysical property of TRPV2. However, the unitary conductance of TRPV2 remains an enigma. Previous studies disagree on what is TRPV2 unitary conductance. Studies by Pottosin et al and McGahon et al both showed small and highly erratic stretch activated current in Jurkat cells and rat retinal arteriole cell respectively[70,104]. Pottosin et al estimate that TRPV2 have a unitary conductance of approximately 40 pS while McGahon et al are not able to measure unitary conductance due to small current size and fast flickering behavior of the channel[70,104]. Also, note that unitary conductance in Pottosin study is not directly measured from single channel record but rather estimated by dividing macroscopic current (*I*) measured by voltage ramp by estimated number of open channels (*NPo*) measured in excised inside-out patch clamp recording[70]. On the other spectrum, Huynh et al show reconstituted homotetrameric purified rTRPV2 in preformed asolectin liposomes have a large conductance; excised inside-out patch clamp shows PBC induced unitary conductance of approximately 304 pS[35]. Finally, Zhang et al report TRPV2-QM have RTx induced unitary conductance of 101 pS at +90mV and 28 pS at -90mV in isometric 140 mM NaCl solution under excised

inside-out patch clamp configuration[43]. The reasons for diverse TRPV2 unitary conductance is not known, as each study in previously published works studies TRPV2 under a variety of experimental conditions and may contain caveats. For example, Pottosin et al measured endogenous stretch activated current in Jurkat cells, and their study suggests stretch activated current is TRPV2 because RNAi knockdown of TRPV2 or application of rTRPV2 antibody and inhibitors abolishes stretch activated current[70,104]. These results indicate TRPV2 is required for stretch activated current but does not indicate TRPV2 conducts stretched activated current. Potentially TRPV2 can be a part of a group of channels that mediate stretch activated current or TRPV2 may simply act as a modulator of an another stretch activated channel. Huynh et al reconstituted homotetrameric purified rTRPV2 in preformed asolectin liposomes, which removes any potential proteins and lipids interaction required for proper TRPV2 function but may provide non-modulated TRPV2 biophysical property[35]. Finally, Zhang et al used RTx sensitive TRPV2-QM[43]. RTx is a TRPV1 selective agonist that does not activate TRPV2 and TRPV3[43]. In order to make TRPV2 sensitive to RTx, Zhang et al mutated TRPV2 channel to more TRPV1 like. Interestingly only four residues are needed to make TRPV2 sensitive to RTx[43], but the overall effect of the mutations on TRPV2 gating is not clear, and perhaps it is not surprising that TRPV2-QM have similar unitary conductance with TRPV1.

Here we report the unitary conductance of heterologously expressed wild-type rTRPV2 in HEK-293 cells in excised inside-out patch clamp configuration. The unitary conductance is 103.8 pS at -80mV and 93.5 pS at +80mV membrane step when 2-APB is used as the agonist. When CBD is used as agonist unitary conductance of rTRPV2 was 104.3 pS at -80mV and 105.4 pS at +80mV membrane step. Those result suggest three characteristics of TRPV2 unitary conductance; TRPV2 unitary conductance remain unchanged whether membrane voltage is stepped to negative or positive potential, TRPV2 unitary conductance remains constant whether 2-ABP or CBD are used as agonist, TRPV2 unitary conductance is approximately 100 pS, similar to that of Zhang et al report and similar to unitary conductance of TRPV1 (approximately 80 pS)[43,106,107].

Several factors may responsible for different unitary conductance observed. The first factor is presence or absence of intracellular molecules and axillary proteins. Proteins and lipids such as $PI(4,5)P_2$ and calmodulin, are known to bind TRPV2 and suggested to enhance TRPV2 current in excised inside-out path clamp[18,124]. Pottosin et al and McGahon et al used cell attached configuration to measure stretch activated TRPV2 unitary current, completely retaining intracellular molecules[70,104]. On the other hand, reconstitution of the purified channel in liposome would strip away any auxiliary subunits and potentially cause large unitary conductance[35]. In excised inside-out voltage clamp, some molecules will be dilated by bath solution while others remain. Interestingly TRPV2 unitary conductance becomes large as intracellular molecules are removed from experimental conditions. Also purified rTRPV2 reconstituted in asolectin liposomes would remove naturally occurring membrane lipids including cholesterols, sphingolipids, and phosphoinositide (i.e. $PI(4,5)P_2$), which are shown to modulate gating of TRP channels[125]. Second, TRPV1 and TRPV3 channel macroscopic current (*I*) measured in the whole cell voltage clamp configuration are shown to undergo the process of pore dilation during prolonged agonist or heat stimulation[25,98,99]. During pore dilation, TRPV currents are shown to increase over time, and their I-V relation and ion selectivity can be altered without any additional stimulations[25,98,99]. Although it is not clear pore dilation affect unitary conductance of TRPV channels, but it is suggested that pore dilation is a process of spontaneous change in pore structure. Potentially purified, reconstituted TRPV2 reside in 'fully dilated' state that produces large unitary conductance in liposomes, while TRPV2 channel expressed in the natural membrane is modulated by intracellular molecules and lipids in the membrane. However, this hypothesis is only a speculation at this time and further experiment is needed to test if any intracellular molecules and lipids in the membrane can reduce unitary conductance of TRPV2.

Some other potential causes of the difference in unitary conductance include different agonists used to elicit TRPV2 current. Pottosin et al and McGahon et al show small and highly erratic unitary current is observed when membrane stretch are used to activate TRPV2[70,104], while PBC induced unitary conductance of 304 pS in purified rTRPV2 in liposome[35]. Interestingly our preliminary result suggests unlike 2-APB and CBD,

PBC only activates TRPV2 when applied exogenously (data not shown), suggesting PBC may have different activation process that 2-APB and CBD. However, our result and Zhang et al show that 2-APB, CBD, and RTx all induced approximately 100 pS current when rTRPV2 are expressed in HEK-293 cells[43]. Whether stretch activation and pharmacological activation result in differential TRPV2 unitary conductance remains to be explored. Also, an argument can be made that the study by Pottosin is performed in Jurkat cell which is human origin[126]. Although the significance of species difference on unitary conductance is not known, human TRPV2 and murine TRPV2 are shown to have different pharmacological profiles[32], illustrating potential species difference in biophysical property of TRPV2. However, this is unlikely since McGahon et al shows similar high erratic, flickering, small single channel current in rat retinal arterioles. Finally, the difference in conducting ion must be considered. The study by Huynh et al used K^+ as the charge carrier, whereas all other experiments used sodium Na^+ as a charge carrier. However, the effect of Na+ compared to K+ on unitary conductance is unlikely since related TRPV1 are shown to have smaller unitary conductance when K^+ instead of Na^+ are used as main conducting ion[127].

Interestingly Zhang et al report strong rectification in unitary conductance; TRPV2 unitary conductance is 103 pS at +90 mV membrane step and 28 pS at -90 mV membrane step[43]. This result contradicts with ours and results in rTRPV2 reconstituted in asolectin liposomes, where no rectification of unitary conductance is observed[35]. RTx is a TRPV1 selective agonist originally have no affinity to TRPV2. Mutations introduced by Zhang et al are thought to convert TRPV2 to more TRPV1 like[43]. Although only four subunit mutation is needed to create TRPV2-QM, the mutation and usage of RTx as agonist may cause rectification. Unlike TRPV2, TRPV1 is shown to have rectified unitary conductance[121,128], and hence it may not surprising that TRPV1 like TRPV2-QM develop rectification.

To summarize agonists, mutations, and presence of intracellular molecules may cause variability in TRPV2 unitary conductance, and differential unitary conductance observed in distinct experimental conditions may provide insight to the biophysical property of TRPV2. However, further examination is needed to elucidate the cause of different unitary conductance. In the end, our result shows agonist induced unitary conductance

in wild-type rTRPV2 channel is approximately 90-105 pS under excised inside-out patch clamp configuration, similar to the unitary conductance of TRPV1. By using commonly used TRPV2 agonists in the commonly used experimental system, our results provide both useful information for future TRPV2 studies and insight to TRPV2 biophysical properties.

3. Electrostatically charged residues E614 and R619 at S5-S6 loop does not determines TRPV2 unitary conductance

We demonstrated that TRPV2 unitary conductance can be increased by a pharmacological reagent (i.e. DCPIB). This suggests that TRPV2 pore structure is relatively flexible and can be potentially modulated. Multiple mutation studies have pointed out alternation of pore structure can drastically affect gating property. For example, in KcsA channel C-type inactivation process is modulated by a multipoint hydrogen-bond network[110]. TRPV channels are thought to have a similar structure to Kv channels; specifically, they have similar pore loop and selectivity filter[7]. As expected similar hydrogen bond structure is found in TRPV1. Furthermore, this hydrogen bond network has been shown to regulate TRPV1 functions; mutating charged amino acid residues at E648 and E651 residue to non-charged amino acid residues alters acid sensitivity[129-131] and mutation of K656 lead to alternation in gating properties such as agonist sensitivity and basal activity of TRPV1[132]. Two of these residues are conserved in TRPV2, E614 (equivalent to E651 in TRPV1) and R619 (equivalent to K656 in TRPV1) respectively. The structure shows that these two residues are located at the tip of S5-S6 loop structure facing extracellular matrix. Two residues are located close to each other which can potentially form a hydrogen bond. This hydrogen bond seems to be able to stabilize S5-S6 poor loop structure. Interestingly these two residues are not present in TRPV3. TRPV3 does not seem to have hydrogen bond network at the extracellular tip S5-S6 pore loop. We hypothesized that TRPV1 and TRPV2 have smaller unitary conductance because of hydrogen bond network at the S5-S6 loop.

However, mutating hydrogen bond forming subunit R619 to proline did not make TRPV2 channels to TRPV3 like. The unitary conductance of TRPV2 remain unchanged, and vice versa adding charged amino acid to S5-S6 pore loop (Q651E-P656R) did not significantly reduce TRPV3 unitary conductance.

The reason for the negative result is unknown. At the time of the experiment, the TRPV2 structure is not resolved and TRPV3 structure is still not resolved today. Hence, rat TRPV1 structure is used to determine the structure of TRPV channel poor loop and location of amino acids. Cryo-EM reports purified channel structures as purification is needed for visualization[1,26,29]. How does purification process affect the structure of the TRPV channel is unknown, but as we described in the previous section, single channel activity of TRPV2 is shown to differ in purified rTRPV2 compared to rTRPV2 expressed in HEK-293 cells; suggesting a potential difference in pore structure determined by cryo-EM and pore structure of expressed channel[35,43]. Furthermore, part of pore turret loop next to S5-S6 loop structure (amino acids 604 and 628) are removed from TRPV1 in order to resolve the cryo-EM structure of TRPV1[1,26]. How does the removal of turret loop affect the accuracy of TRPV1 pore structure visualized in cryo-EM is unknown. However, the comparison between turret loop truncated rabbit TRPV2 structure and full-length rat TRPV2 structure reveal that full-length rat TRPV2 have wider upper and lower gates and truncation of the pore turret loop reduced the sensitivity of rat TRPV2 to 2-APB[1]. On the other hand, truncation of rabbit TRPV2 pore turret loop did not affect rabbit TRPV2 sensitivity to 2-APB[29]. It is not known whether observed differences in size of upper and lower gate and 2-APB sensitivity are species dependent[32,96], but rat TRPV2 pore turret loop is shown to affect agonist sensitivity and potentially affect TRPV2 pore structure. Due to purification process and truncation of turret loop, it is possible that rat TRPV1 pore loop may have different conformation than reported, and the charged residues are never close enough to form hydrogen bond network. The full-length structure of rat TRPV2 shows charged amino acids are located at the tip of TRPV2 S5-S6 pore loop and facing extracellular matrix. The localization of potential hydrogen bond in full-length rat TRPV2 is farther away from pore loop (Fig 11) compared to truncated rat TRPV1. The hydrogen bond network in TRPV1 may also locate in a different position than initially estimated and may locate in a

different position than KcsA. It is possible that difference in positions and conformations result in negative result.

Our result indicates R619 in TRPV2 and Q651E-P656R in TRPV3 does determine unitary conductance of TRPV channels. However, other gating mechanisms may be altered by removal or addition of charged residues at R619 in TRPV2, and Q651E and P656R in TRPV3.Whether mutations affect agonist sensitivity and channel open duration are to be addressed in the future.

4. Hydrogen peroxide is a co-agonist of TRPV2

The identity of endogenous agonists is one of the greatest question remaining for TRPV2 studies. Multiple stimuli have been suggested to activate TRPV2 including; mechanical stretch[70,104], heat[8], membrane depolarization, PI(4,5)P2[18], and organic compounds such as 2-APB [27,96], PBC [47] and phytocannabinoids including Δ^9-THC[44] and CBD [97]. However TRPV2 is not activated at physiological temperature[8], and their endogenous agonist in physiological condition is not known. For example, PI(4,5)P_2 is required for 2-ABP induced TRPV2 current, however, PI(4,5)P_2 is not known to activate TRPV2 by itself[18]. We also demonstrate membrane depolarization of up to 80 mV did not induce TRPV2 current in BV-2 or in rTRPV2 transfected HEK-293 cells. TRP channels are characterized by their 'polymodal' gating, and it is suggested that multiple stimulations may be needed to activate channel[7,22]. For the first time, we demonstrate H_2O_2 is also a co-agonist of TRPV2. Co-application of CBD and H_2O_2 enhances TRPV2 *NPo* but not unitary conductance. Also, H_2O_2 by itself did not activate TRPV2 indicating additional stimuli is needed for H_2O_2 to activate TRPV2. The effect is consistent with the observation in TRPV1. H_2O_2 is shown to sensitize TRPV1 to capsaicin and heat, and co-application of H_2O_2 with other agonist have shown to enhance TRPV1 current[91,111,112]. Similarly, H_2O_2 also modulate TRPV4[86], TRPM2[87,88], and TRPA1[89-91] gating. Our results suggest that a larger TRPV2 current is expected in an environment with high H_2O_2 concentration.

This result implies potential biological function of TRPV2. H_2O_2 is ubiquitously produced in the body, and its concentration is shown to increase in multiple disease conditions. Physiologically H_2O_2 is converted from superoxide ($O_2^{\bullet}$) by superoxide dismutase. $O_2^{\bullet}$ is generated by NADPH oxidase on membrane and electron transport chain in mitochondria[133,134]. This result suggests that TRPV2 activation is enhanced in an environment with high ROS. In the central nervous system, ROS is produced following traumatic injury[135] and stroke[103,136]. High level of ROS also associated with the development of neurodegenerative diseases such as Alzheimer's disease[137] and Parkinson's disease[83,136]. In the heart, H_2O_2 is increased following ischemia and ROS level directly affect recovery following ischemia[138,139]. H_2O_2 also plays important role in immune regulation. H_2O_2 production is enhanced during acute and chronicle inflammation, and H_2O_2 level regulated phagocyte activities[75,76,134]. Not surprisingly, TRPV2 is found to affect the function of immune cells and heart cells. Conditional knockout of TRPV2 is shown to reduce phagocytosis in macrophage[64], while application of CBD to BV-2 microglia-like cells increases phagocytosis of amino-modified polystyrene beads[67]. Furthermore, knockdown of TRPV2 inhibits LPS induced cytokine production and NF-κB nuclear translocation in macrophage[66]. Conditional knockout of TRPV2 from heart result in cardiac dysfunction in 3 day[115], while dominant negative suppression of TRPV2 mediated calcium influx is suggested to prevent muscle dystrophy[140].

Despite their effect, H_2O_2 did not activate TRPV2 by itself, indicating TRPV2 need another endogenous molecule for activation in physiological conditions. TRPV2 activation in a physiological condition still remains an enigma despite our finding. It is possible TRPV2 do not have single activator in physiological condition. Instead, TRPV2 activation may co-regulated by body temperature, membrane depolarization, H_2O_2 and potentially membrane stretch, and TRPV2 may remain closed until all conditions are met. For example, our experiment is conducted under room temperature (18-24°C). Given TRPV2 is a heat sensitive channel, it is possible that H_2O_2 may activate TRPV2 at a higher temperature (i.e. 37°C). Normally TRPV2 is activated temperature >53°C[8], but co-application of H_2O_2 may shift the temperature sensitivity to the physiological range (i.e. 37°C). Whether the combination of H_2O_2, temperature and membrane

depolarization can activate TRPV2 without pharmacological reagents remain to be examined. Also, 1mM H_2O_2 is used to enhance TRPV2 activity in the study. However, human body are expected to produce H_2O_2 in lower concentration. In the physiological condition intracellular concentration of H_2O_2 is thought to be 1 – 100 nM, while the intracellular concentration of H_2O_2 is thought to increase to 100 nM – 10 μM[133]. Whether lower concentration of H_2O_2 has the same effect on the TRPV2 need to be addressed in future experiments. Nevertheless, our study demonstrates a concept that TRPV2 *NPo* can be modulated by H_2O_2 and suggests enhanced TRPV2 activity in high ROS environment.

5. Cysteine 206 in ARD and 704 in CTD are required for TRPV2 hydrogen peroxide sensitivity

H_2O_2 are shown to modify TRPV channel gating, however, the mechanism of regulation remained elusive. Through single mutations, we identified C206 and C704 are required for TRPV2 H_2O_2 sensing. If those two cysteines are replaced by alanine, H_2O_2 may no longer enhance CBD induced current in TRPV2. Two residues are located on the cytosolic side of two separate motifs; C206 is located on ARD and C704 is located on CTD. This result suggests cytosolic H_2O_2 concentration is important in regulating TRPV channel function, and both ARD and CTD are involved in H_2O_2 modulation of TRPV2 gating. Both ARD and CTD have shown to modulate TRP channel gating. For example, swapping ARD of TRPV1 with TRPV2 have been shown to convert temperature sensitivity of TRPV1 to TRPV2 and temperature sensitivity of TRPV2 to TRPV1 like[34]. Similarly, swapping CTD of heat sensitive TRPV1 with CTD of cold sensitive TRPM8 are able to convert TRPV1 to cold sensitive and TRPM8 to heat sensitive[141]. Those results indicate that both ARD and CTD are a modulator of temperature dependent activation of TRP channels. Furthermore, ARD of TRPV2 are shown to modulate agonist sensitivity as swapping ARD of human TRPV2 with ARD of mouse TRPV2 alters their 2-APB sensitivity[32]. This result shows 2-ABP binding site can locate near the C206 in TRPV2, but no direct evidence have been found to indicate the exact location of the 2-APB binding site. Lastly, the proximal C-terminal region is suggested $PI(4,5)P_2$ binding site needed for $PI(4,5)P_2$ modulation of TRPV1. Specifically, amino acid 682–725 are needed for the $PI(4,5)P_2$ binding[28]. Together

those results indicate both ARD and CTD modulate TRPV2 gating, and perhaps it is not a surprise that cysteines in those two motifs are needed for H_2O_2 sensitivity in TRPV2. However, it is possible there are additional cysteines required for H_2O_2 sensitivity outside of ARD and CTD.

One question remains, whether mutations modulate H_2O_2 sensitivity or modulate CBD sensitivity and basal activity of TRPV2. Application of CBD increased wild-type TRPV2 I_{tail} approximately 6 times to that of the control condition (leak current), and co-application of H_2O_2 and CBD increased I_{tail} approximately 12 times to that of the control condition (Fig 14). Interestingly, CBD increased C206A mutant TRPV2 I_{tail} approximately 10 times to that of control condition, and further addition of H_2O_2 did not enhance CBD current further. CBD increased C219A mutant TRPV2 I_{tail} approximately 4 times to that of control, while CBD increased C334 and C704 mutant TRPV2 I_{tail} approximately 7 times to that of control. The question remains whether mutation alters sensitivity to CBD. For example, it is possible that addition of H_2O_2 did not enhance CBD induced C206A rTRPV2 current because C206A mutation itself stabilize open configuration of rTRPV2 and application of 300 μM CBD achieves maximum Po of rTRPV2. Hence C206A mutation mimics H_2O_2 effect instead of abolishes H_2O_2 effect. Mutations in ARD and CTD have shown to alter TRP channel sensitivity to agonists. Mutations in ARD of TRPV1 channel have shown to alters heat, CAP, calmodulin, ATP, and $PI(4,5)P_2$[45,141]. Truncation and mutations of TRPV1 CTD have shown to alter CAP, pH, and heat sensitivity of TRPV1 channel[141,142]. In TRPV2 CTD is suggested to be $PI(4,5)P_2$ binding site and required for $PI(4,5)P_2$ modulation of TRPV2[18,143]. It is possible that mutation in ARD and CTD of TRPV2 also modulate sensitivity to CBD as well. Whole cell current is determined by functional channel in membrane (*N*), unitary current (*i*) and open probability of the channel (*Po*; see equation 6). In our experiment amount of TRPV2 expressed is not controlled, and a number of functional channel in the membrane (*N*) can differ from cell to cell. C206A mutant TRPV2 may simply better expressed (larger *N*) and result in a difference in CBD induced rTRPV2 current. Currently, whether mutations affect Po or N is not determined. TRPV2 sensitivity to CBD can be measured by dose-response experiment in a regulated expression system or in excised inside-out patch clamp where a small number of

channels (*N*) are present in membrane patch. Although the effect of the mutation on TRPV2 sensitivity to CBD is not known, our experiment shows the addition of H_2O_2 enhances 300 μM CBD induced current in same cells, where the concentration of CBD remains constant and little change of *N* is expected. Furthermore, our result suggests C206 and C704 are required for H_2O_2 modulation of the TRPV2 activity.

How mutation of C206 and C704 affect H_2O_2 sensitivity is not known. Interestingly C206 is located near to C704 of neighboring subunit. Cysteine residue in ARD is suggested to form covalent interaction with neighboring CTD in TRPV1, linking two neighboring subunit together[38]. Specifically, C258 in ARD interact with and C742 on CTD in TRPV1[38]. However, the functional significance of disulfide bond formation in TRPV1 is not fully understood. In TRPV2 C206 in ARD and C704 in CTD may play a similar role, suggesting potential disulfide bond formation in TRPV2. However, it is not known if covalent bonding forms between subunits in TRPV2 at this time. In addition to C206 and C704, TRPV2 contains two additional cysteine residues, C219 and C334, located in close proximity of the interaction surface (Fig 18 gray space fill plots). However, mutation of C219 and C334 to alanine did not alter TRPV2 H_2O_2 sensitivity. The reason for the lack of sensitivity in those two residues are not known, it is possible that two cysteines are hindered from H_2O_2 interaction by surrounding amino acids. In addition to C258 and C742, Ogawa et al indicate C158 and C363 also affect dimerization of the TRPV1 suggesting they also participate in intra-subunit disulfide bond formation[38]. TRPV2 also contains several cysteines in ARD, including C135, C157, C364 and more. Their effect on H_2O_2 sensitivity is not determined at this point.

How do cytosolic motifs such as ARD and CTD regulate TRPV channel opening is not determined. One theory is that rotation of ARD causes TRPV channel opening[29]. During heat and agonist mediated activation, TRPV1 ARD is thought to move close to neighboring CTD and this movement is transduced to S5-S6 pore loop to open that gate[29]. This hypothesis is derived from structure analysis of TRPV1 by cryo-EM. Compared to apo-TRPV1, capsaicin and DkTx bound form of TRPV1, which is thought to be locked in "open channel state", shows that ARD is rotated counterclockwise and comes close to CTD of neighboring subunit[4,26]. TRPV2 may have a similar mechanism of activation; ARD and neighboring subunit CTD may

locate close to each other when TRPV2 is activated. This may explain why H_2O_2 enhances CBD induced TRPV2 *NPo* but by itself does not activate TRPV2. It is possible that agonist is required for C206 and C704 residues close together for H_2O_2 to function. However whether activation of TRPV channel brings ARD and CTD of two neighboring subunits close enough to form a disulfide bond, and whether inter-subunit disulfide bond enhances TRPV *NPo* is not determined. It is entirely possible that cysteines form intra-subunit disulfide bonds or regulate TRPV gating property thought other mechanisms[38].

In addition to C206 and C704, we also report C678 modulate TRPV2 H_2O_2 sensitivity. C678 is located on tip of a hook structure unique to TRPV2 (Fig 26)[1,29]. This hook structure is not found in apo TRPV1 or DkTx bond TRPV1[4,26]. The hook structure contains multiple ionizable amino acids and one cysteine residue at the tip. The importance of the hook structure is not previously examined. Interestingly this cysteine residue is not conserved across species. C678 is conserved in most of the mammals but replaced with arginine in most of the bird species (data not shown). When C678 is mutated to arginine TRPV2 become less sensitive to H_2O_2. This result implies TRPV2 in bird species may have less sensitivity to H_2O_2 compared to mammals. The full function of this hook structure is not known, however, this unique structure may underlie biophysical difference of TRPV1 and TRPV2 such as agonist sensitivity, sensitivity to membrane stretch, $PI(4,5)P_2$ sensitivity and H_2O_2 sensitivity[18,27,28,50,70,104,106,112].

In summary, our result highlights three cytosolic structures ARD, hook, and CTD is important in H_2O_2 sensitivity. Especially three cysteines C206, C678, and C704 affect the H_2O_2 sensitivity of rTRPV2. However, additional cysteine sites for H_2O_2 sensitivity as well as mutation effect on TRPV2 agonist sensitivity need to be examined in the future.

6. TRPV2, but not TRPV1, TRPV3 or TRPA1 is functionally expressed in microglia

Multiple TRP channels are known to be present in the CNS including TRPV1, TRPV2, TRPV4, TRPA1, TRPM2, and TRPM8[144]. Of those channels, TRPV1[61,67] and TRPV4[63] have been shown to present in mice brain microglia while TRPV2 are known to present in BV-2 microglia-like cells[67]. However, the presence of related TRPV3 and TRPA1 protein and functional expression of these channels are not known as TRP

channel current response is not fully established in microglia. In this study, we demonstrate that TRPV2 and TRPA1 protein are present in both BV-2 microglia and dissociated neonatal mice microglia, however, TRPV3 protein is not found in BV-2. Furthermore, we demonstrate TRPV2 current is present in BV-2 microglia-like cells. TRPV2 are likely to be main functional TRPV in microglia.

TRPV2 is important in mediating phagocyte activity. TRPV2 protein is present in macrophage[64,65], and shown to mediate a wide variety of functions including; mediates Ca^{2+} entry during podosome assembly, NFKB nuclear translocation, inflammasome assembly, cytokine production, chemotaxis and phagocytosis in macrophages [64-66,68]. Identification of functional TRPV2 expression in those study suggests TRPV2 can mediate similar function in microglia. Indeed, CBD is shown to increase phagocytosis of BV-2 microglia like cells[67].

TRPA1 is shown to present in brain and suggested to the mediate pain sensation in DRG neurons following traumatic brain injury[145,146]. However, their functional expression is not established in microglia. Our result shows TRPA1 protein in BV-2 and primary microglia, but no current detected by AITC. Similarly, no TRPV1 current is found in BV-2 and primary microglia despite their protein is detected in both[61,67]. The reason for the lack of TRPV1 current may be related to its cellular localization. In brain microglia, TRPV1 is thought to localize mainly in intercellular organelles, specifically shown to localize on mitochondria[61,102]. This is consistent with our results that no TRPV1 current is detected by whole cell voltage clamp electrophysiology in BV-2 and dissociated neonatal mice primary microglia[102]. TRPA1 localization is not known, but may also not expressed on the membrane. The trpv2 expression on the membrane is facilitated by growth factors and chemokines in macrophage[65,68]. It is possible that TRPV1 and TRPA1 translocate on plasma membrane with specific inflammatory stimuli, but whether translocation occurs in microglia is not examined. TRPV1 is suggested to localized on mitochondria and regulate their function. CAP stimulation induces mitochondrial transition pore formation and cytochrome c mediated cell death of microglia[61]. Furthermore, TRPV1 is shown to promote mitochondrial ROS production and chemotaxis when activated, but TRPV1 knockdown does not inhibit NO production or cytokine production[102,147]. Alternatively, TRPV1

on the membrane may exist in a form not sensitive to CAP. For example, TRPV1 is known to associate with TRPV3 during heterologous expression in HEK-293 cells[10], and associate with TRPV2 in the brain and when co-expressed in mammalian cell line[116,117]. Furthermore, TRPV1 is suggested to form heteromeric TRP channel with TRPA1 in dorsal root ganglion neurons (DRG)[148]. Formation of heteromeric TRPV1/TRPA1 channels can modify their sensitivity to agonist. Wild-type mice TRPV1 have CAP sensitivity of EC50 approximately 9.1 nM[149], and TRPA1 have AITC sensitivity of EC50 approximately 11 μM[150]. CAP sensitivity of heteromeric TRPV1 and AITC sensitivity of heteromeric TRPA1 are not tested. Potentially more than 100 μM of CAP is needed to activate TRPV1 and more than 20 μM of AITC are needed to activate TRPA1 in microglia. TRPA1 may also not localized on membrane similar to TRPV1, or associated with another channel making them insensitive to agonist stimulation. It is possible that more than 20 μM of AITC may be needed to activate heteromeric AITC in microglia. However, the further experiment is needed to identify if TRPA1 play a role in microglial physiology.

Our result confirms TRPV2 is main functional TRPV channel present on the membrane of cultured microglia. This suggests TRPV2 activation will lead to influx of Ca^{2+} from extracellular fluid. Indeed, TRPV2 increases calcium influx following the addition of chemokine fMLP and elevated basal calcium level in the macrophage[68]. Removal of extracellular Ca^{2+} abolishes the elevation of basal calcium level in macrophage, indicating calcium influx is the cause of elevated basal $[Ca^{2+}]_i$[65,68]. Furthermore knockdown of TRPV2 prevents the elevated basal $[Ca^{2+}]_i$ following fMLP peptide stimulation suggesting TRPV2 may regulate chemokine induced rise of $[Ca^{2+}]_i$[65,68]. Whether TRPV2 in phagocyte are activated by other stimuli are unknown, however, we demonstrated H_2O_2 enhances TRPV2 *NPo*. This would suggest potentially TRPV2 current is enhanced in the high H_2O_2 environment and lead to increase of $[Ca^{2+}]_i$ in microglia. The exact function of TRPV2 in microglia is not fully examined. Knockdown of TRPV2 in macrophage have shown to reduce inflammatory activation, specifically, TRPV2 are needed for phagocytosis[64], cytokine production[66], and podosome assembly[65,68] and inflammasome assembly[151] in the macrophage. It is likely similar effect will be observed in microglia. Initial data suggests CBD promote phagocytosis of microglia

via activation of TRPV2[67] consistent with findings in the macrophage. Further examination is needed to fully understand TRPV2 function in microglia. Overall we demonstrated that TRPV2 and TRPA1 protein are present in microglia but only TRPV2 are functionally expressed in plasma membrane, and potentially modulate the function of microglia.

7. TRPV2 is primed for activation in pro-inflammatory environment

TRPV2 have shown to play important role in phagocytes; they regulate extracellular Ca^{2+} influx[65,68], NF-κB nuclear translocation[66] pro-inflammatory cytokine production[66], and phagocytosis[64,67]. Our study demonstrated two facts; TRPV2 is functionally expressed in microglia and TRPV2 current is enhanced by hydrogen peroxide. Hydrogen peroxide is both product and activator of microglia[76]. A constant level of H_2O_2 is required for maintaining microglia activation while activated microglia produces ROS including H_2O_2[76]. These results suggest TRPV2 have increased current in pro-inflammatory activated microglia. Indeed we demonstrate that LPS pretreated microglia has enhanced microglia activation. We have demonstrated that LPS pretreatment reduced $V_{0.5}$, indicating TRPV2 in microglia is activated at more negative membrane potential after LPS stimulation. Furthermore, LPS pretreatment slowed TRPV2 I_{tail} decay time, indicating TRPV2 remains in the open state longer after LPS treatment.

However, no statistical difference is found in size of maximum I_{tail} partially dues to large variance between measurements, and slope factor *dx* did not change following LPS stimulation, suggesting LPS did not modulate valance of gating charge. Since I_{tail} is proportional to *NPo*, this suggests maximum *NPo* did not change by LPS pretreatment. The result seems to contradict with our previous finding where the addition of H_2O_2 enhanced CBD induced I_{tail} following +80 mV membrane step. One possibility is the large variance. H_2O_2 experiments are conducted in the same cell; H_2O_2 is added to rTRPV2 expressing HEK-293 cells to enhance 300 μM CBD induced current in the same cell. Under this experimental condition, the number of channel in the membrane, *N*, is expected to remain constant. In LPS experiment, a group of LPS pre-treated BV-2 cells is compared to a group of control media treated BV-2 cells that may contain a different number

of the functional channel on the membrane. The second difference is the cell used. H_2O_2 experiments are performed in rTRPV2 transfected HEK-293 cells while LPS experiment is performed in BV-2. It is possible that TRPV2 phosphorylation state or $PI(4,5)P_2$ binding may differ in two cells, and furthermore, it is possible that TRPV2 form heteromer in BV-2 cells. Heteromeric channel formation and auxiliary molecule binding state of TRPV2 in BV-2 and HEK-293 cells need to be examined in the future. The third difference is the pro-inflammatory stimuli used. H_2O_2 and LPS may or may not have same mechanisms of activation. LPS are known to cause H_2O_2 production in microglia cells[75,76]. However, there is no evidence LPS dependent modulation of TRPV2 gating is mediated by H_2O_2. LPS may modify TRPV2 channel gating in addition to H_2O_2. For example, LPS are shown to activate phosphoinositide 3-kinases (PI3K) pathway and modulate $PI(4,5)P_2$ concentration[152]. In turn, the $PI(4,5)P_2$ level can modulate TRPV2 activities[18]. In addition to the PI3K pathway, LPS are also known to activate TGF-β-activated kinase 1 pathway and NF-κB pathway. The compounded effect of all LPS induced cellular changes on TRPV2 is unknown, and it is possible this difference in agonist used causes difference in I_{tail}. Also, note that a high concentration of LPS (2 μg/ml) are used to induce a change in TRPV2 channel gating. High concentration of LPS is used to activate macrophage-1 antigen (MAC1) receptor and ensures production of H_2O_2[75,153]. However, even 2 μg/ml LPS are not expected to induce H_2O_2 concentration as high as 1mM. 100 nM to 10 μM of intracellular H_2O_2 concentration are expected during inflammation[133]. A higher level of H_2O_2 is thought to induce apoptosis of the microglia[75,133]. Lower expected H_2O_2 concentration in LPS treated BV-2 cells may cause smaller I_{tail} enhancement in LPS treated BV-2 cells compared to direct application of 1mM H_2O_2. Also, note that H_2O_2 effect is measured by direct application of H_2O_2, but LPS effect is measured by pre-treatment of LPS and pro-inflammatory stimuli have been removed at the time of whole cell voltage clamp; potentially further reducing the amount of H_2O_2 at the time of electrophysiological measurements. This also suggests LPS modulated TRPV2 channel gating prior to whole cell voltage clamp. Whether pre-treatment and low concentration of H_2O_2 also modulate TRPV2 gating is to be examined in the future. To summarize, our result shows pro-inflammatory stimulation shift voltage dependent activation of TRPV2 to more negative potential and retains a population of TRPV2 in the open state longer in BV-2 cells.

Our result implies that TRPV2 in BV-2 with LPS pretreatment would conduct more current and more likely to increase $[Ca^{2+}]_i$ at any given membrane potential between -40 mV and +70 mV. Increased I_{tail} decay time also suggest TRPV2 channel activated by membrane depolarization and agonists stimulation will likely to remain in the open state longer after LPS stimulation. The resting membrane potential of mice microglia shows two distinct populations. One population of microglia in hippocampal slices have membrane potential of approximately -23 mV and another population of microglia have approximately -50 mV[154]. In cultured mice microglia, the resting membrane potential is approximate -31 mV in one population and -64 mV in the second population[154]. Our result shows that membrane potential of -20 to -30 mV would activate approximately 20 – 30 % of LPS pretreated TRPV2, while only 5 – 10% of no-LPS treated TRPV2 would be activated. This suggests residual TRPV2 current in LPS stimulated BV-2 without the requirement of further membrane depolarization. This moderate increase of TRPV2 *NPo* may underline maintaining basal $[Ca^{2+}]_i$ and mediate inflammatory process including, nitric oxide production[92], NF-κB nuclear translocation[92], NFLP inflammasome formation[94,95] and cytokine production[85,92,93]. These results suggest activation of TRPV2 may enhance microglia activation. Microglia is crucial to physiological and pathophysiological CNS functions. For example, microglia activation is shown to modulate progression and recovery of neurotrauma[81,155], Alzheimer's disease[156,157], Parkinson disease[75,153], and multiple sclerosis[158,159]. Microglia also maintains synaptic structure by synaptic pruning and synaptic stripping, indicating alternation of microglia activity can modulate synaptic plasticity during brain development[160,161] and impaired microglia activity is correlated to cognitive dysfunctions[162]. Microglia also maintains the integrity of blood brain barrier and angiogenesis[163]. Finally, microglia maintains a healthy environment for neurons and glia through phagocytosis of damaged and old cells[164,165]. Microglia has multiple functions in CNS and it is difficult to predict the effect of TRPV2 activation in the alternation of physiological microglia function and development of neurological diseases. However, our result suggests TRPV2 activation may modulate microglia activities and TRPV2 can be a potential therapeutic target for neurological dysfunctions.

The exact mechanism of how LPS mediated TRPV2 gating is not known. It is not likely that LPS binds to TRPV2 directly as no evidence of LPS interaction with TRPV2 is previously published. In our study, LPS are removed prior to whole cell voltage clamp, and hence there is less probability that LPS is directly binding to TRPV2 during current measurement. Furthermore, our preliminary result shows the application of LPS do not enhance TRPV2 current directly (data not shown). Previously we have demonstrated that H_2O_2 enhances TRPV2 *NPo*, which is expected to be produced following pro-inflammatory stimulations[75,76]. Application of high concentration of LPS (2 μM) ensures production O_2• from NADPH oxidase trough binding to TLR4 or MAC1 receptor[75,76]. O_2• are converted to H_2O_2 by superoxide dismutase which can modulate gating of TRPV2 (Fig 35). Furthermore, LPS treated BV-2 microglia-like cells are cultured in a high oxygen environment, which can potentially produce a higher level of H_2O_2 than the physiological environment. Whether H_2O_2 is required for LPS modulation of TRPV2 gating is not known, and whether the physiological concentration of H_2O_2 modulates TRPV2 gating is not known. It is possible that LPS modulate TRPV2 through other molecules such as preventing hydrolysis of $PI(4,5)P_2$[18]. The exact mechanism of LPS modulation of TRPV2 gating needs to be examined in the future. Despite exact mechanism is unknown, our result reveals TRPV2 is primed for activation following pro-inflammatory stimulation.

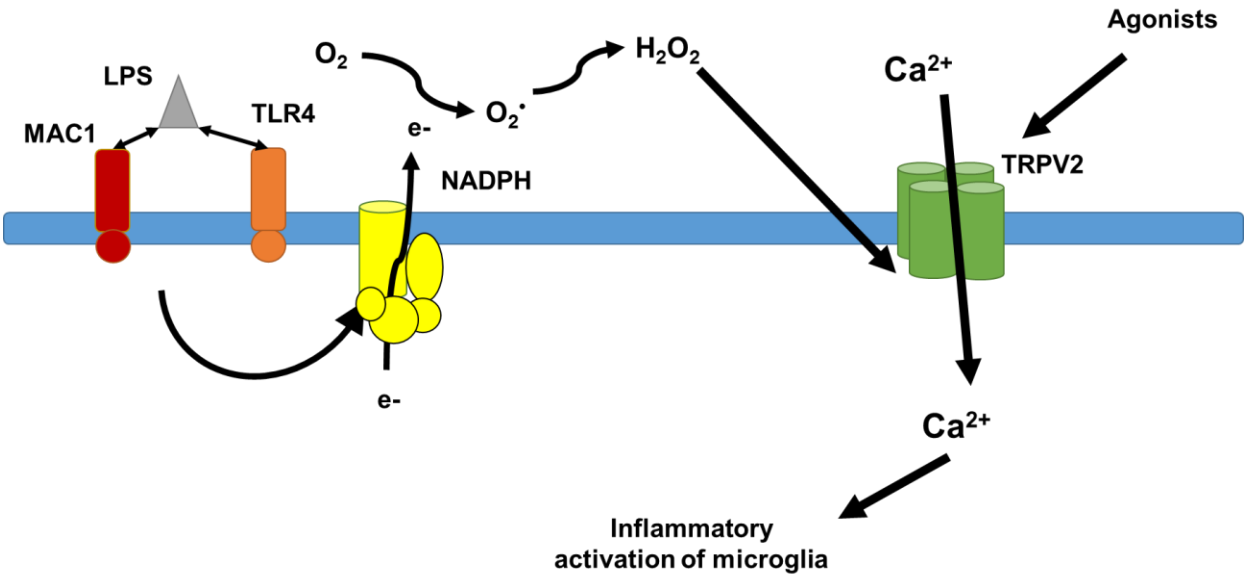

Figure 35: The working hypothesis of the LPS modification of TRPV2.

LPS binds to receptors such as MAC1 and TLR4. LPS is thought to activate NADPH oxidase complex and produce O_2•. Subsequently. Is converted to H_2O_2 which enhances TRPV2 activity together with other endogenous agonists. Enhanced TRPV2 activity would increase Ca^{2+} influx and promote microglia activation.

8. Summary

The biophysical property of TRPV2 remains poorly understood compared to related TRPV1 despite their suggested role in multiple physiological processes including osmosensation, mechanosensation, cardiac cell function, innate immunity, and cancer[20,66,70,113-115]. Rapid advances in TRPV2 research in recent years including successful visualization of the TRPV2 structure using cryo-EM and presentation of single channel activity in liposome have provided insight of TRPV2 biophysical properties. However, a gap of knowledge still exists. For example, the single channel activity of wild-type TRPV2 was not fully understood, and the process of TRPV2 activation in physiological condition remained to be an enigma. In this study we confirmed

1. TRPV2 have fast flickering, erratic activity with subconductance.

2. TRPV2 have a unitary conductance of approximately to 100 pS, similar to TRPV1.

3. TRPV2 have a constant unitary conductance that is neither affected by negative or positive membrane steps nor agonist used.

4. TRPV2 single channel property can be modulated by pharmacological reagents such as DCPIB.

5. TRPV2 are functionally expressed in both BV-2 microglia-like cells and neonatal murine primary brain microglia.

6. Application of exogenous H_2O_2 is sufficient to potentiate the agonist-dependent activity of TRPV2.

7. Cysteines in ARD (C206), hook structure (C678), and C-terminal loop (C704) are required for H_2O_2 modulation of TRPV2.

8. Acute treatment of microglia with LPS is sufficient to shift voltage depended activation of endogenous TRPV2 currents.

In this study, we aimed to contribute to the understanding of TRPV2 biophysical properties by reporting characteristics of wild-type TRPV2 single channel activities and demonstrated pro-inflammatory stimuli such as H_2O_2 and LPS can modulate TRPV2 channel gating and suggests potentially serve as an endogenous agonist. Furthermore, we identified 3 cysteine residues that modulate TRPV2 H_2O_2 sensitivity. Although the exact mechanism of H_2O_2 and LPS modulation of TRPV2 gating is not fully understood, our results infer endogenously produced ROS in macrophages and microglia is likely to promote Ca^{2+} influx through TRPV2 channels and thereby promote pro-inflammatory phagocyte activation.

However, four major questions remain to be answered.

1. Whether the addition of pharmacological agents such as DCPIB or ROS such as H_2O_2 modulates duration of TRPV2 opening. Our result shows that pro-inflammatory stimuli such as LPS treated BV-2 microglia-like cells have TRPV2 remain in the open state longer compared to media treated BV-2 microglia-like cells. Dwell time analysis of excised inside-out patch clamp electrophysiology can be used to examine the duration of channel opening after DCPIB or H_2O_2 application.

2. Whether physiological concentration of H_2O_2 can enhance agonist induced TRPV2 current. Our result demonstrates 1 mM H_2O_2 enhance CBD induced TRPV2 activation. A dose response measurement H_2O_2 effect on CBD induced TRPV2 current is needed to elucidate if lower concentration (1 – 10 μM) of H_2O_2 can also enhance TRPV2 activity.
3. Whether the combination of H_2O_2 and other endogenous stimuli such as temperature increase and membrane stretch activate TRPV2. Our result has demonstrated H_2O_2 alone do not activate TRPV2. TRPV2 are known to be activated by heating above 53°C and potentially by membrane stretch. It is possible that H_2O_2 shifts TRPV2 sensitivity of temperature and stretch; allowing TRPV2 to be activated by normal body temperature (37°C) and membrane stretch. This can be tested by comparing the TRPV2 current response to temperature ramp and stretch prior and after application of H_2O_2.
4. Whether inter-subunit disulfide connection is needed for sensitivity to H_2O_2. Our result identified C206 and C704 are required for TRPV2 sensitivity to H_2O_2, and study in TRPV1 suggest that two residues may form an inter-subunit disulfide bond that potentially affects TRPV channel activity[38]. However, whether inter-subunit bond forms in TRPV2, and whether inter-subunit disulfide bond is needed for H_2O_2 sensitivity is not known. Change in oligomer formation in wild-type TRPV2, C206A mutant TRPV2 and C704A mutant TRPV2 can be tested by non-reducing western blotting.
5. Whether LPS induced alteration of TRPV2 gating is mediated by H_2O_2. LPS is known to induce H_2O_2 production in microglia and we have demonstrated H_2O_2 enhances TRPV2 activity. LPS can be co-applied with DPI or catalase to prevent or remove H_2O_2 production in BV-2 microglia-like cells to test whether is H_2O_2 production is needed for LPS effect on TRPV2 gating.

In the end, this thesis demonstrates TRPV2 is present and mediate current transduction in microglia, described rTRPV2 single channel activities, H_2O_2 enhances TRPV2 NPo and three intracellular cysteine subunits that are required for TRPV2 sensitivity to H_2O_2. Although further works are needed to confirm H_2O_2 affect TRPV2 NPo in cells and examine the effect of to enhance heat and stretch induced TRPV2 current, our study suggests TRPV2 is sensitized during pro-inflammatory and high redox potential

environments. Modulation of TRPV2 function can be a potential future drug target for modulation inflammatory processes.

References

1 Huynh, K. W. *et al.* Structure of the full-length TRPV2 channel by cryo-EM. *Nature communications* **7**, 11130, doi:10.1038/ncomms11130 (2016).

2 Harteneck, C., Plant, T. D. & Schultz, G. From worm to man: three subfamilies of TRP channels. *Trends in neurosciences* **23**, 159-166 (2000).

3 Clapham, D. E., Runnels, L. W. & Strubing, C. The TRP ion channel family. *Nature reviews. Neuroscience* **2**, 387-396, doi:10.1038/35077544 (2001).

4 Cao, E., Liao, M., Cheng, Y. & Julius, D. TRPV1 structures in distinct conformations reveal activation mechanisms. *Nature* **504**, 113-118, doi:10.1038/nature12823 (2013).

5 Phelps, C. B., Huang, R. J., Lishko, P. V., Wang, R. R. & Gaudet, R. Structural analyses of the ankyrin repeat domain of TRPV6 and related TRPV ion channels. *Biochemistry* **47**, 2476-2484, doi:10.1021/bi702109w (2008).

6 Saotome, K., Singh, A. K., Yelshanskaya, M. V. & Sobolevsky, A. I. Crystal structure of the epithelial calcium channel TRPV6. *Nature* **534**, 506-511, doi:10.1038/nature17975 (2016).

7 Clapham, D. E. TRP channels as cellular sensors. *Nature* **426**, 517-524, doi:10.1038/nature02196 (2003).

8 Caterina, M. J., Rosen, T. A., Tominaga, M., Brake, A. J. & Julius, D. A capsaicin-receptor homologue with a high threshold for noxious heat. *Nature* **398**, 436-441, doi:10.1038/18906 (1999).

9 Xu, H. *et al.* TRPV3 is a calcium-permeable temperature-sensitive cation channel. *Nature* **418**, 181-186, doi:10.1038/nature00882 (2002).

10 Smith, G. D. *et al.* TRPV3 is a temperature-sensitive vanilloid receptor-like protein. *Nature* **418**, 186-190, doi:10.1038/nature00894 (2002).

11 Caterina, M. J. *et al.* The capsaicin receptor: a heat-activated ion channel in the pain pathway. *Nature* **389**, 816-824, doi:10.1038/39807 (1997).

12 Story, G. M. *et al.* ANKTM1, a TRP-like channel expressed in nociceptive neurons, is activated by cold temperatures. *Cell* **112**, 819-829 (2003).

13 Peier, A. M. *et al.* A TRP channel that senses cold stimuli and menthol. *Cell* **108**, 705-715 (2002).

14 McKemy, D. D., Neuhausser, W. M. & Julius, D. Identification of a cold receptor reveals a general role for TRP channels in thermosensation. *Nature* **416**, 52-58, doi:10.1038/nature719 (2002).

15 Rohacs, T. & Nilius, B. Regulation of transient receptor potential (TRP) channels by phosphoinositides. *Pflugers Archiv : European journal of physiology* **455**, 157-168, doi:10.1007/s00424-007-0275-6 (2007).

16 Brauchi, S. *et al.* Dissection of the components for PIP2 activation and thermosensation in TRP channels. *Proceedings of the National Academy of Sciences of the United States of America* **104**, 10246-10251, doi:10.1073/pnas.0703420104 (2007).

17 Hille, B., Dickson, E. J., Kruse, M., Vivas, O. & Suh, B. C. Phosphoinositides regulate ion channels. *Biochimica et biophysica acta* **1851**, 844-856, doi:10.1016/j.bbalip.2014.09.010 (2015).

18 Mercado, J., Gordon-Shaag, A., Zagotta, W. N. & Gordon, S. E. Ca2+-dependent desensitization of TRPV2 channels is mediated by hydrolysis of phosphatidylinositol 4,5-bisphosphate. *The Journal of neuroscience : the official journal of the Society for Neuroscience* **30**, 13338-13347, doi:10.1523/JNEUROSCI.2108-10.2010 (2010).

19 Davis, J. B. *et al.* Vanilloid receptor-1 is essential for inflammatory thermal hyperalgesia. *Nature* **405**, 183-187, doi:10.1038/35012076 (2000).

20 Caterina, M. J. *et al.* Impaired nociception and pain sensation in mice lacking the capsaicin receptor. *Science* **288**, 306-313 (2000).
21 Jordt, S. E. & Julius, D. Molecular basis for species-specific sensitivity to "hot" chili peppers. *Cell* **108**, 421-430 (2002).
22 Ramsey, I. S., Delling, M. & Clapham, D. E. An introduction to TRP channels. *Annual review of physiology* **68**, 619-647, doi:10.1146/annurev.physiol.68.040204.100431 (2006).
23 Liedtke, W. *et al.* Vanilloid receptor-related osmotically activated channel (VR-OAC), a candidate vertebrate osmoreceptor. *Cell* **103**, 525-535 (2000).
24 Strotmann, R., Harteneck, C., Nunnenmacher, K., Schultz, G. & Plant, T. D. OTRPC4, a nonselective cation channel that confers sensitivity to extracellular osmolarity. *Nature cell biology* **2**, 695-702, doi:10.1038/35036318 (2000).
25 Chung, M. K., Guler, A. D. & Caterina, M. J. TRPV1 shows dynamic ionic selectivity during agonist stimulation. *Nature neuroscience* **11**, 555-564, doi:10.1038/nn.2102 (2008).
26 Liao, M., Cao, E., Julius, D. & Cheng, Y. Structure of the TRPV1 ion channel determined by electron cryo-microscopy. *Nature* **504**, 107-112, doi:10.1038/nature12822 (2013).
27 Hu, H. Z. *et al.* 2-aminoethoxydiphenyl borate is a common activator of TRPV1, TRPV2, and TRPV3. *The Journal of biological chemistry* **279**, 35741-35748, doi:10.1074/jbc.M404164200 (2004).
28 Ufret-Vincenty, C. A., Klein, R. M., Hua, L., Angueyra, J. & Gordon, S. E. Localization of the PIP2 sensor of TRPV1 ion channels. *The Journal of biological chemistry* **286**, 9688-9698, doi:10.1074/jbc.M110.192526 (2011).
29 Zubcevic, L. *et al.* Cryo-electron microscopy structure of the TRPV2 ion channel. *Nature structural & molecular biology* **23**, 180-186, doi:10.1038/nsmb.3159 (2016).
30 Peralvarez-Marin, A., Donate-Macian, P. & Gaudet, R. What do we know about the transient receptor potential vanilloid 2 (TRPV2) ion channel? *The FEBS journal* **280**, 5471-5487, doi:10.1111/febs.12302 (2013).
31 McCleverty, C. J., Koesema, E., Patapoutian, A., Lesley, S. A. & Kreusch, A. Crystal structure of the human TRPV2 channel ankyrin repeat domain. *Protein science : a publication of the Protein Society* **15**, 2201-2206, doi:10.1110/ps.062357206 (2006).
32 Neeper, M. P. *et al.* Activation properties of heterologously expressed mammalian TRPV2: evidence for species dependence. *The Journal of biological chemistry* **282**, 15894-15902, doi:10.1074/jbc.M608287200 (2007).
33 Zheng, W. & Qin, F. A combined coarse-grained and all-atom simulation of TRPV1 channel gating and heat activation. *The Journal of general physiology* **145**, 443-456, doi:10.1085/jgp.201411335 (2015).
34 Yao, J., Liu, B. & Qin, F. Modular thermal sensors in temperature-gated transient receptor potential (TRP) channels. *Proceedings of the National Academy of Sciences of the United States of America* **108**, 11109-11114, doi:10.1073/pnas.1105196108 (2011).
35 Huynh, K. W. *et al.* Structural insight into the assembly of TRPV channels. *Structure* **22**, 260-268, doi:10.1016/j.str.2013.11.008 (2014).
36 Zheng, J. & Ma, L. Structure and function of the thermoTRP channel pore. *Current topics in membranes* **74**, 233-257, doi:10.1016/B978-0-12-800181-3.00009-9 (2014).
37 Joseph, J., Wang, S., Lee, J., Ro, J. Y. & Chung, M. K. Carboxyl-terminal domain of transient receptor potential vanilloid 1 contains distinct segments differentially involved in capsaicin- and heat-induced desensitization. *The Journal of biological chemistry* **288**, 35690-35702, doi:10.1074/jbc.M113.513374 (2013).
38 Ogawa, N. *et al.* Functional and Structural Divergence in Human TRPV1 Channel Subunits by Oxidative Cysteine Modification. *The Journal of biological chemistry* **291**, 4197-4210, doi:10.1074/jbc.M115.700278 (2016).
39 Vriens, J., Appendino, G. & Nilius, B. Pharmacology of vanilloid transient receptor potential cation channels. *Molecular pharmacology* **75**, 1262-1279, doi:10.1124/mol.109.055624 (2009).

40 Ferrer-Montiel, A. *et al.* Advances in modulating thermosensory TRP channels. *Expert opinion on therapeutic patents* **22**, 999-1017, doi:10.1517/13543776.2012.711320 (2012).
41 Jancso, G., Kiraly, E., Such, G., Joo, F. & Nagy, A. Neurotoxic effect of capsaicin in mammals. *Acta physiologica Hungarica* **69**, 295-313 (1987).
42 Song, M. Y. & Yuan, J. X. Introduction to TRP channels: structure, function, and regulation. *Advances in experimental medicine and biology* **661**, 99-108, doi:10.1007/978-1-60761-500-2_6 (2010).
43 Zhang, F. *et al.* Engineering vanilloid-sensitivity into the rat TRPV2 channel. *eLife* **5**, doi:10.7554/eLife.16409 (2016).
44 De Petrocellis, L. *et al.* Effects of cannabinoids and cannabinoid-enriched Cannabis extracts on TRP channels and endocannabinoid metabolic enzymes. *British journal of pharmacology* **163**, 1479-1494, doi:10.1111/j.1476-5381.2010.01166.x (2011).
45 Lishko, P. V., Procko, E., Jin, X., Phelps, C. B. & Gaudet, R. The ankyrin repeats of TRPV1 bind multiple ligands and modulate channel sensitivity. *Neuron* **54**, 905-918, doi:10.1016/j.neuron.2007.05.027 (2007).
46 Aoyagi, K., Ohara-Imaizumi, M., Nishiwaki, C., Nakamichi, Y. & Nagamatsu, S. Insulin/phosphoinositide 3-kinase pathway accelerates the glucose-induced first-phase insulin secretion through TrpV2 recruitment in pancreatic beta-cells. *The Biochemical journal* **432**, 375-386, doi:10.1042/BJ20100864 (2010).
47 Bang, S., Kim, K. Y., Yoo, S., Lee, S. H. & Hwang, S. W. Transient receptor potential V2 expressed in sensory neurons is activated by probenecid. *Neuroscience letters* **425**, 120-125, doi:10.1016/j.neulet.2007.08.035 (2007).
48 Doerner, J. F., Hatt, H. & Ramsey, I. S. Voltage- and temperature-dependent activation of TRPV3 channels is potentiated by receptor-mediated PI(4,5)P2 hydrolysis. *The Journal of general physiology* **137**, 271-288, doi:10.1085/jgp.200910388 (2011).
49 Lukacs, V. *et al.* Distinctive changes in plasma membrane phosphoinositides underlie differential regulation of TRPV1 in nociceptive neurons. *The Journal of neuroscience : the official journal of the Society for Neuroscience* **33**, 11451-11463, doi:10.1523/JNEUROSCI.5637-12.2013 (2013).
50 Lukacs, V. *et al.* Dual regulation of TRPV1 by phosphoinositides. *The Journal of neuroscience : the official journal of the Society for Neuroscience* **27**, 7070-7080, doi:10.1523/JNEUROSCI.1866-07.2007 (2007).
51 Voets, T. *et al.* The principle of temperature-dependent gating in cold- and heat-sensitive TRP channels. *Nature* **430**, 748-754, doi:10.1038/nature02732 (2004).
52 Brauchi, S., Orio, P. & Latorre, R. Clues to understanding cold sensation: thermodynamics and electrophysiological analysis of the cold receptor TRPM8. *Proceedings of the National Academy of Sciences of the United States of America* **101**, 15494-15499, doi:10.1073/pnas.0406773101 (2004).
53 Nie, L., Oishi, Y., Doi, I., Shibata, H. & Kojima, I. Inhibition of proliferation of MCF-7 breast cancer cells by a blocker of Ca(2+)-permeable channel. *Cell calcium* **22**, 75-82 (1997).
54 Mihara, H. *et al.* Involvement of TRPV2 activation in intestinal movement through nitric oxide production in mice. *The Journal of neuroscience : the official journal of the Society for Neuroscience* **30**, 16536-16544, doi:10.1523/JNEUROSCI.4426-10.2010 (2010).
55 Nie, L., Kanzaki, M., Shibata, H. & Kojima, I. Activation of calcium-permeable cation channel by insulin in Chinese hamster ovary cells expressing human insulin receptors. *Endocrinology* **139**, 179-188, doi:10.1210/endo.139.1.5674 (1998).
56 Park, U. *et al.* TRP vanilloid 2 knock-out mice are susceptible to perinatal lethality but display normal thermal and mechanical nociception. *The Journal of neuroscience : the official journal of the Society for Neuroscience* **31**, 11425-11436, doi:10.1523/JNEUROSCI.1384-09.2011 (2011).
57 Liedtke, W. & Friedman, J. M. Abnormal osmotic regulation in trpv4-/- mice. *Proceedings of the National Academy of Sciences of the United States of America* **100**, 13698-13703, doi:10.1073/pnas.1735416100 (2003).
58 Suzuki, M., Mizuno, A., Kodaira, K. & Imai, M. Impaired pressure sensation in mice lacking TRPV4. *The Journal of biological chemistry* **278**, 22664-22668, doi:10.1074/jbc.M302561200 (2003).

59 Huang, S. M., Li, X., Yu, Y., Wang, J. & Caterina, M. J. TRPV3 and TRPV4 ion channels are not major contributors to mouse heat sensation. *Molecular pain* **7**, 37, doi:10.1186/1744-8069-7-37 (2011).
60 Cai, X. *et al.* Transient receptor potential vanilloid 2 (TRPV2), a potential novel biomarker in childhood asthma. *The Journal of asthma : official journal of the Association for the Care of Asthma* **50**, 209-214, doi:10.3109/02770903.2012.753454 (2013).
61 Kim, S. R., Kim, S. U., Oh, U. & Jin, B. K. Transient receptor potential vanilloid subtype 1 mediates microglial cell death in vivo and in vitro via Ca2+-mediated mitochondrial damage and cytochrome c release. *Journal of immunology* **177**, 4322-4329 (2006).
62 Sappington, R. M. & Calkins, D. J. Contribution of TRPV1 to microglia-derived IL-6 and NFkappaB translocation with elevated hydrostatic pressure. *Investigative ophthalmology & visual science* **49**, 3004-3017, doi:10.1167/iovs.07-1355 (2008).
63 Konno, M. *et al.* Stimulation of transient receptor potential vanilloid 4 channel suppresses abnormal activation of microglia induced by lipopolysaccharide. *Glia* **60**, 761-770, doi:10.1002/glia.22306 (2012).
64 Link, T. M. *et al.* TRPV2 has a pivotal role in macrophage particle binding and phagocytosis. *Nature immunology* **11**, 232-239, doi:10.1038/ni.1842 (2010).
65 Nagasawa, M., Nakagawa, Y., Tanaka, S. & Kojima, I. Chemotactic peptide fMetLeuPhe induces translocation of the TRPV2 channel in macrophages. *Journal of cellular physiology* **210**, 692-702, doi:10.1002/jcp.20883 (2007).
66 Yamashiro, K. *et al.* Role of transient receptor potential vanilloid 2 in LPS-induced cytokine production in macrophages. *Biochemical and biophysical research communications* **398**, 284-289, doi:10.1016/j.bbrc.2010.06.082 (2010).
67 Hassan, S. *et al.* Cannabidiol enhances microglial phagocytosis via transient receptor potential (TRP) channel activation. *British journal of pharmacology* **171**, 2426-2439, doi:10.1111/bph.12615 (2014).
68 Nagasawa, M. & Kojima, I. Translocation of calcium-permeable TRPV2 channel to the podosome: Its role in the regulation of podosome assembly. *Cell calcium* **51**, 186-193, doi:10.1016/j.ceca.2011.12.012 (2012).
69 Stokes, A. J., Shimoda, L. M., Koblan-Huberson, M., Adra, C. N. & Turner, H. A TRPV2-PKA signaling module for transduction of physical stimuli in mast cells. *The Journal of experimental medicine* **200**, 137-147, doi:10.1084/jem.20032082 (2004).
70 Pottosin, I. *et al.* Mechanosensitive Ca(2)(+)-permeable channels in human leukemic cells: pharmacological and molecular evidence for TRPV2. *Biochimica et biophysica acta* **1848**, 51-59, doi:10.1016/j.bbamem.2014.09.008 (2015).
71 Schilling, T. & Eder, C. Non-selective cation channel activity is required for lysophosphatidylcholine-induced monocyte migration. *Journal of cellular physiology* **221**, 325-334, doi:10.1002/jcp.21857 (2009).
72 Monet, M. *et al.* Lysophospholipids stimulate prostate cancer cell migration via TRPV2 channel activation. *Biochimica et biophysica acta* **1793**, 528-539, doi:10.1016/j.bbamcr.2009.01.003 (2009).
73 Henn, A. *et al.* The suitability of BV-2 cells as alternative model system for primary microglia cultures or for animal experiments examining brain inflammation. *Altex* **26**, 83-94 (2009).
74 Ransohoff, R. M. & Cardona, A. E. The myeloid cells of the central nervous system parenchyma. *Nature* **468**, 253-262, doi:10.1038/nature09615 (2010).
75 Block, M. L., Zecca, L. & Hong, J. S. Microglia-mediated neurotoxicity: uncovering the molecular mechanisms. *Nature reviews. Neuroscience* **8**, 57-69, doi:10.1038/nrn2038 (2007).
76 Block, M. L. & Hong, J. S. Microglia and inflammation-mediated neurodegeneration: multiple triggers with a common mechanism. *Progress in neurobiology* **76**, 77-98, doi:10.1016/j.pneurobio.2005.06.004 (2005).
77 Davalos, D. *et al.* ATP mediates rapid microglial response to local brain injury in vivo. *Nature neuroscience* **8**, 752-758, doi:10.1038/nn1472 (2005).
78 Fetler, L. & Amigorena, S. Neuroscience. Brain under surveillance: the microglia patrol. *Science* **309**, 392-393, doi:10.1126/science.1114852 (2005).
79 Jack, C. S. *et al.* TLR signaling tailors innate immune responses in human microglia and astrocytes. *Journal of immunology* **175**, 4320-4330 (2005).

80 Town, T., Nikolic, V. & Tan, J. The microglial "activation" continuum: from innate to adaptive responses. *Journal of neuroinflammation* **2**, 24, doi:10.1186/1742-2094-2-24 (2005).
81 Cao, T., Thomas, T. C., Ziebell, J. M., Pauly, J. R. & Lifshitz, J. Morphological and genetic activation of microglia after diffuse traumatic brain injury in the rat. *Neuroscience* **225**, 65-75, doi:10.1016/j.neuroscience.2012.08.058 (2012).
82 Bowler, R. M., Koller, W. & Schulz, P. E. Parkinsonism due to manganism in a welder: neurological and neuropsychological sequelae. *Neurotoxicology* **27**, 327-332, doi:10.1016/j.neuro.2005.10.011 (2006).
83 Block, M. L. *et al.* Nanometer size diesel exhaust particles are selectively toxic to dopaminergic neurons: the role of microglia, phagocytosis, and NADPH oxidase. *FASEB journal : official publication of the Federation of American Societies for Experimental Biology* **18**, 1618-1620, doi:10.1096/fj.04-1945fje (2004).
84 Wilkinson, B., Koenigsknecht-Talboo, J., Grommes, C., Lee, C. Y. & Landreth, G. Fibrillar beta-amyloid-stimulated intracellular signaling cascades require Vav for induction of respiratory burst and phagocytosis in monocytes and microglia. *The Journal of biological chemistry* **281**, 20842-20850, doi:10.1074/jbc.M600627200 (2006).
85 Hoffmann, A., Kann, O., Ohlemeyer, C., Hanisch, U. K. & Kettenmann, H. Elevation of basal intracellular calcium as a central element in the activation of brain macrophages (microglia): suppression of receptor-evoked calcium signaling and control of release function. *The Journal of neuroscience : the official journal of the Society for Neuroscience* **23**, 4410-4419 (2003).
86 Suresh, K. *et al.* Hydrogen peroxide-induced calcium influx in lung microvascular endothelial cells involves TRPV4. *American journal of physiology. Lung cellular and molecular physiology* **309**, L1467-1477, doi:10.1152/ajplung.00275.2015 (2015).
87 Chung, M. K. *et al.* The role of TRPM2 in hydrogen peroxide-induced expression of inflammatory cytokine and chemokine in rat trigeminal ganglia. *Neuroscience* **297**, 160-169, doi:10.1016/j.neuroscience.2015.03.067 (2015).
88 Kraft, R. *et al.* Hydrogen peroxide and ADP-ribose induce TRPM2-mediated calcium influx and cation currents in microglia. *American journal of physiology. Cell physiology* **286**, C129-137, doi:10.1152/ajpcell.00331.2003 (2004).
89 Bessac, B. F. *et al.* TRPA1 is a major oxidant sensor in murine airway sensory neurons. *The Journal of clinical investigation* **118**, 1899-1910, doi:10.1172/JCI34192 (2008).
90 Sawada, Y., Hosokawa, H., Matsumura, K. & Kobayashi, S. Activation of transient receptor potential ankyrin 1 by hydrogen peroxide. *The European journal of neuroscience* **27**, 1131-1142, doi:10.1111/j.1460-9568.2008.06093.x (2008).
91 Ruan, T. *et al.* Sensitization by pulmonary reactive oxygen species of rat vagal lung C-fibers: the roles of the TRPV1, TRPA1, and P2X receptors. *PloS one* **9**, e91763, doi:10.1371/journal.pone.0091763 (2014).
92 Zhou, X., Yang, W. & Li, J. Ca2+- and protein kinase C-dependent signaling pathway for nuclear factor-kappaB activation, inducible nitric-oxide synthase expression, and tumor necrosis factor-alpha production in lipopolysaccharide-stimulated rat peritoneal macrophages. *The Journal of biological chemistry* **281**, 31337-31347, doi:10.1074/jbc.M602739200 (2006).
93 Lichtman, S. N., Wang, J., Zhang, C. & Lemasters, J. J. Endocytosis and Ca2+ are required for endotoxin-stimulated TNF-alpha release by rat Kupffer cells. *The American journal of physiology* **271**, G920-928 (1996).
94 Murakami, T. *et al.* Critical role for calcium mobilization in activation of the NLRP3 inflammasome. *Proceedings of the National Academy of Sciences of the United States of America* **109**, 11282-11287, doi:10.1073/pnas.1117765109 (2012).
95 Lee, G. S. *et al.* The calcium-sensing receptor regulates the NLRP3 inflammasome through Ca2+ and cAMP. *Nature* **492**, 123-127, doi:10.1038/nature11588 (2012).
96 Juvin, V., Penna, A., Chemin, J., Lin, Y. L. & Rassendren, F. A. Pharmacological characterization and molecular determinants of the activation of transient receptor potential V2 channel orthologs by 2-

aminoethoxydiphenyl borate. *Molecular pharmacology* **72**, 1258-1268, doi:10.1124/mol.107.037044 (2007).
97 Qin, N. *et al.* TRPV2 is activated by cannabidiol and mediates CGRP release in cultured rat dorsal root ganglion neurons. *The Journal of neuroscience : the official journal of the Society for Neuroscience* **28**, 6231-6238, doi:10.1523/JNEUROSCI.0504-08.2008 (2008).
98 Bautista, D. & Julius, D. Fire in the hole: pore dilation of the capsaicin receptor TRPV1. *Nature neuroscience* **11**, 528-529, doi:10.1038/nn0508-528 (2008).
99 Chung, M. K., Guler, A. D. & Caterina, M. J. Biphasic currents evoked by chemical or thermal activation of the heat-gated ion channel, TRPV3. *The Journal of biological chemistry* **280**, 15928-15941, doi:10.1074/jbc.M500596200 (2005).
100 Stotz, S. C., Vriens, J., Martyn, D., Clardy, J. & Clapham, D. E. Citral sensing by Transient [corrected] receptor potential channels in dorsal root ganglion neurons. *PloS one* **3**, e2082, doi:10.1371/journal.pone.0002082 (2008).
101 Nilius, B. *et al.* Gating of TRP channels: a voltage connection? *The Journal of physiology* **567**, 35-44, doi:10.1113/jphysiol.2005.088377 (2005).
102 Miyake, T., Shirakawa, H., Nakagawa, T. & Kaneko, S. Activation of mitochondrial transient receptor potential vanilloid 1 channel contributes to microglial migration. *Glia* **63**, 1870-1882, doi:10.1002/glia.22854 (2015).
103 Laskin, D. L., Sunil, V. R., Gardner, C. R. & Laskin, J. D. Macrophages and tissue injury: agents of defense or destruction? *Annual review of pharmacology and toxicology* **51**, 267-288, doi:10.1146/annurev.pharmtox.010909.105812 (2011).
104 McGahon, M. K. *et al.* TRPV2 Channels Contribute to Stretch-Activated Cation Currents and Myogenic Constriction in Retinal Arterioles. *Investigative ophthalmology & visual science* **57**, 5637-5647, doi:10.1167/iovs.16-20279 (2016).
105 Billen, B. *et al.* Different ligands of the TRPV3 cation channel cause distinct conformational changes as revealed by intrinsic tryptophan fluorescence quenching. *The Journal of biological chemistry* **290**, 12964-12974, doi:10.1074/jbc.M114.628925 (2015).
106 Caires, R. *et al.* Hyaluronan modulates TRPV1 channel opening, reducing peripheral nociceptor activity and pain. *Nature communications* **6**, 8095, doi:10.1038/ncomms9095 (2015).
107 Studer, M. & McNaughton, P. A. Modulation of single-channel properties of TRPV1 by phosphorylation. *The Journal of physiology* **588**, 3743-3756, doi:10.1113/jphysiol.2010.190611 (2010).
108 Baumgarten, C. M., Browe, D. M. & Ren, Z. in *Mechanosensitivity in Cells and Tissues* (eds A. Kamkin & I. Kiseleva) (2005).
109 Lemonnier, L., Prevarskaya, N., Mazurier, J., Shuba, Y. & Skryma, R. 2-APB inhibits volume-regulated anion channels independently from intracellular calcium signaling modulation. *FEBS letters* **556**, 121-126 (2004).
110 Cordero-Morales, J. F., Jogini, V., Chakrapani, S. & Perozo, E. A multipoint hydrogen-bond network underlying KcsA C-type inactivation. *Biophysical journal* **100**, 2387-2393, doi:10.1016/j.bpj.2011.01.073 (2011).
111 Susankova, K., Tousova, K., Vyklicky, L., Teisinger, J. & Vlachova, V. Reducing and oxidizing agents sensitize heat-activated vanilloid receptor (TRPV1) current. *Molecular pharmacology* **70**, 383-394, doi:10.1124/mol.106.023069 (2006).
112 DelloStritto, D. J. *et al.* Differential regulation of TRPV1 channels by H2O2: implications for diabetic microvascular dysfunction. *Basic research in cardiology* **111**, 21, doi:10.1007/s00395-016-0539-4 (2016).
113 Selvaggi, F. P., Laurentaci, G. & Losacco, T. [Relations between heterophilic antibodies and natural lymphocytotoxic antibodies in rabbits with allogenic skin grafts]. *Chirurgia e patologia sperimentale* **25**, 231-237 (1977).
114 Monet, M. *et al.* Role of cationic channel TRPV2 in promoting prostate cancer migration and progression to androgen resistance. *Cancer research* **70**, 1225-1235, doi:10.1158/0008-5472.CAN-09-2205 (2010).

115 Katanosaka, Y. *et al.* TRPV2 is critical for the maintenance of cardiac structure and function in mice. *Nature communications* **5**, 3932, doi:10.1038/ncomms4932 (2014).
116 Rutter, A. R., Ma, Q. P., Leveridge, M. & Bonnert, T. P. Heteromerization and colocalization of TrpV1 and TrpV2 in mammalian cell lines and rat dorsal root ganglia. *Neuroreport* **16**, 1735-1739 (2005).
117 Liapi, A. & Wood, J. N. Extensive co-localization and heteromultimer formation of the vanilloid receptor-like protein TRPV2 and the capsaicin receptor TRPV1 in the adult rat cerebral cortex. *The European journal of neuroscience* **22**, 825-834, doi:10.1111/j.1460-9568.2005.04270.x (2005).
118 Best, L., Yates, A. P., Decher, N., Steinmeyer, K. & Nilius, B. Inhibition of glucose-induced electrical activity in rat pancreatic beta-cells by DCPIB, a selective inhibitor of volume-sensitive anion currents. *European journal of pharmacology* **489**, 13-19, doi:10.1016/j.ejphar.2004.02.030 (2004).
119 Decher, N. *et al.* DCPIB is a novel selective blocker of I(Cl,swell) and prevents swelling-induced shortening of guinea-pig atrial action potential duration. *British journal of pharmacology* **134**, 1467-1479, doi:10.1038/sj.bjp.0704413 (2001).
120 Liu, B., Hui, K. & Qin, F. Thermodynamics of heat activation of single capsaicin ion channels VR1. *Biophysical journal* **85**, 2988-3006, doi:10.1016/S0006-3495(03)74719-5 (2003).
121 Hui, K., Liu, B. & Qin, F. Capsaicin activation of the pain receptor, VR1: multiple open states from both partial and full binding. *Biophysical journal* **84**, 2957-2968, doi:10.1016/S0006-3495(03)70022-8 (2003).
122 Kim, D., Cavanaugh, E. J. & Simkin, D. Inhibition of transient receptor potential A1 channel by phosphatidylinositol-4,5-bisphosphate. *American journal of physiology. Cell physiology* **295**, C92-99, doi:10.1152/ajpcell.00023.2008 (2008).
123 Tang, M., Wu, G. Y., Dong, X. Z. & Tang, Z. X. Phosphoinositide interacting regulator of TRP (Pirt) enhances TRPM8 channel activity in vitro via increasing channel conductance. *Acta pharmacologica Sinica* **37**, 98-104, doi:10.1038/aps.2015.110 (2016).
124 Holakovska, B., Grycova, L., Bily, J. & Teisinger, J. Characterization of calmodulin binding domains in TRPV2 and TRPV5 C-tails. *Amino acids* **40**, 741-748, doi:10.1007/s00726-010-0712-2 (2011).
125 Rosenhouse-Dantsker, A., Mehta, D. & Levitan, I. Regulation of ion channels by membrane lipids. *Comprehensive Physiology* **2**, 31-68, doi:10.1002/cphy.c110001 (2012).
126 Schneider, U., Schwenk, H. U. & Bornkamm, G. Characterization of EBV-genome negative "null" and "T" cell lines derived from children with acute lymphoblastic leukemia and leukemic transformed non-Hodgkin lymphoma. *International journal of cancer* **19**, 621-626 (1977).
127 Samways, D. S. & Egan, T. M. Calcium-dependent decrease in the single-channel conductance of TRPV1. *Pflugers Archiv : European journal of physiology* **462**, 681-691, doi:10.1007/s00424-011-1013-7 (2011).
128 Premkumar, L. S., Agarwal, S. & Steffen, D. Single-channel properties of native and cloned rat vanilloid receptors. *The Journal of physiology* **545**, 107-117 (2002).
129 Welch, J. M., Simon, S. A. & Reinhart, P. H. The activation mechanism of rat vanilloid receptor 1 by capsaicin involves the pore domain and differs from the activation by either acid or heat. *Proceedings of the National Academy of Sciences of the United States of America* **97**, 13889-13894, doi:10.1073/pnas.230146497 (2000).
130 Ryu, S., Liu, B., Yao, J., Fu, Q. & Qin, F. Uncoupling proton activation of vanilloid receptor TRPV1. *The Journal of neuroscience : the official journal of the Society for Neuroscience* **27**, 12797-12807, doi:10.1523/JNEUROSCI.2324-07.2007 (2007).
131 Jordt, S. E., Tominaga, M. & Julius, D. Acid potentiation of the capsaicin receptor determined by a key extracellular site. *Proceedings of the National Academy of Sciences of the United States of America* **97**, 8134-8139, doi:10.1073/pnas.100129497 (2000).
132 Myers, B. R., Bohlen, C. J. & Julius, D. A yeast genetic screen reveals a critical role for the pore helix domain in TRP channel gating. *Neuron* **58**, 362-373, doi:10.1016/j.neuron.2008.04.012 (2008).
133 Sies, H. Hydrogen peroxide as a central redox signaling molecule in physiological oxidative stress: Oxidative eustress. *Redox biology* **11**, 613-619, doi:10.1016/j.redox.2016.12.035 (2017).
134 Wittmann, C. *et al.* Hydrogen peroxide in inflammation: messenger, guide, and assassin. *Advances in hematology* **2012**, 541471, doi:10.1155/2012/541471 (2012).

135 Bains, M. & Hall, E. D. Antioxidant therapies in traumatic brain and spinal cord injury. *Biochimica et biophysica acta* **1822**, 675-684, doi:10.1016/j.bbadis.2011.10.017 (2012).
136 Kleinschnitz, C. *et al.* Post-stroke inhibition of induced NADPH oxidase type 4 prevents oxidative stress and neurodegeneration. *PLoS biology* **8**, doi:10.1371/journal.pbio.1000479 (2010).
137 Milton, N. G. Role of hydrogen peroxide in the aetiology of Alzheimer's disease: implications for treatment. *Drugs & aging* **21**, 81-100 (2004).
138 Slezak, J. *et al.* Hydrogen peroxide changes in ischemic and reperfused heart. Cytochemistry and biochemical and X-ray microanalysis. *The American journal of pathology* **147**, 772-781 (1995).
139 Petrosillo, G. *et al.* Mitochondrial dysfunction associated with cardiac ischemia/reperfusion can be attenuated by oxygen tension control. Role of oxygen-free radicals and cardiolipin. *Biochimica et biophysica acta* **1710**, 78-86, doi:10.1016/j.bbabio.2005.10.003 (2005).
140 Iwata, Y., Katanosaka, Y., Arai, Y., Shigekawa, M. & Wakabayashi, S. Dominant-negative inhibition of Ca2+ influx via TRPV2 ameliorates muscular dystrophy in animal models. *Human molecular genetics* **18**, 824-834, doi:10.1093/hmg/ddn408 (2009).
141 Brauchi, S., Orta, G., Salazar, M., Rosenmann, E. & Latorre, R. A hot-sensing cold receptor: C-terminal domain determines thermosensation in transient receptor potential channels. *The Journal of neuroscience : the official journal of the Society for Neuroscience* **26**, 4835-4840, doi:10.1523/JNEUROSCI.5080-05.2006 (2006).
142 Vlachova, V. *et al.* Functional role of C-terminal cytoplasmic tail of rat vanilloid receptor 1. *The Journal of neuroscience : the official journal of the Society for Neuroscience* **23**, 1340-1350 (2003).
143 Gordon-Shaag, A., Zagotta, W. N. & Gordon, S. E. Mechanism of Ca(2+)-dependent desensitization in TRP channels. *Channels* **2**, 125-129 (2008).
144 Vennekens, R., Menigoz, A. & Nilius, B. TRPs in the Brain. *Reviews of physiology, biochemistry and pharmacology* **163**, 27-64, doi:10.1007/112_2012_8 (2012).
145 Corrigan, F., Mander, K. A., Leonard, A. V. & Vink, R. Neurogenic inflammation after traumatic brain injury and its potentiation of classical inflammation. *Journal of neuroinflammation* **13**, 264, doi:10.1186/s12974-016-0738-9 (2016).
146 Barabas, M. E., Kossyreva, E. A. & Stucky, C. L. TRPA1 is functionally expressed primarily by IB4-binding, non-peptidergic mouse and rat sensory neurons. *PloS one* **7**, e47988, doi:10.1371/journal.pone.0047988 (2012).
147 Schilling, T. & Eder, C. Amyloid-beta-induced reactive oxygen species production and priming are differentially regulated by ion channels in microglia. *Journal of cellular physiology* **226**, 3295-3302, doi:10.1002/jcp.22675 (2011).
148 Weng, H. J. *et al.* Tmem100 Is a Regulator of TRPA1-TRPV1 Complex and Contributes to Persistent Pain. *Neuron* **85**, 833-846, doi:10.1016/j.neuron.2014.12.065 (2015).
149 Correll, C. C., Phelps, P. T., Anthes, J. C., Umland, S. & Greenfeder, S. Cloning and pharmacological characterization of mouse TRPV1. *Neuroscience letters* **370**, 55-60, doi:10.1016/j.neulet.2004.07.058 (2004).
150 Jordt, S. E. *et al.* Mustard oils and cannabinoids excite sensory nerve fibres through the TRP channel ANKTM1. *Nature* **427**, 260-265, doi:10.1038/nature02282 (2004).
151 Compan, V. *et al.* Cell volume regulation modulates NLRP3 inflammasome activation. *Immunity* **37**, 487-500, doi:10.1016/j.immuni.2012.06.013 (2012).
152 Brown, J., Wang, H., Hajishengallis, G. N. & Martin, M. TLR-signaling networks: an integration of adaptor molecules, kinases, and cross-talk. *Journal of dental research* **90**, 417-427, doi:10.1177/0022034510381264 (2011).
153 Levesque, S. *et al.* The role of MAC1 in diesel exhaust particle-induced microglial activation and loss of dopaminergic neuron function. *Journal of neurochemistry* **125**, 756-765, doi:10.1111/jnc.12231 (2013).
154 Boucsein, C. *et al.* Purinergic receptors on microglial cells: functional expression in acute brain slices and modulation of microglial activation in vitro. *The European journal of neuroscience* **17**, 2267-2276 (2003).

155 McKee, C. A. & Lukens, J. R. Emerging Roles for the Immune System in Traumatic Brain Injury. *Frontiers in immunology* **7**, 556, doi:10.3389/fimmu.2016.00556 (2016).
156 Du, L. *et al.* Role of Microglia in Neurological Disorders and Their Potentials as a Therapeutic Target. *Molecular neurobiology*, doi:10.1007/s12035-016-0245-0 (2016).
157 Hickman, S. E., Allison, E. K. & El Khoury, J. Microglial dysfunction and defective beta-amyloid clearance pathways in aging Alzheimer's disease mice. *The Journal of neuroscience : the official journal of the Society for Neuroscience* **28**, 8354-8360, doi:10.1523/JNEUROSCI.0616-08.2008 (2008).
158 Bhasin, M., Wu, M. & Tsirka, S. E. Modulation of microglial/macrophage activation by macrophage inhibitory factor (TKP) or tuftsin (TKPR) attenuates the disease course of experimental autoimmune encephalomyelitis. *BMC immunology* **8**, 10, doi:10.1186/1471-2172-8-10 (2007).
159 Heppner, F. L. *et al.* Experimental autoimmune encephalomyelitis repressed by microglial paralysis. *Nature medicine* **11**, 146-152, doi:10.1038/nm1177 (2005).
160 Cunningham, C. L., Martinez-Cerdeno, V. & Noctor, S. C. Microglia regulate the number of neural precursor cells in the developing cerebral cortex. *The Journal of neuroscience : the official journal of the Society for Neuroscience* **33**, 4216-4233, doi:10.1523/JNEUROSCI.3441-12.2013 (2013).
161 Bilimoria, P. M. & Stevens, B. Microglia function during brain development: New insights from animal models. *Brain research* **1617**, 7-17, doi:10.1016/j.brainres.2014.11.032 (2015).
162 Parkhurst, C. N. *et al.* Microglia promote learning-dependent synapse formation through brain-derived neurotrophic factor. *Cell* **155**, 1596-1609, doi:10.1016/j.cell.2013.11.030 (2013).
163 Fantin, A. *et al.* Tissue macrophages act as cellular chaperones for vascular anastomosis downstream of VEGF-mediated endothelial tip cell induction. *Blood* **116**, 829-840, doi:10.1182/blood-2009-12-257832 (2010).
164 Nimmerjahn, A., Kirchhoff, F. & Helmchen, F. Resting microglial cells are highly dynamic surveillants of brain parenchyma in vivo. *Science* **308**, 1314-1318, doi:10.1126/science.1110647 (2005).
165 Sierra, A. *et al.* Microglia shape adult hippocampal neurogenesis through apoptosis-coupled phagocytosis. *Cell stem cell* **7**, 483-495, doi:10.1016/j.stem.2010.08.014 (2010).